Frank J. Ferrell
Goddard

03635-1-T

The Measurement of Atmospheric Ozone Using Satellite Infrared Observations in the 9.6 μm Band

JAMES MADISON RUSSELL III

July 1970

National Aeronautics and Space Administration
Contract No. NSR 23-005-376
Washington, D.C.

High Altitude Engineering Laboratory
Departments of Aerospace Engineering
Meteorology and Oceanography

This report was also a dissertation submitted in partial fulfillment of the requirements for the degree of Doctor of Philosophy in the University of Michigan, 1970.

THE UNIVERSITY OF MICHIGAN
COLLEGE OF ENGINEERING
High Altitude Engineering Laboratory
Departments of
Aerospace Engineering
Meteorology and Oceanography

Technical Report

THE MEASUREMENT OF ATMOSPHERIC OZONE USING SATELLITE INFRARED OBSERVATIONS IN THE 9.6 μm BAND

ORA Project 03635

under contract with:

NATIONAL AERONAUTICS AND SPACE ADMINISTRATION
CONTRACT NO. NSR-23-005-376
WASHINGTON, D. C.

administered through

OFFICE OF RESEARCH ADMINISTRATION ANN ARBOR

July 1970

ACKNOWLEDGEMENTS

The author wishes to thank those who assisted him in this study. Special appreciation is given to Professor S. Roland Drayson for his guidance and counsel while serving as Chairman of the Doctoral Committee. The author also expresses gratitude to the other members of the Doctoral Committee, Professor Frederick L. Bartman, Professor William R. Kuhn, and Professor Gwynn H. Suits for their help and suggestions during the course of this work.

The help of colleagues and the staff of the High Altitude Engineering Laboratory is also gratefully acknowledged. The author expresses thanks to Mr. L. W. Chaney for several helpful discussions concerning instrumentation aspects of the problem.

Financial support for this work was received from a number of sources. The author appreciates direct assistance provided by the Institute of Science and Technology and the Aeronomy Program of the University of Michigan and by the Langley Research Center of the National Aeronautics and Space Administration. The author also acknowledges additional support received from the National Aeronautics and Space Administration under contracts NASr-54(03) and NGR 23-005-394 and from the Environmental Science Services Administration under contract E92-69-N.

Finally, the author would like to thank his wife for her support and encouragement during the course of this work and for her help in refining the manuscript.

TABLE OF CONTENTS

TABLE OF CONTENTS (concluded)

LIST OF TABLES

LIST OF FIGURES

LIST OF FIGURES (Continued)

LIST OF FIGURES (Continued)

LIST OF SYMBOLS

A_v	Avogadro number
a	mean radius of earth
$B(\bar{\nu}, T)$	Planck Radiance
c	velocity of light in a vacuum
$\bar{d}$	mean spacing of absorption lines in an interval $\Delta\bar{\nu}$ wide
E_o	ground state energy
$f(\bar{\nu}, \bar{\nu}_i)$	absorption line profile function
F_i	ratio of perturbed to unperturbed line strength
$F_{\nu\infty}$	solar flux entering the atmosphere at the top
g	acceleration of gravity
H	width factor in Green's ozone profile function
h	Planck constant
hm	altitude of the maximum ozone partial pressure
k	Boltzmann constant
$L(\bar{\nu}, \theta)$	spectral radiance
L_{z_k}	radiance for a horizon line of sight passing through a tangent height of Z_k
$\bar{\ell}$	effective length of a homogeneous absorption path
M	gram molecular weight
m	mass per molecule in grams
N	total number of absorption lines in a band
N'	total number of absorption lines in an interval $\Delta\bar{\nu}$ wide
n_2	number density of oxygen
n_3	number density of ozone
n_m	number density of a third body
nO_{3e}	photochemical equilibrium number density of ozone

n_s	the number density of air at standard temperature and pressure
P	atmospheric pressure
PO_3	ozone partial pressure
PO3m	maximum ozone partial pressure in Green's ozone profile function
Pm	atmospheric pressure at the level of the maximum ozone partial pressure
q	mass mixing ratio of an absorbing gas
$\bar{q}_2$	number of dissociating photons absorbed per unit volume per unit time by oxygen
$\bar{q}_3$	number of dissociating photons absorbed per unit volume per unit time by ozone
R_o	universal gas constant
S_i	intensity of the ith absorption line
$S_{j,k}$	distance along the line of sight from the kth tangent point out to the boundary of the jth layer
T	atmospheric temperature
u	integrated mass in an atmospheric column of unit cross-section
v_i	ith eigenvector
$W(\bar{\nu}_o, P)$	weighting function
W_k	vertical weighting function in the horizon direction
Z	height in the local vertical
Z_k	tangent height
α_{Li}	Lorentz half-width
α_{Di}	Doppler half-width
$\beta_{\bar{\nu}}$	the mean absorption line intensity for the interval $\Delta\bar{\nu}$ (when the Goody Random Exponential band model is used)
γ_i	unperturbed line strength in the ground state representation
$\epsilon_g(\bar{\nu})$	emissivity of the lower boundary under a satellite

θ	zenith angle
$\kappa(\bar{\nu}, P)$	absorption coefficient
λ	wavelength
λ_i	ith eigenvalue
ν	frequency
$\bar{\nu}$	wave number = $1/\lambda$
ρ	atmospheric mass density
ρO_3	atmospheric ozone mass density
σ	standard deviation of a random variable
σ_ν	absorption cross section per molecule
$\tau(\bar{\nu}, P)$	transmittance
$\phi(\bar{\nu})$	radiometer instrument function

ABSTRACT

Atmospheric ozone is significantly involved, both directly and indirectly, in the fundamental physical processes affecting the energetics and motions of the stratosphere and mesosphere. There is also a correlation between ozone concentration and meteorological conditions. Consequently, widespread interest exists in global ozone measurements. This paper analyzes two approaches to the measurement of ozone from a satellite using the 9.6 μm band; the nadir experiment and the horizon experiment.

First, a technique is developed for inverting radiances measured in the nadir direction. A method is formulated for computing the emission from the lower boundary under the satellite which circumvents the difficult analytical problems caused by the presence of atmospheric clouds and the water vapor continuum absorption. The inversion equations are expanded in terms of the eigenvectors and eigenvalues of a least squares solution matrix and an analysis is performed to determine the information content of the radiance measurements. The results show that under favorable conditions there are only two pieces of independent information available from the measurements: the total ozone (u) and the altitude (hm) of the primary maximum in the ozone profile. An error analysis shows that errors in u are most affected by random radiance noise, lower boundary temperature errors, and ozone absorption line intensity errors. Errors in hm are most affected by the former two errors and by temperature profile bias errors. The results when all errors are considered simultaneously indicate that it should ultimately be possible

to determine u to within 10% or less and to determine hm to within 1.5 km when the RMS radiance noise level is .1% or less. The calculations are also done for various degrees of cloudiness in the troposphere. The data shows that the presence of clouds will not seriously effect results as long as there is some contrast between the ozone spectrum and the lower boundary emission spectrum. Finally, the inversion technique is applied to radiances measured from a balloon over Palestine, Texas and to Nimbus III satellite data measured over the Bahama Islands.

Next, a method is developed for inverting radiances measured in the horizon direction. The ensuing study proves the feasibility of the horizon experiment for determining ozone information and shows that the ozone partial pressure can be determined in the altitude range from 50 km down to 25 or 30 km. A study of individual error effects shows that ozone partial pressure errors are very sensitive to small temperature profile bias errors. The next most significant effect is caused by tangent height error. These calculations are performed for both a low latitude and a high latitude horizon radiance profile. In the final set of error calculations, all error sources are considered simultaneously. The results show that in the absence of a temperature profile bias error, it should ultimately be possible to determine the ozone partial pressure to within 15 or 20% for most of the range 25 to 50 km. It may be possible to reduce this error to 10% or less by smoothing the solution profile. Since a small temperature bias error would seriously degrade these results, great emphasis should be placed on methods of minimizing this source of error in an actual experiment.

Data provided by the nadir and horizon experiments would aid in several areas of research. The extensive geographic coverage made possible by satellite measurements would be helpful in documenting the relationship between ozone amount and weather conditions and the data should lead to a better understanding of global air mass circulation. The measurements would also be useful in the study of sudden stratospheric warmings and in clarifying unanswered questions regarding stratospheric photochemistry. Furthermore, the experiments would provide data routinely in previously unsounded or infrequently probed regions, such as over the oceans, over remote locations in the Southern Hemisphere, and in the upper stratosphere.

CHAPTER I

INTRODUCTION

Ozone is only a minor atmospheric constituent, yet it has held the attention of scientists ever since it was first suggested by the chemist Schonbein in 1840. The first conclusive evidence of an ozone layer in the atmosphere was deduced from ultraviolet absorption measurements made by Fabry and Buisson (1913). Later, their conclusions were given theoretical support by the British geophysicist Chapman (1930) who first explained the presence of ozone in the upper atmosphere using photochemical principles. At about the same time, Dobson (1930) published his paper describing the development of Fabry and Buisson's technique into a convenient method for routinely measuring the total ozone above an observer.[1]

After the work by Dobson and his co-workers the real meteorological significance of atmospheric ozone began to emerge. The systematic measurements of total ozone made possible by the Dobson instrument revealed a strong correlation between ozone amount and day-to-day weather variations. Later, with the advent of rocketsondes and high altitude balloons, instruments were developed to measure, in-situ, the vertical distribution of ozone as well as temperature and wind field profiles. These measurements showed definite correlations between significant changes in the ozone partial pressure and changes in the temperature lapse rate and the wind field frequency (see for example Brieland, 1964, or for an extensive list of references, Duardo,

[1]This is the total (integrated) ozone amount in an atmospheric column of unit cross-section which extends from the ground to the top of the atmosphere. The phrases "total ozone" and "ozone amount" will be used synonymously throughout this report.

1967). Other measurements showed an unquestionable dependence of total ozone content on the position of the subtropical jet stream relative to the location of the ozone observations (Paetzold, 1953 and Sticksel, 1966). Measurements by Godson (1960) revealed correlations on a finer scale. He compared the 10-day running mean of 100 mb temperature with the total ozone for data taken over a nine month period at Edmonton, Canada. His results showed that the average daily temperature variation was almost exactly correlated with the average daily variation in ozone amount.

As measurements of the vertical distribution of ozone accumulated and the photochemical theory was developed, important discrepancies were noticed between the distributions observed and the profiles predicted based on photochemistry. These discrepancies gave the first indication of the significant inter-relationship between ozone content and atmospheric motions. Wulf (1945) was apparently the first to propose a general circulation model which explained the ozone spring polar maximum. After his work, other papers were published concerning the relation between ozone and atmospheric motions and the role of ozone in this regard became widely accepted (see for example Normand, 1951; Kellogg and Schilling, 1951; Bekoryukov, 1965; and Lindzen and Goody, 1965.)

The complex interplay between ozone and other atmospheric properties, especially atmospheric motions, caused widespread interest in global measurements of both total ozone and the vertical ozone distribution. In 1965, the National Academy of Sciences published a report outlining goals for an international observation program. The

report cited several areas of research which would be advanced by global ozone measurements. These areas include the study of atmospheric dynamics in the region of the upper troposphere and lower stratosphere, the analysis and study of the circulation patterns of the Northern and Southern hemispheres and the exchange processes that take place between them, the study of the mechanics of the tropospheric-stratospheric exchange process, the study of stratospheric photochemistry, and the study of atmospheric phenomena such as the "explosive warming" of the winter-spring stratosphere and the 26-month oscillation in the stratospheric wind and temperature.

The general interest in global scale measurements of atmospheric ozone resulted in the conception of a number of satellite measurement techniques. These methods include the measurement of backscattered solar uv light (Singer and Wentworth, 1957; Sekera and Dave, 1961; Twomey, 1961; Dave and Mateer, 1967; Herman and Yarger, 1969; and Anderson et al, 1969), the measurement of visible and near uv solar radiation passing tangentially through the atmosphere (Frith, 1961; Rawcliffe, 1963; and Miller, 1969), the measurement of the uv spectrum of a star during occultation from a satellite (Hays and Roble, 1967), and the use of laser transmission from the ground to a satellite or vice-versa (Duardo, 1967). The use of atmospheric emission measurements in an infrared band (9.6μm) of ozone has also been suggested (see for example Conrath, 1967). This method is attractive since it does not contain many of the problems of the other schemes. In the infrared technique, the measurements are not restricted to specific geographic areas and the method is applicable on both the day and night side of the planet. Also,

since scattering is unimportant in the infrared spectral region, the analysis is comparatively simple and the multiple scattering problem of the uv backscatter method does not exist.

Studies dealing with the determination of atmospheric ozone amounts from satellite measurements in the infrared have been reported by Sekihara and Walshaw(1969), and Prabhakara (1969a). A more recent paper by Prabhakara (1969b) discusses inversion results for radiance measurements taken from the Nimbus III satellite. These papers deal with the problem of inversion of vertically measured radiances. In the latter report, the atmospheric transmission due to ozone is computed using a statistical band model. The ozone absorption line parameters used in the computations are empirically determined with the help of an ozone sounding and Nimbus III radiance measurements. The water vapor continuum is considered but absorption by water vapor line centers is not. Although the results are useful, it would be of interest to perform a study using absorption line parameters based only on physics and using atmospheric transmission values computed by the line-by-line method. In treating water vapor absorption it would be informative to consider the line absorption which is superimposed on the continuum. A comprehensive error analysis would also be useful as a guide for future research. After studying the inversion of vertically measured radiances it would be especially interesting to consider the inversion of measurements of the 9.6μm band emission coming from the horizon.

This paper will present the results of a detailed study of the general infrared technique for measuring atmospheric ozone from a satellite. Chapter 2 contains a brief review of general features of the atmospheric

ozone profile and a summary of some properties of the ozone molecule. Next, two different methods of applying the infrared technique are presented. Chapter 3 is a study of the inversion of vertically measured radiances. It includes an extensive parametric error analysis and inversion results for radiance measurements taken from a high altitude balloon and from the Nimbus III satellite. The work is concluded in Chapter 4 with a feasibility study to determine how much ozone information can be deduced from horizon radiance measurements.

CHAPTER 2

OZONE

2.1 ATMOSPHERIC PROPERTIES[1]

2.1.1 Introduction

Atmospheric ozone is usually described by the vertical distribution or by the total ozone. Extensive measurements of the vertical distribution have been made both from the ground by the Umkehr method and in-situ using balloons and rockets. Also, total ozone has been regularly measured with the Dobson instrument since 1930. But, there are only a few stations that routinely make these observations and no measurements have been made over vast ocean areas and over most of the Southern Hemisphere. Furthermore, much of the existing data are inaccurate because of measurement difficulties related to calibration. Consequently, there is not an abundance of data available concerning the climatology of ozone and the information which does exist is mostly qualitative. A summary of this information is included in sub-section 2.1.3. The topics which are covered include latitudinal, longitudinal, daily, and seasonal effects as well as inter-hemispherical differences in these effects and in the ozone concentrations. The ozone altitude profile and the mechanisms leading to its formation are described in subsection 2.1.2.

2.1.2 The Vertical Ozone Distribution and the Related Photochemistry.

The ozone partial pressure is usually small and constant in the troposphere at any given time and location. But in the stratosphere it

[1] In addition to those specifically cited, references for this section are Craig (1965), Vassy (1965), Griggs (1966), and Duardo(1967).

varies with altitude in a manner similar to a gaussian function. The curve starts to increase near the tropopause and it continues to rise until it reaches a maximum value in the middle or lower stratosphere. In the upper stratosphere, the function has a negative slope and in the region 40-50 km it follows, very closely, a curve of constant ozone mixing ratio. Most of the time, there is only one peak observed during the daylight hours, but occasionally a second maximum is observed which is almost always smaller in magnitude than the primary maximum and which always occurs at a lower altitude. This second peak was first suggested by Gotz, et al (1934) and later confirmed by Ramanthan (1949). The most probable explanation of the phenomenon is downward transport of ozone from above by vertical winds (Normand, 1951). During the night, a third maximum is expected at around 70 km according to photochemical theory but apparently only one observation has been reported (Reed and Scolnick, 1964). The data showed the peak to be smaller and to occur at a lower altitude (63 km) than predicted. Fine structure, consisting of a number of very small peaks, is also observed in addition to the dominant features. This structure is most pronounced in the part of the profile which extends from the ground to the altitude of the primary maximum. The main peak of the ozone profile, can be explained by considering the mechanisms responsible for the creation and destruction of ozone in the atmosphere.

Ozone is formed photochemically in the upper stratosphere. When Chapman (1930) first explained the photochemistry, he used only reactions involving the oxygen allotropes. However, recent laboratory measurements of important rate coefficients (Benson and Axworthy, 1965) have

cast doubt on the completeness of the original explanation. It now appears that additional reactions are needed to reconcile the quantitative differences between theory and observations. Roney (1965) and Hunt (1966a, 1966b) have included in their calculations, equations involving H_2O, HO_2 and OH. They show reasonably good results but their results are not conclusive and the matter remains unsettled, principally because of uncertainties in the values of the rate coefficients. These constants are difficult to measure in the laboratory, particularly under conditions directly applicable to the atmosphere. Even with the new rate coefficients the calculations of Hunt (1966b) differ with observations by almost 100% in part of the range 30 to 50 km.

Although other reactions may be important in quantitative calculations of the vertical ozone distribution, the oxygen reactions alone are sufficient to explain the general shape of the profile. The important photochemical reactions in the stratosphere are,

$$O_2 + h\nu\ (\lambda \leq 2423A) \longrightarrow O + O \qquad (2.1.1)$$

$$O_2 + O + M \longrightarrow O_3 + M \qquad (2.1.2)$$

$$O_3 + h\nu\ (\lambda \leq 11,000A) \longrightarrow O + O_2 \qquad (2.1.3)$$

$$O_3 + O \longrightarrow 2O_2 \qquad (2.1.4)$$

$$O + O + M \longrightarrow O_2 + M \qquad (2.1.5)$$

where $h\nu$ is the dissociation energy, h is Planck's constant, ν is the frequency of the dissociating radiation, λ is wavelength, and M is any third body, presumably N_2 in most cases. Craig (1965) has used this set of reactions to obtain an expression for the photochemical equilibrium number density of ozone. His result shows that

$$nO_{3e} \propto n_2 n_m \frac{\bar{q}_2}{\bar{q}_2 + \bar{q}_3} \tag{2.1.6}$$

where nO_{3e} is the equilibrium number density of ozone, n_2 is the number density of oxygen, n_m is the number density of the third body, and $\bar{q}_2$ and $\bar{q}_3$ are the number of dissociating photons absorbed per unit volume per unit time by oxygen and ozone respectively. These latter quantities are defined by the equations,

$$\bar{q}_2 = n_2 \int_0^\infty \sigma_{\nu 2} F_{\nu \infty} \tau_\nu \, d\nu \tag{2.1.7}$$

$$\bar{q}_3 = n_3 \int_0^\infty \sigma_{\nu 3} F_{\nu \infty} \tau_\nu \, d\nu \tag{2.1.8}$$

where σ_{ν_3} is the absorption cross section per ozone molecule, n_3 is the number density of ozone, F_{ν_∞} is the solar flux entering the atmosphere at the top, and τ_ν is the transmittance of the atmosphere from the volume in question outward in a direction toward the sun. Similar quantities apply for q_2. The integration is over a frequency range which results in dissociation. According to (2.1.6), the equilibrium ozone profile results from two opposing factors. The factor $n_2 n_m$ is acutely dependent on air density. Therefore, it tends to cause the ozone density to continually increase with decreasing altitude. The quantity q_2, however, has the opposite effect since it is constantly decreasing with decreasing altitude. These processes acting simultaneously cause the ozone profile to peak at a point in the atmosphere where the two effects are in balance.

Ozone is in photochemical equilibrium at altitudes of about 35 km and higher in the stratosphere. But in the lower stratosphere, photochemic

balance does not exist. Craig (1950), among others, has computed the time required for the ozone concentration to be photochemically restored to its equilibrium value after being perturbed. The half-restoration time varies from about an hour at 50 km, to a month at 30 km, to a year or more below the primary maximum in the ozone profile. So ozone is neither produced nor destroyed in the lower stratosphere and troposphere. It is generally believed that ozone in this lower region originates in the upper stratosphere and is transported downward by air motions. However, the exact transport mechanisms are not well understood at the present time. Once in the lower stratosphere, ozone is a conservative property of the air and its concentration becomes critically dependent on atmospheric dynamics.

2.1.3 The Variability of Atmospheric Ozone

Most changes in the ozone profile occur at altitudes below 30 km. Bojkov (1968) concludes that ozone variations in the upper stratosphere, where photochemical equilibrium prevails, are only about one-third to one-fifth as large as variations that occur in lower regions. Thus it appears that the variability in the ozone profile and also in the total ozone is caused mainly by dynamical effects. A brief summary of abailable information concerning these variations follows.

The vertical ozone distribution exhibits marked latitudinal variations. In the tropics, the value of the maximum ozone partial pressure is low, the profile is narrow, and it peaks at a high altitude (about 26 km at the equator). As the geographic location changes toward high latitudes

the value of the maximum partial pressure increases, the profile broadens and the altitude of the peak shifts downward (to about 19 km in polar regions). In equatorial zones, the ozone partial pressure starts to slowly increase just above the tropopause but at high latitudes the increase is more rapid and it occurs at or sometimes below the tropopause. The low altitude secondary peak is only observed at middle and high latitudes and the high latitude profiles are generally more irregular than the comparatively smooth curves of the tropics.

Extended measurements at a given latitude reveal the seasonal variations in the profile. The measurements show that during the winter-spring months the maximum ozone partial pressure is higher, the peak in the profile occurs at a lower altitude, and the low altitude secondary maximum is observed more frequently. Particularly interesting variations occur during these months at the times of sudden stratospheric warming events. During the major stratospheric warming of 1958 which originated over western Europe, the ozone partial pressure at Arosa, Switzerland increased at all levels up to about 40 km (Dütsch, 1962). The increase varied from almost 50% in part of the upper stratosphere to more than 200% at some levels in the lower region.

Total ozone varies in accordance with changes in the vertical ozone distribution. Ozone amounts are smallest at low latitudes and they increase poleward. The seasonal variation at a given location is approximately sinusoidal with a maximum in spring and a minimum in autumn. The amplitude of the variation depends upon latitude with the greatest amplitude occurring at high latitudes. Perl and Dütsch (1959) have published a curve showing the annual variation. They computed long term

average values of ozone amount for each month using data taken at Arosa, Switzerland during the period 1926-1958. They also calculated the root-mean-square (RMS) deviations of individual monthly means from the long-term mean for each month. The maximum deviation occurred in February and was about seven percent. Besides the monthly and seasonal changes, the Arosa observations show pronounced daily variations. Craig (1965) used data taken during the period 1949 to 1958 to compute these daily changes and he found a maximum RMS deviation of about nine percent. While these variations do not seem to be very large, it should be noted that they are RMS deviations and that the peak deviations will be greater. These effects are even larger at latitudes higher than at Arosa (47^{o}N). Total ozone also changes significantly during a sudden stratospheric warming. During the 1958 event the ozone amount increased almost 200% (Dütsch, 1962). In addition, it appears that the long term variation in ozone amount in the equatorial zone follows a 26-month cycle which is strongly correlated with the 26-month oscillation in equatorial stratospheric temperature (Reed, 1965). The variation is roughly sinusoidal with an amplitude of about 10%.

Measurements distributed in longitude over the Northern Hemisphere show that ozone amounts are largest at all seasons over eastern North America, eastern Asia, and central Europe. The observations show also that the total ozone longitudinal gradient is greatest in the spring (London, 1962).

There are also inter-hemispherical differences in both the ozone amount and its variation. It appears that the seasonal and latitudinal variations are similar in the two hemispheres. But daily changes seem

to be smaller in the Southern Hemisphere and there is more total ozone in the middle latitudes below the equator. Regarding the polar regions, Bojkov (1968) concludes that there is less ozone above the Antarctic and that the spring maximum in total ozone occurs later than in the Arctic. He also concludes that the variability of ozone over the Antartic is only about one-third to one-fifth that of ozone over the Northern polar region.

2.2 MOLECULAR PROPERTIES

Herzberg (1945) and Trambarulo, et al (1953), among others, have discussed the chemical structure of the ozone molecule. The best available data indicates that the three oxygen atoms form an isosceles triangle with an apex angle of $116^{\circ}\ 49' \pm 30'$. The two end oxygen atoms are joined to the central atom by chemical bonds of length 1.278 ± 0.003A. This distance is intermediate between the characteristic lengths of single and double oxygen-oxygen bonds.

Ozone has absorption bands in the ultraviolet, visible, and infrared regions of the spectrum. The primary absorption in the ultraviolet spectrum is in the Hartley bands extending from 2000 to 3200A. On the long wavelength side of these bands are the Huggins bands between 3200 and 3600 A. Absorption in the visible spectrum is by the weaker Chappius bands extending from 4400 to 7400 A. There are several vibration-rotation bands in the infrared spectrum. The strongest of these is the $\bar{\nu}_3$ band centered at 9.6μm with a companion $\bar{\nu}_1$ band located at 8.8μm and a weaker $\bar{\nu}_2$ band at 14.3μm. These bands result from quantum transitions between energy levels corresponding to the three fundamental vibration wavelengths of the ozone molecule. There are also other bands, which are weaker, located at 3.3μm, 3.6μm,

4.8μm, and 5.7μm(Griggs, 1966).[1]

The success of any infrared technique for determining ozone amounts from remote measurements will depend upon the accuracy of the method used to determine the ozone absorption as a function of altitude. This can be accomplished either analytically or by using experimental data techniques. The former approach is preferred in this report. A two-step process is required in computing the absorption. First, the positions, intensities, and half-widths of absorption lines in the band must be determined and after this, a method must be developed to compute the integrated effect of these lines on the absorption at any given wave number. A discussion of this latter problem is deferred until Chapter 3. The absorption line parameters are determined by combining experimental measurements with an analysis based on the physics of the ozone molecule. Ozone is a planar, slightly asymmetric rotor of C_{2v} symmetry and such configurations are difficult to analyze. Consequently, past theoretical studies of the ozone molecule have been limited. The best analysis to date was by Clough and Kneizys (1966). These authors found it necessary to include vibration-rotation coupling between the $\bar{\nu}_1$ (1103 cm^{-1}) and $\bar{\nu}_3$ (1042 cm^{-1}) bands in order to explain an intensity anomaly in the $\bar{\nu}_1$ band. This coupling was in the form of a strong Coriolis interaction and a weaker distortion interaction. The band parameters from their analysis (Clough and Kneizys, 1965) are used throughout this report.

A good indication of errors that may exist in the absorption line parameters can be obtained by comparing theoretical and experimental

[1] Hereafter the absorption band centers will be discussed in terms of wave numbers, $\bar{\nu}$, where $\bar{\nu} = 1/\lambda$. Thus the fundamental bands would appear at 1042 cm^{-1}, 1103 cm^{-1}, and 701 cm^{-1}.

absorption spectra for a homogeneous path. The most accurate method, numerically, for computing the absorption is the direct integration technique.[1] Drayson and Young (1967) have used this method and the line parameters of Clough and Kneizys (1965) and they have compared their calculations with experimental measurements made by McCaa and Shaw (1967). The experimental values are believed to be accurate to within ten percent or less. The comparisons were made for a variety of conditions of pressure, temperature and absorber concentration. A comparison of the computed and experimental spectra for a set of conditions similar to those encountered in the atmosphere is shown in Figure 1. The theory predicts too little absorption on the low wave number side of the band-center and too much absorption on the high wave number side. Also, the discrepancies are much greater than the experimental inaccuracies. It appears, therefore, that there are large errors in the absorption line parameters. This problem is very critical, as will be seen in Chapter 3, and further work is necessary to advance our understanding of the physics of the ozone molecule.

[1] This method will be described in Chapter 3. Let it suffice here to say that if the absorption line parameters are known precisely, this technique will predict the absorption almost exactly.

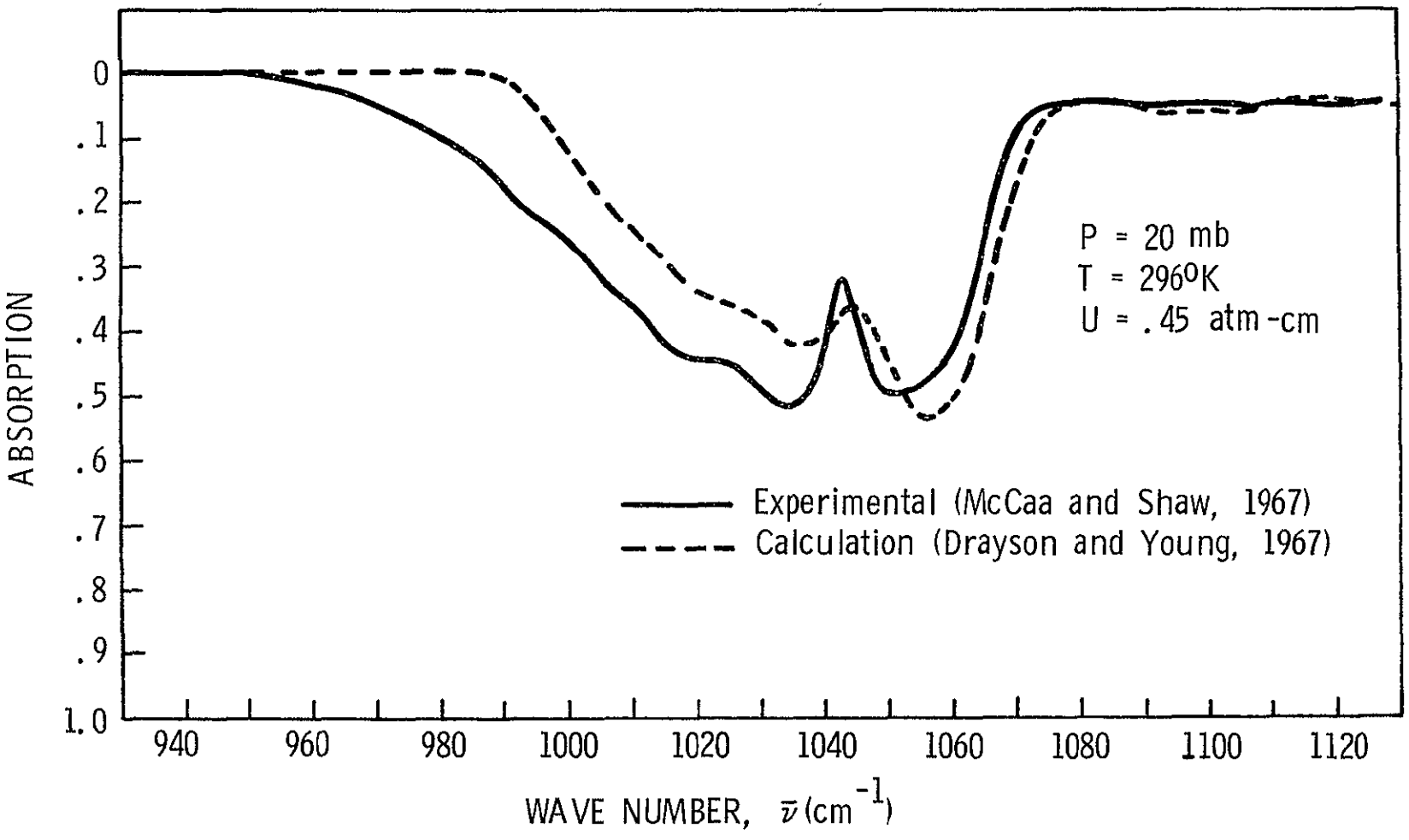

Fig. 1. A Comparison of experimental and calculated absorption in the 1042 cm^{-1} ozone band.

CHAPTER 3

THE NADIR EXPERIMENT

3.1 INTRODUCTION

The thermal energy measured by a satellite instrument pointed vertically toward the earth is a function of several variables. It depends on the temperature of the lower boundary (if the atmosphere is not opaque in the wave number region of interest), on the temperature profile in the atmosphere, and on the amount and vertical distribution of of gases that emit energy in the spectral pass-band of the instrument. It should be possible, because of this dependence, to infer the values of these parameters from the measured energy. The prospect of remotely measuring such quantities from a satellite was originally discussed by King (1956). After the first artifical earth satellite was launched, widespread interest developed in the technique and today, a copious list of references exists on the subject of remote sensing from a satellite.[1] The main reason for the extensive attention given to the method is the satellite's ability to cover vast areas of the globe daily and to obtain information over the oceans and other isolated regions where ground based measurements are seldom made.

To determine the temperature profile from a satellite, the instrument must measure energy in the absorption band of a gas whose mixing ratio is known. Two gases in the atmosphere, CO_2 and O_2, meet this requirement since their mixing ratio is constant at least up to 50 or 60 km. Kaplan (1959) proposed using the 667 cm^{-1} infrared band of carbon dioxide for this application and his suggestion has been generally followed. Once the temperature structure is known, the

[1] See Wark and Fleming (1966) and references therein for a historical review. See Conrath (1968) and Gille (1968a) for a review of various approaches to the problem.

distributions and amounts of the variable gases can, in principle, be determined by combining the temperature data with other measurements. For example, Conrath, (1966 and 1969) has used the 1587 cm^{-1} water vapor band to determine the distribution of water vapor and suggestions regarding ozone have already been referenced in Chapter 1.

Two types of satellite instruments have been developed to vertically sound the atmosphere using the infrared spectral region. These are the Satellite Infrared Spectrometer (SIRS) and the Infrared Interferometer Spectrometer (IRIS). Both devices are currently in orbit onboard the Nimbus III and Nimbus IV satellites launched in April, 1969 and April, 1970 respectively. These instruments were discussed in a recent report by Bandeen (1968). The SIRS is a Fastie-Ebert grating spectrometer which has a series of fixed channels distributed throughout the 667 cm^{-1} carbon dioxide band and the rotation band of water vapor. The IRIS is a scanning Michelson-type interferometer spectrometer which provides a continuous spectrum over the range 500 cm^{-1} to 2000 cm^{-1}. Each instrument has a resolution of 5 cm^{-1}. A breadboard version of the IRIS was flown on a high altitude balloon from Palestine, Texas, on May 8, 1966. The experiment was conducted by the High Altitude Engineering Laboratory of the University of Michigan for the NASA, Goddard Space Flight Center. A spectrum obtained from that flight is shown in Figure 2. (Chaney, et al, 1967; Conrath, 1967). This spectrum shows, in addition to the carbon dioxide and water vapor bands, marked structure in the 1042 cm^{-1} band of ozone. The remainder of this chapter is devoted to the problem of assessing how much and what kind of ozone information can be obtained from such a spectrum.

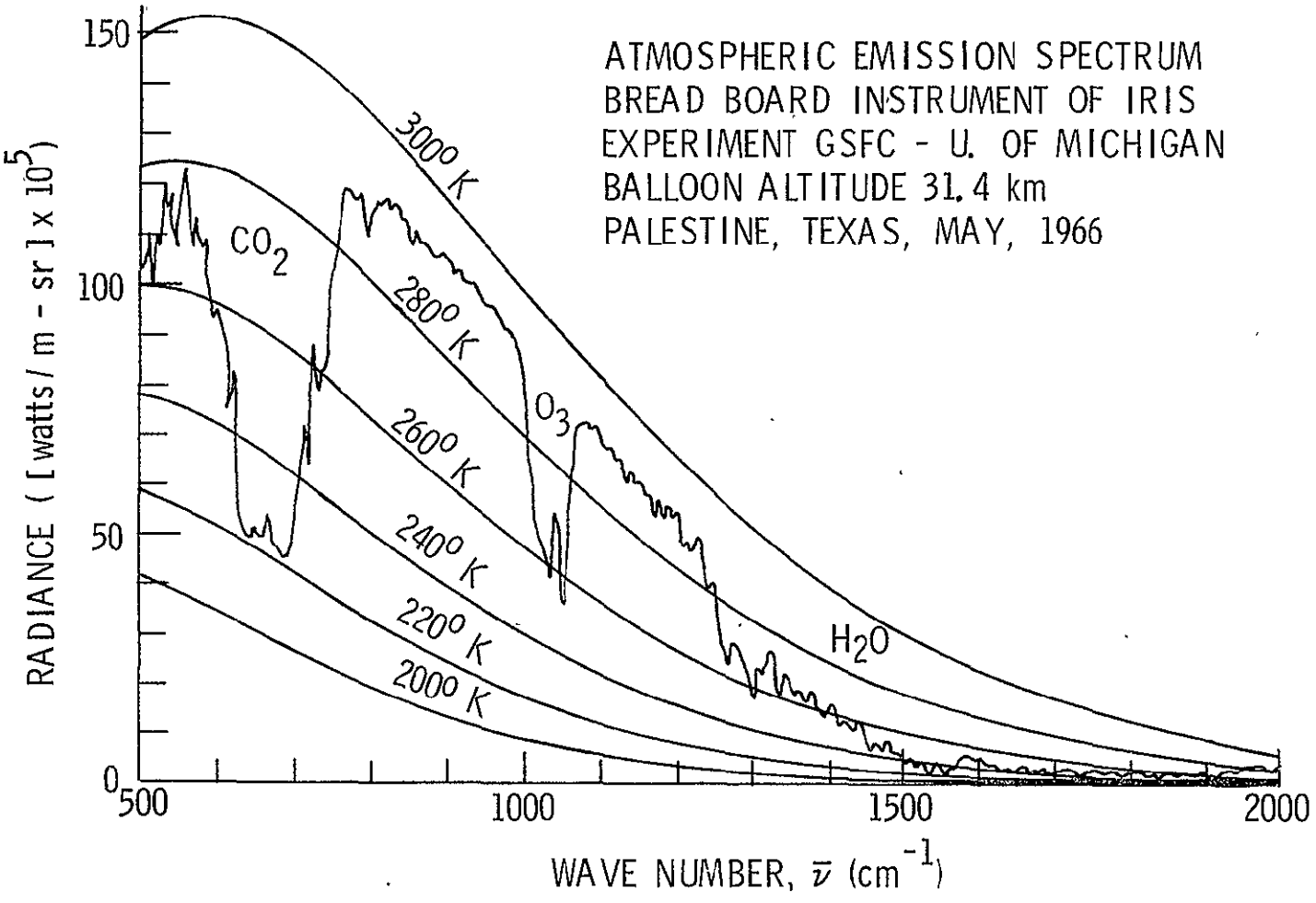

Fig. 2. Atmospheric spectrum acquired with a breadboard version of an IRIS instrument in a balloon flight, 8 May 1966, from Palestine, Texas (After Conrath, 1967).

3.2 ANALYSIS

3.2.1 Basic Relations

The fundamental relationship between the energy measured by a satellite instrument, the temperature profile, and the optical properties of the atmosphere is the equation of radiative transfer. The form of the equation used in this chapter is based on the following assumptions:

a) The atmosphere is plane-parallel

b) Scattering at the wavelengths under consideration can be neglected

c) Atmospheric refraction can be neglected

d) The absorbing gases are in local thermodynamic equilibrium up to an altitude of 60 or 70 km (Kuhn and London, 1969).

Under these conditions, the radiative transfer equation at a single wave number $\bar{\nu}$, as stated in Chandrasekhar (1960), is

$$dL(\bar{\nu}, \theta) = \left\{-L(\bar{\nu}, \theta)+B[\bar{\nu}, T(Z)]\right\} \kappa(\bar{\nu}, Z)\rho(Z)SEC(\theta)dZ \qquad (3.2.1)$$

where $L(\bar{\nu}, \theta)$ is the spectral radiance at a wave number $\bar{\nu}$, $\kappa(\bar{\nu}, Z)$ is the absorption coefficient of the absorbing gas, $\rho(Z)$ is the density of that gas, θ is the zenith angle relative to the local vertical, Z is the height in the local vertical, $T(Z)$ is the atmospheric temperature, and $B[\bar{\nu}, T(Z)]$ is the Planck radiance. This last quantity can be expressed by

$$B[\bar{\nu}, T(Z)] = 2hc^2 \bar{\nu}^3 \cdot \left\{ \exp[hc\bar{\nu}/kT(Z)]-1 \right\}^{-1} \qquad (3.2.2)$$

where h is Planck's constant, c is the velocity of light in a vacuum, and k is Boltzmann's constant.

If we transform the variable from Z to pressure and we assume that the instrument views in a narrow cone in the vertical so that everywhere in the cone $SEC\theta \approx 1$, equation (3.2.1) can be written in integral form as follows,

$$L(\bar{\nu}, 0) = \epsilon_g(\bar{\nu}) B[\bar{\nu}, T(P_g)] \tau(\bar{\nu}, P_g) - \int_0^{P_g} B[\bar{\nu}, T(P)] \frac{d\tau(\nu, P)}{d(\log P)} d(\log P) \quad (3.2.3)$$

where $L(\bar{\nu}, 0)$ is the radiance at the top of the atmosphere, $\epsilon_g(\bar{\nu})$ and P_g are the emissivity and pressure respectively at the lower boundary, and $\tau(\nu,P)$ is the transmittance of the atmosphere from the satellite down to an arbitrary height where the atmospheric pressure is P. The descending energy which is reflected at the lower boundary has been neglected in (3.2.3). The first term on the right in (3.2.3) represents the contribution to the radiance at the top of the atmosphere due to emission by the lower boundary. The second term accounts for the contribution made by atmospheric emissions.

The transmissivity depends upon wave number and pressure according to the relation

$$\tau(\bar{\nu}, P) = \exp - \left[\int_0^P \kappa(\bar{\nu}, P) \frac{q(P)}{g(P)} \, dP \right] \quad (3.2.4)$$

where q(P) is the mass mixing ratio of the absorbing gas and g(P) is the acceleration of gravity. The transmittance is also weakly dependent upon temperature through the absorption coefficient $\kappa(\bar{\nu}, P)$, but the introduction of this relationship is deferred until sub-section 3.2.2. If there is more than one gas absorbing at the wave number $\bar{\nu}$ then the transmittance is (Goody, 1964a, p. 123)

$$\tau(\bar{\nu}, P) = \pi_i \tau_i(\bar{\nu}, P) \qquad (3.2.5)$$

where the subscript i denotes the ith gas and symbol π denotes multiplication.

Equation (3.2.3) is written for the case of monochromatic radiation. However, in practice an instrument can only measure radiation over a finite bandwidth. So the computed radiance must be weighted and normalized according to some function $\phi(\bar{\nu})$ which adequately represents the frequency response of the instrument. The IRIS instrument function covers only a narrow spectral interval (5 cm^{-1}) and it is virtually symmetric and approximately triangular (Hanel and Chaney, 1966). When this function is used, the average Planck function for the interval can be equated with negligible error to the value at the center of the interval. This is possible because of the symmetry of $\phi(\bar{\nu})$ and because of the fact that the Planck function is slowly varying and approximately linear in the middle infrared. A similar argument can be advanced for the emissivity $\epsilon_g(\bar{\nu})$ of the lower boundary. With these approximations, the averaged form of (3.2.3) becomes,

$$\overline{L(\bar{\nu}_o, 0)} = \epsilon_g(\bar{\nu}_o)\, B\left[\bar{\nu}_o, T(P_g)\right] \overline{\tau(\bar{\nu}_o, P_g)} - \int_o^{P_g} B\left[\bar{\nu}_o, T(p)\right] \frac{d\overline{\tau(\bar{\nu}_o, P)}}{d(\log P)}\, d(\log P) \qquad (3.2.6)$$

where the o subscript denotes the wave number at the center of the interval spanned by $\phi(\bar{\nu})$ and the bars above the symbols denote that these quantities are average values. The average transmittance is computed in the following way,

$$\overline{\tau(\bar{\nu}_o, P)} = \frac{\int_{\bar{\nu}_1}^{\bar{\nu}_2} \tau(\bar{\nu}, P)\phi(\bar{\nu})d\bar{\nu}}{\int_{\bar{\nu}_1}^{\bar{\nu}_2} \phi(\bar{\nu})d\,\bar{\nu}} \qquad (3.2.7)$$

where $\bar{\nu}_1$, and $\bar{\nu}_2$ are the bounds of the interval covered by the instrument function.

Equation (3.2.6) is the basis for all remaining calculations in this chapter. The radiances computed with that equation can be directly compared to measured quantities. Before we consider the problem of inverting (3.2.6) to obtain ozone information, there are two important points which must be discussed; 1) The method for computing the atmospheric transmittance and 2) The method for computing the lower boundary emission. These topics are treated in the next two sub-sections.

3.2.2 Atmospheric Transmittances

The transmission of the atmosphere in the vicinity of 1042 cm^{-1} is influenced by water vapor and carbon dioxide as well as ozone. The water vapor continuum absorption must be considered as well as absorption by water vapor lines superimposed on the continuum. However, carbon dioxide absorption is weak and it will be neglected in the current calculations. The estimated upper limit to the transmittance error caused by this assumption is about 5% based on calculations using the weak line approximation. The actual error is probably only about 2-3% Carbon dioxide effects should not be neglected in future computations once the accuracies of the ozone transmittances are improved.

Water vapor line absorption can be accurately computed if the vertical water vapor distribution is known and even if the vertical profile

is not known, an adequate treatment is possible. But the water vapor continuum spectrum is difficult to model analytically since it arises from absorption in the wings of many lines located in distant rotation and vibration-rotation bands. There are presently no totally acceptable theories available concerning this problem. Consequently, the influence of water vapor on the atmospheric transmittance in the ozone band will not be computed directly in this study. Instead, the effect will be treated as part of the problem of determining the lower boundary emission. The way this is done is discussed in sub-section 3.2.3. Thus, the problem of computing the transmittance of the atmosphere is, in a sense, reduced to one of computing the transmittance due to ozone alone. Two methods of accomplishing this are described in the following paragraphs.

An expression for the atmospheric transmittance at a wave number $\bar{\nu}$ at a height where the pressure is P was given in (3.2.4). Assume now that the atmosphere is divided into small incremental slabs in the vertical and consider the transmission through only one of these layers. If each layer is considered to be homogeneous, the transmittance for the jth layer is,

$$\tau_j(\bar{\nu}, P_j) \approx \exp\left[-\kappa(\bar{\nu}, P_j)\, u_j\right]. \qquad (3.2.8)$$

where P_j is the mean pressure for the layer and u_j is the integrated mass across the layer given by

$$u_j = \int_{P_1}^{P_2} \frac{q(P)}{g(P)}\, dP \qquad (3.2.9)$$

P_1 and P_2 are the pressures at the boundaries of the layer. Equation (3.2.8) is not an exact expression since in reality, an atmospheric slab is inhomogeneous and the absorption coefficient varies with pressure across the layer. But errors which arise in using (3.2.8) can be made as small as desired by using very thin slabs. Fundamentally, the problem of computing the transmittance of the atmosphere is one of calculating the absorption coefficient for each of the j layers in the atmosphere. This is not a simple problem since the absorption coefficient at any given wave number $\bar{\nu}$ is the sum of the coefficients at $\bar{\nu}$ due to each of a large number of absorption lines in a band and each of these lines varies with pressure and temperature.

Consider first the absorption coefficient at $\bar{\nu}$ due to a single line centered at a wave number $\bar{\nu}_i$ in the band. For this ith line and the jth atmospheric layer,

$$\kappa_i(\bar{\nu}, P_j) = S_i \cdot f(\bar{\nu}, \bar{\nu}_i) \tag{3.2.10}$$

where S_i is the line intensity or strength and $f(\bar{\nu}, \bar{\nu}_i)$ is the profile function which describes the line shape. The profile function is normalized so that

$$\int_0^\infty f(\bar{\nu}, \bar{\nu}_i)d\bar{\nu} = 1 \tag{3.2.11}$$

and

$$S_i = \int_0^\infty \kappa_i(\bar{\nu}, P_j)\, d\bar{\nu} \tag{3.2.12}$$

The absorption coefficient varies with altitude because of changes in both the line strength and the profile function. The line strength

contributes to the variation through a temperature dependence. The relationship used by Clough and Kneizys (1965) for ozone is given by

$$S_i(T_j) = K\gamma_i F_i \left(\frac{273}{T_j}\right)^{5/2} \exp\left[-E_o/\mathcal{R}T_j\right] \qquad (3.2.13)$$

where K is a constant, γ_i is the unperturbed line strength in the ground state representation, F_i is the ratio of perturbed to unperturbed line strength, and E_o is the ground state energy. The profile function varies with altitude because of both a temperature and a pressure dependence. The variation in the profile function for the range of physical conditions considered here, can be described by two limiting cases; the Lorentz and Doppler line shapes. A third case, the natural line shape, can be neglected since the width of the natural broadened line is much smaller than the width for either of the other two cases.

The Lorentz line shape is caused by molecular collisions and is described by the function

$$f_L(\bar{\nu}, \bar{\nu}_i) = \frac{1}{\pi} \frac{\alpha_{Li}}{(\bar{\nu}-\bar{\nu}_i)^2+\alpha_{Li}^2} \qquad (3.2.14)$$

where α_{Li} is the Lorentz half-width at half maximum. The half-width depends on pressure and temperature according to

$$\alpha_{Li}(T_j,P_j) = \alpha_{oi} \frac{P_j}{P_o} \sqrt{\frac{T_o}{T_j}} \qquad (3.2.15)$$

where α_{oi} is the half-width at temperature T_o and pressure P_o.

The Doppler line shape arises because of thermal motions of the molecules. In this case

$$f_D(\bar{\nu}, \bar{\nu}_i) = \left(\frac{\ell n 2}{\pi \cdot \alpha_{Di}^2}\right)^{1/2} \exp(-x^2) \qquad (3.2.16)$$

where

$$x = \left(\frac{\ell n 2}{\alpha_{Di}^2}\right)^{1/2} \cdot (\bar{\nu} - \bar{\nu}_i)$$

and where α_{Di} is the Doppler half-width at half maximum which is expressed by

$$\alpha_{Di} = \frac{\bar{\nu}_i}{c} (\ell n 2 \cdot \frac{2kT_i}{m})^{1/2} \qquad (3.2.17)$$

The quantity m is the mass per molecule in grams.

The transition from the region of the atmosphere where one limiting shape is important to the region where the other dominates is not abrupt. Therefore, a range of pressures is encountered where both thermal and collisional effects are important in determining the absorption line profile. Under these conditions, the correct line shape is given by a convolution of the Doppler and Lorentz shapes. This shape, called the Voigt function, is represented by

$$f_v(\bar{\nu}, \bar{\nu}_i) = \left[\frac{\ell n 2}{\pi^3 \alpha_{Di}^2}\right]^{1/2} \cdot y \cdot \int_{-\infty}^{\infty} \frac{e^{-t^2}}{y^2 + (x - t^2)} \, dt \qquad (3.2.18)$$

where

$$y = \frac{\alpha_{Li}}{\alpha_{Di}} (\ell n 2)^{1/2}$$

So far we have been concerned with a single absorbing line and we have seen how the absorption coefficient for this line varies as a function

of the atmospheric parameters, pressure and temperature. To compute the integrated effect of all lines in a band on the absorption at a given wave number $\bar{\nu}$ we must sum the values of absorption coefficients at $\bar{\nu}$ due to each absorption line. Thus for N lines, the monochromatic absorption coefficient is, ,

$$\kappa(\bar{\nu}, P_j) = \sum_{i=1}^{N} \kappa_i(\bar{\nu}, P_j) \qquad (3.2.19)$$

The monochromatic transmittance is computed by inserting (3.2.19) into (3.2.8) and the average value is calculated as in (3.2.7). Equation (3.2.19) is a lengthy calculation because of the large number of lines normally found in an absorption band. The equation is also complicated because of the requirement that the computations be done for all j layers in the atmosphere, in which case the line strength and shape variability must be included. These difficulties prompted the development of the band model concept to compute the transmittances. In this approach, the actual distributions of absorption line positions and intensities are simulated and instead of computing (3.2.19) and the average transmittance from (3.2.7) directly, the calculations are approximated by an analytical integration using the assumed distributions of the line parameters. Even though band models are still frequently used today, it is now possible, because of the existence of high-speed computers, to perform the calculations directly by the direct integration (or line-by-line) method (Drayson, 1965; Drayson, 1966; Drayson and Young, 1966). The advantages and disadvantages of each of these approaches were discussed by Drayson (1967) and will not be repeated here. Both procedures were used in this present work and a brief description of each method follows.

The direct integration method is numerically the most accurate of the two techniques. The method will predict the absorption almost exactly if the absorption line parameters are known precisely. In the program developed by Drayson and Young (1966) the monochromatic transmittance is computed at various wave numbers in the absorption band. Since the values are computed monochromatically, the transmittance from the top of the atmosphere down to a height where the pressure is P can be computed by multiplying the transmittances for each of the K layers. Accordingly,

$$\tau(\bar{\nu}, P) = \prod_{j=1}^{K} \tau_j(\bar{\nu}, P_j) \qquad (3.2.20)$$

These monochromatic transmittances are then averaged over .1 cm^{-1} intervals at the bottom of each Kth layer. With this technique, the atmosphere can be divided up into a series of thin homogeneous layers each of which has values of pressure and temperature equal to the average values for the layer. Since each transmittance value is computed for a thin atmospheric layer, it is relatively easy to include in the calculations, the appropriate absorption line shape and intensity for that region of the atmosphere. The Drayson and Young (1966) program includes all three absorption line broadening regimes, it allows for the variation of line half-width with wave number, and it accounts for the variation of line intensity with temperature. The chief drawback to using the method is that it is very time consuming, even when modern, high-speed computers are used. Nevertheless, the versatility and exactness of the approach make it worthwhile to contend with this problem. One way of reducing the time required for a calculation is to use a library method; i. e.

compute the transmittance for a range of conditions, store the values, and interpolate for each calculation thereafter. This will be discussed in more detail in section 3.4. Professor Drayson kindly provided a duplicate deck of his program for use in this current work. However, because the calculations are so lengthy, the method was used only in a weighting function study, in calculating the effect of the line intensity temperature dependence, and in applying the inversion method developed in sub-section 3.2.4 to the Nimbus III and Palestine, Texas flight data. The error study transmittances were calculated using the Random-Exponential band model (Goody, 1952; Mayer, 1947). A description of this model follows.

The major gain in using the band model technique rather than the line-by-line method is a great reduction in the time required for a calculation. The line parameter distribution functions used with the most success in the ozone band are a random distribution of line positions and an exponential distribution of line intensities (see for example, Goldman and Kyle, 1968). The probability distribution function for the line positions is $P(\bar{\nu}) = \frac{1}{\Delta\bar{\nu}}$ where $\Delta\bar{\nu}$ is the width of the spectral interval, and the function for line intensities is,

$$P(S) \quad \frac{1}{\beta_{\bar{\nu}}} \exp\left(-S/\beta_{\bar{\nu}}\right) \qquad (3.2.21)$$

where $\beta_{\bar{\nu}}$ is a constant for the interval $\Delta\bar{\nu}$. With these distributions, the average transmittance at a wave number $\overline{\nu}$ through a single atmospheric layer is (Goody, 1964a, Chapter 4)

$$\overline{\tau\left(\bar{\nu}, P_j\right)} = \exp\left(-\omega\right) \qquad (3.2.22)$$

The argument of the exponential is computed as follows,

$$\omega = \frac{1}{\bar{d}} \int_{-\infty}^{\infty} \frac{\beta_{\bar{\nu}} f(\bar{\nu}, \bar{\nu}_i)\, u_j}{1+\beta_{\bar{\nu}} f(\bar{\nu}, \bar{\nu}_i) u_j} \, d\bar{\nu} \qquad (3.2.23)$$

where $\bar{d}=\Delta\bar{\nu}\ /N'$ is the mean line spacing and N' is the number of lines in the interval $\Delta\bar{\nu}$. Since the transmittance computed with the band model is an average value for the spectral interval, the transmittance through K layers cannot be computed simply by multiplying the values for each jth layer (Goody, 1964a, p. 123). Instead, the transmittance must be calculated for an equivalent homogeneous slab defined by the K layers. The reduction of an arbitrary path in the atmosphere to an equivalent homogeneous path is usually done by means of the Curtis-Godson approximation (e.g. Armstrong, 1968). This approximation is not very accurate for atmospheric ozone (e.g. Walshaw and Rodgers, 1963; Goody, 1964b) but the accuracy is good enough that the method can still be used in the error study calculations discussed later. There are two other approximations which will be used in the band model calculations. It will be assumed that purely collisional line broadening is valid throughout the range of altitudes considered and that the line intensities do not vary with temperature. The assumption of collisional broadening causes a small transmittance error above an altitude of $\approx$30km since in this region the Voigt profile function is important (Kuhn and London, 1969). However the estimated maximum error is only about 2% according to the correction table published by Gille and Ellingson (1968). The effect of neglecting the line intensity temperature dependence is discussed in section 3.3. These approximations cannot be used in precision calculations but they should have little effect upon

the error study results. Goody (1964a, Chapter 4) integrated (3.3.23) for a Lorentz profile function to give,

$$\overline{\tau(\bar{\nu}, P_k)} = \exp\left[-\frac{(\beta_{\bar{\nu}}/d)\,\bar{u}_k}{\left(1+2\left[\frac{\beta_{\bar{\nu}}}{2\pi\alpha_{L_o}(\bar{\nu})}\right]\bar{\ell}_k\right)^{1/2}}\right] \qquad (3.2.24)$$

where $\bar{\ell}_k$ and $\bar{u}_k$ are the effective length and absorber amount respectively of the homogeneous path and $\alpha_{L_o}(\bar{\nu})$ is the Lorentz half-width at the wave number $\bar{\nu}$ and at standard temperature and pressure. The subscript k refers to the effective value for a homogeneous slab defined by K layers. The methods for computing the various quantities in (3.2.24) are discussed in Appendix A. A spectral interval of 5 cm^{-1} was used in all calculations with (3.2.24) to simulate the resolution of an IRIS.

Figure 3 is a plot against wave number of the percent difference between the spectral radiance at the top of the atmosphere computed using (3.2.24) and that computed using the numerically exact direct integration method. The calculations were done using a mid-latitude ozone profile and a corresponding temperature profile published by Hering and Borden (1967). The maximum difference is 11.6% and the difference at the wave numbers of strongest and weakest absorption is negligible. So even though the band model approach is not as accurate as the direct integration technique, the errors are not so large that they prohibit use of the model in an error study. The quantitative results would not differ drastically from data determined by the direct integration method and the calculations would certainly be useful in identifying the most important error effects.

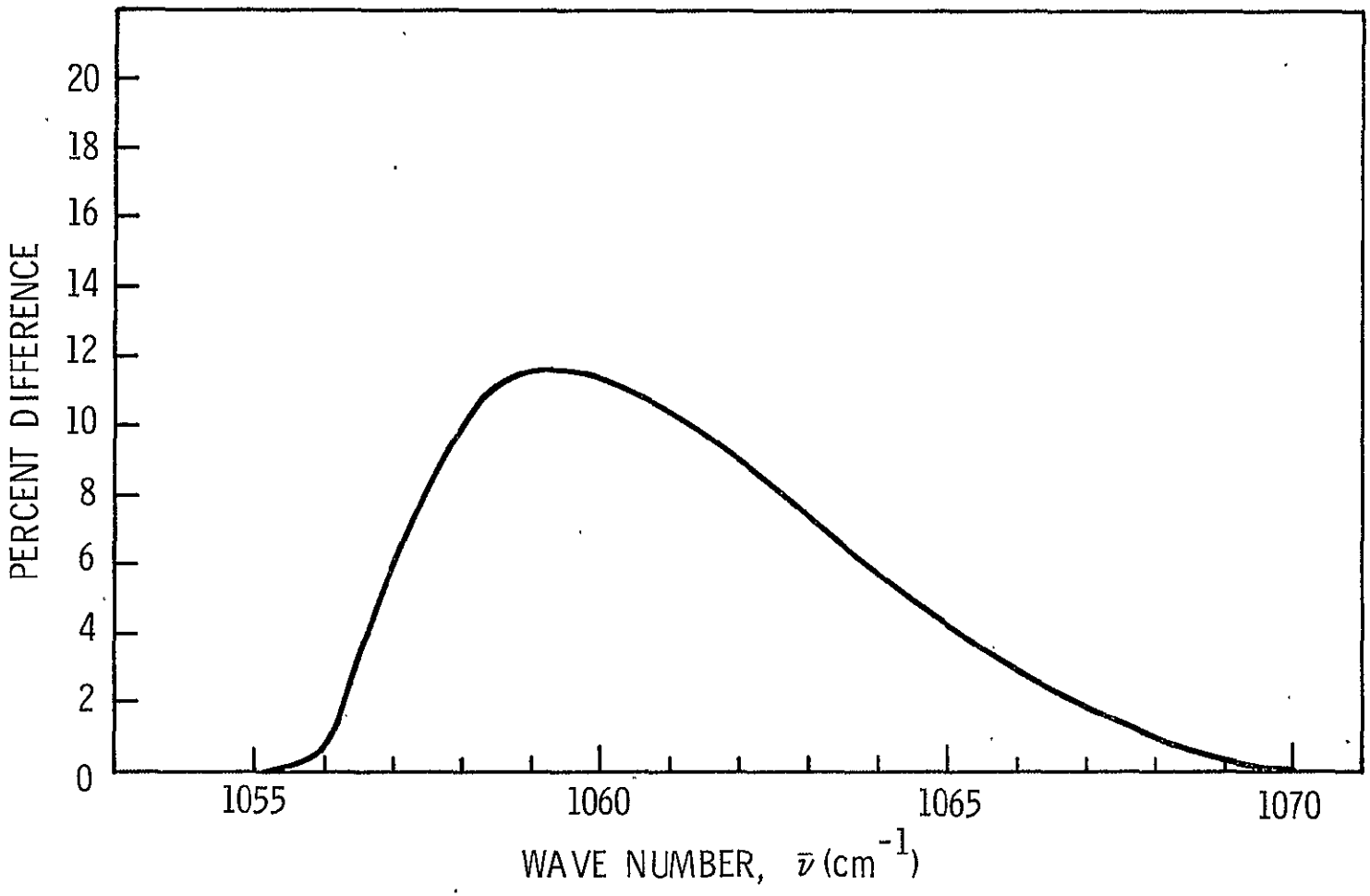

Fig. 3. Percent difference between the spectral radiance computed using the random exponential band model and the radiance computed using the direct integration method.

3.2.3 Lower Boundary Emission

Background emission from the underlying boundary can significantly alter the ozone spectrum measured at the top of the atmosphere. Sometimes, in high latitude areas of the globe, the combined effect due to atmospheric and lower boundary emissions can create the condition where there is little or no contrast between the background emission spectrum and the ozone spectrum. Under these conditions, it may be difficult or impossible to determine ozone information from satellite measurements. These effects are discussed in Appendix B. This subsection describes the technique used in this study to compute the lower boundary emission.

The lower boundary emission is clearly represented by the first term on the righthand side of (3.2.6). However, the evaluation of this term is not straight-forward. For example, if the underlying boundary is the earth's surface, it is difficult to determine the surface conditions which should be used. The field of view of a satellite instrument covers a large area and since both the surface temperature and surface emissivity vary with terrain, appropriate average values must be found for these quantities. If the sky contains clouds, the emissivity of the clouds must be considered and the emissions from the clouds and surface must be weighted in some way according to the percentage of cloud cover. The problem is further compounded by the presence of the water vapor continuum absorption which is difficult to compute. This absorption attenuates the energy emitted by the earth's surface before it reaches the top of the atmosphere. But these difficulties can be circumvented to a large extent by using the fact that the ozone partial pressure is small in the troposphere.

This property of atmospheric ozone makes it possible to divide the atmosphere into two broad layers; an upper layer containing pure ozone and a lower layer devoid of ozone containing the earth's surface and all the atmospheric water vapor and clouds. This approach greatly simplifies the problem as will be seen in the following paragraphs.

If the spectral interval is sufficiently wide so that there is no correlation between O_3 and H_2O absorption, then the transmission through a water vapor-ozone atmosphere is given by (Goody, 1964a, p. 123),

$$\overline{\tau(\bar{\nu}, P)} = \overline{\tau_{H_2O}(\bar{\nu}, P)} \cdot \overline{\tau_{O_3}(\bar{\nu}, P)} \qquad (3.2.25)$$

If, for the present, the parentheses are dropped and we use the subscript g to denote the lower boundary and o to denote the top of the atmosphere (3.2.6) can be written,

$$\bar{L}_o = \epsilon_g B_g \bar{\tau}_{gH_2O} \cdot \bar{\tau}_{gO_3} + \int_{\tau_g}^{1} B \, d\left[\bar{\tau}_{H_2O} \cdot \bar{\tau}_{O_3}\right] \qquad (3.2.26)$$

where the relation of (3.2.25) is used. Upon expanding (3.2.26) we have,

$$L_o = \epsilon_g B_g \bar{\tau}_{gH_2O} \cdot \bar{\tau}_{gO_3} + \int_{\tau_{gH_2O}}^{1} B\bar{\tau}_{O_3} \, d\bar{\tau}_{H_2O} + \int_{\tau_{gO_3}}^{1} B\bar{\tau}_{H_2O} \, d\bar{\tau}_{O_3} \qquad (3.2.27)$$

Consider now Figure 4 which shows typical water vapor, ozone, and temperature distributions and which illustrates the two-layer concept. Since the water vapor content is very small in the stratosphere and the O_3 content

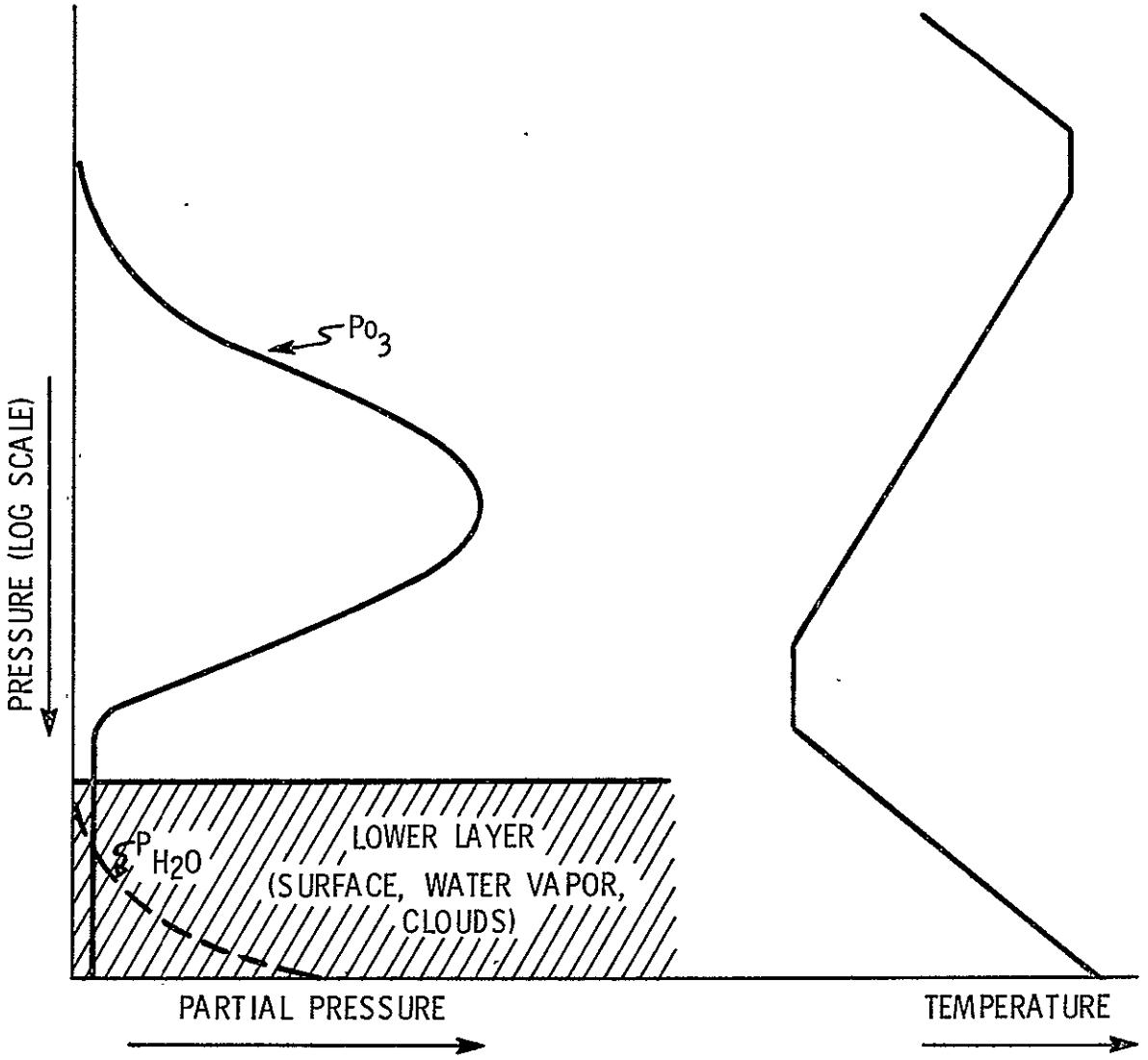

Fig. 4. The two-layer concept.

is small in the troposphere $\bar{\tau}_{O_3} \approx$ constant in the lower layer and $\bar{\tau}_{H_2O} \approx 1$ (in the spectral vicinity of 1042 cm^{-1}) in the upper region. For these conditions $\bar{\tau}_{gO_3} \approx \bar{\tau}_{uO_3}$ where $\bar{\tau}_{uO_3}$ is the transmittance from the top of the atmosphere down to the bottom of the ozone layer. Therefore (3.2.27) can be written,

$$\bar{L}_o = \left[\epsilon_g B_g \bar{\tau}_{gH_2O} + \int_{\tau_{gH_2O}}^{1} B d\bar{\tau}_{H_2O}\right] \bar{\tau}_{uO_3} + \int_{\tau_{uO_3}}^{1} B d\bar{\tau}_{O_3} \qquad (3.2.28)$$

where the bracketed portion of the first term on the righthand side is the emission from the lower layer. If the water vapor line absorption spectrum is excluded for the present and the emissivity (ϵ_g) is considered to be constant in the spectral regions immediately adjacent to and including the ozone band, the spectrum at the top of the atmosphere can be viewed as consisting of the Planck radiance of the lower layer at some effective temperature T_{Eff} and the superimposed absorption spectrum of a pure ozone layer. The temperature T_{Eff} will depend on the surface, water vapor, and cloud conditions. The value of T_{Eff} is determined by selecting a value which gives a match between the Planck radiance and the measured spectrum on either side of the ozone band. Since the measurements will contain noise, T_{Eff} is found by least squares fitting a Planck function through the maximum radiance points of the measured spectrum. This is illustrated by the dashed line in the bottom spectrum of Figure 5. The spectral structure in Figure 5. is due to ozone absorption and line absorption by water vapor. It is not obvious that water vapor line structure exists in the part of the spectrum where ozone absorbs. This is because the effects of the lines are reduced in the center of the band by absorption of the upwelling lower boundary energy in the ozone layer

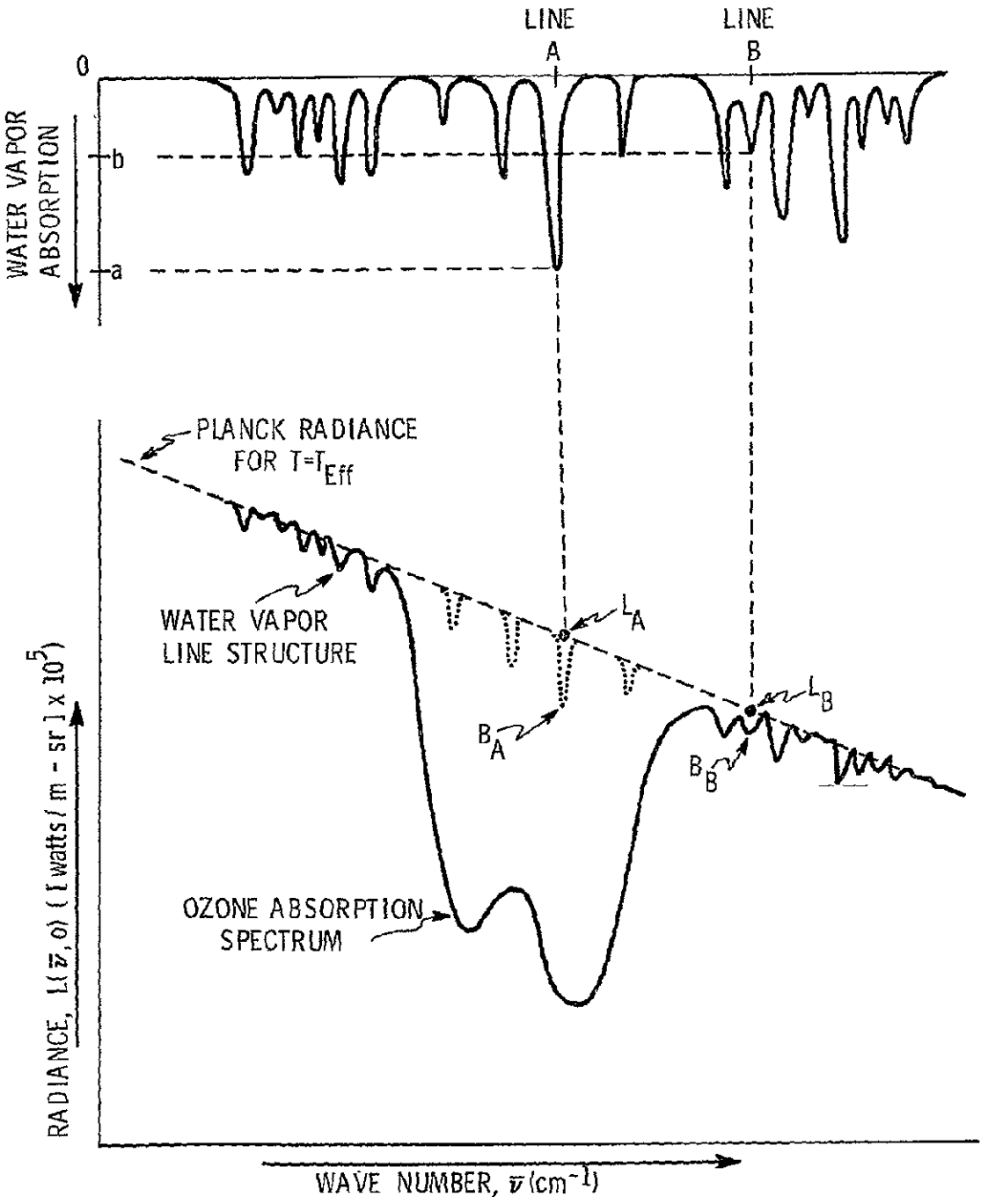

Fig. 5. A sketch of typical ozone and water vapor absorption spectra.

and they are hidden in other spectral regions because of the slope of the ozone spectrum. Nevertheless, line structure is present throughout the band as part of the background emission. This is illustrated in the lower spectrum of Figure 5. by the dotted water vapor lines (the magnitudes of these lines are not drawn to scale relative to the ozone spectrum and the positions do not necessarily coincide with the positions in an actual water vapor spectrum). The effect of water vapor lines is considered by computing a line absorption spectrum for tropospheric water vapor using the direct integration technique. The top spectrum in Figure 5 illustrates this computation. Preferably the calculations would be done using an actual sounding of the water vapor altitude distribution. However, if there is no sounding available, the mean climatological profile can be used. After computing the water vapor line spectrum, the water vapor absorption at any point in the measured spectrum can be predicted based on the relative absorption in the computed water vapor line spectrum. For example, suppose it is desired to compute the background emission B_A at the position of the line A in the measured spectrum. The ratio of the absorption by line A to that by line B in the computed line spectrum is a/b. Therefore, the lower boundary emission B_A at the position of water vapor line A is,

$$B_A = L_A - (a/b) \cdot (L_B - B_B) \qquad (3.2.29)$$

This method was used with the Nimbus and Palestine, Texas flight data. The direct integration method and the H_2O line parameters of Benedict and Calfe (1967) were used to compute the line absorption. Some calculations were done for water vapor absorption centers located outside the spectral region of ozone absorption. It was possible with this procedure

to evaluate the accuracy of lower boundary emission values determined by this method. The calculations showed that the background emission could be computed to within 5×10^{-5} watts/m-sr or less. This corresponds to an effective background temperature error of $\leq .5^{\circ}K$ in the wings of the ozone band and a smaller error toward the center. The background emission computed in this manner at various wave numbers can be used to replace the quantity $\epsilon(\nu_o)\, B\left[\bar{\nu}_o, T(P_g)\right]$ in the first term on the right-hand side of (3.2.6). When this is done, the transmittances in that equation correspond to the transmittances of the atmosphere due to ozone alone.

3.2.4 The Inversion Method

The problem to be solved is the following: given the temperature variation with altitude, find an atmospheric ozone profile which gives a match between the radiance $\bar{L}_c(\bar{\nu}_o,0)$ which is calculated with (3.2.6) and the radiance $\bar{L}_m(\bar{\nu}_o,0)$ which is measured. Equation (3.2.6) behaves like a Fredholm integral equation of the first kind (Wark and Fleming, 1966). Therefore, an infinite number of ozone profiles can be found which will provide a radiance match to within any given error limits. This family of results will include a multitude of solutions which bear no physical resemblance to a realistic ozone profile. Therefore, one is faced with the problem of filtering out those solutions which are mathematically valid but which are physically unrealistic. This is normally accomplished by pre-selecting a form of the solution which is known to be physically valid based on other information, i.e. climatology.[1] A function is needed

[1] For example, in the temperature inversion problem discussed by Wark and Fleming(1966), the temperature solution is expressed in terms of empirical orthogonal functions which are determined from a large number of temperature soundings in a given area of the globe (see Alishouse, et al, 1967).

which adequately represents the general shape of the vertical ozone distribution described in Chapter 2. It would be desirable to include enough parameters in the function to define the dominant features; i. e. the magnitudes and altitudes (or pressure levels) of the three major peaks in the profile. But there may not be sufficient information contained in the radiance measurements to determine such details. A good indication of the information content of the measurements is provided by the weighting functions. The weighting function is contained in the second term on the righthand side of (3. 2. 6) and is given by,

$$W(\bar{\nu}_o, P) = \frac{d\,\tau(\bar{\nu}_o, P)}{d(\log P)} \qquad (3.2.30)$$

The function derives its name from the fact that it vertically weights the energy emitted by the atmosphere; i. e. the atmospheric layer which contributes most to the radiance at the top of the atmosphere is near the layer where $W(\bar{\nu}_o, P)$ is a maximum. If the $W(\bar{\nu}_o, P)$'s for several wave numbers are sharply peaked and do not significantly overlap in the vertical, it may be possible to determine several parameters independently from the measurements. If there is a high degree of overlap it may be possible to determine only a few parameters. The weighting functions for three wave numbers in the ozone band are shown in Figure 6. The functions were computed by the line-by-line integration technique for the ozone profile of Figure 7. A triangular shaped instrument function was used in the calculations with a half-width at the base of 5 cm^{-1} to simulate the resolution of an IRIS. The wave numbers for the calculations were selected in regions of strong (1056 cm^{-1}), moderate

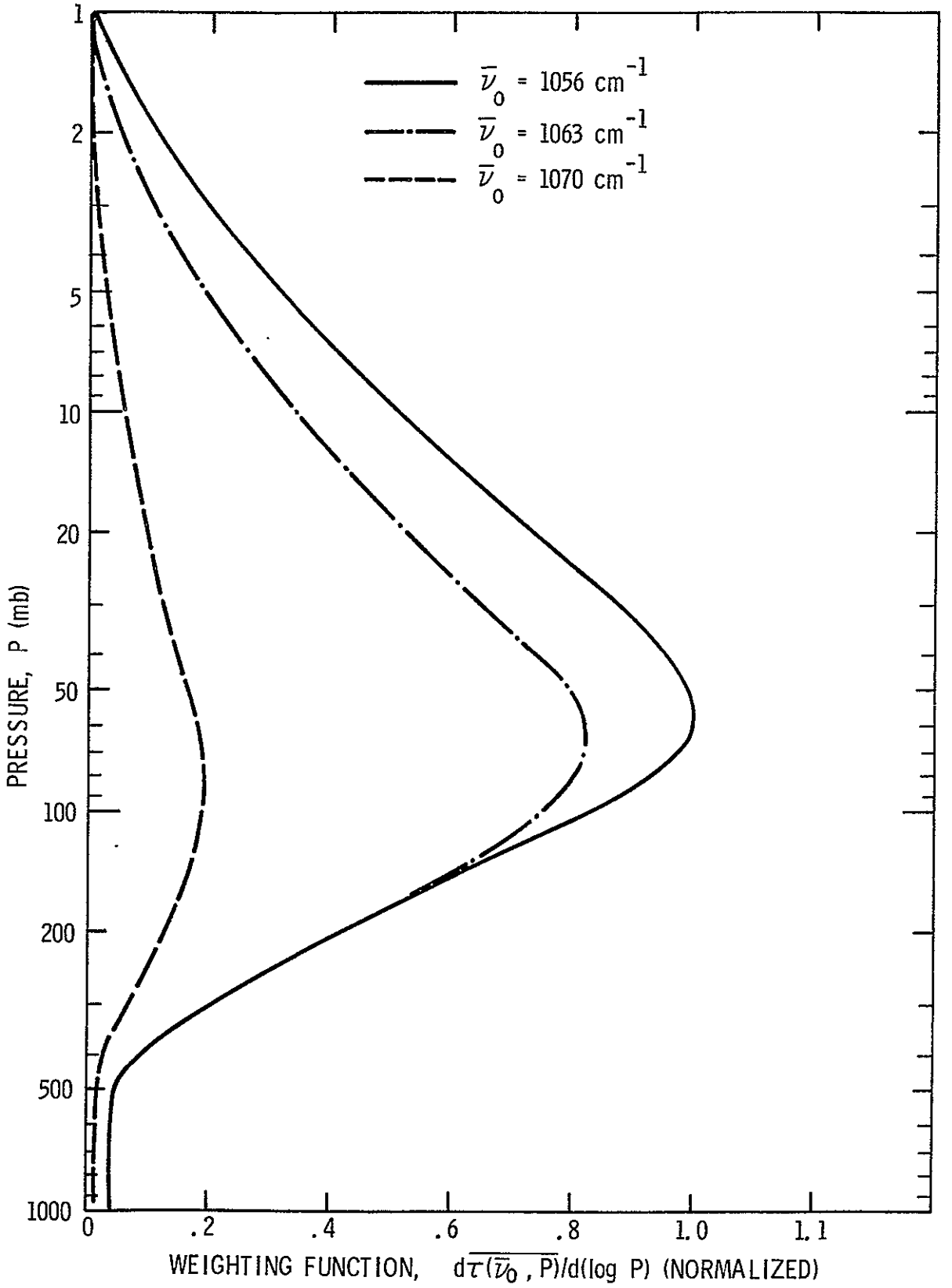

Fig. 6. Ozone weighting function for $\bar{\nu}_0$ = 1056, 1063, and 1070 cm^{-1}.

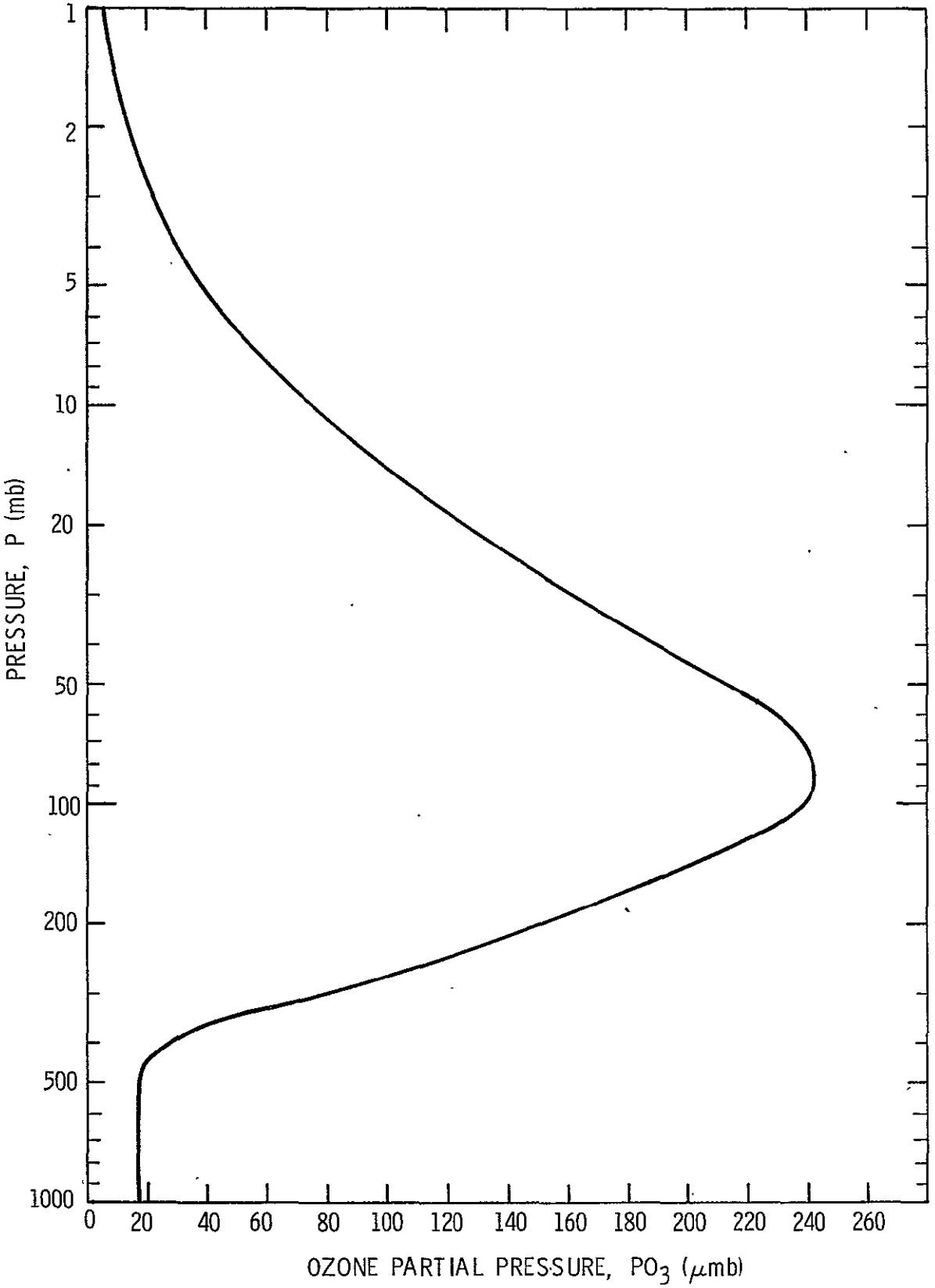

Fig. 7. Ozone profile used to compute weighting functions.

(1063 cm^{-1}), and weak (1070 cm^{-1}) absorption to show the maximum degree of separation which can be expected. These functions are highly overlapping and it appears that it is not possible to obtain more than three pieces of information which are independent of each other from the measued radiances; and probably the limit is two pieces or less.

Because of the low information content of the measurements, the most that can be expected from an inversion is data that defines the gross features of atmospheric ozone, i. e. properties such as the total ozone, the altitude where the main peak in the profile occurs, and the value of the maximum partial pressure at the main peak. A function which characterizes the profile by just a few parameters is all that is required, since greater detail is not available from the measurements. Green (1964) used a relationship that is well suited for this purpose. It is expressed in terms of the value of the maximum partial pressure -P03m, the atmospheric pressure -Pm at the altitude where the maximum partial pressure occurs, and a width factor-H. The function is given by the following equation:

$$PO_3 = 4 \cdot PO3m \frac{e^x}{\left[1+e^x\right]^2} \qquad (3.2.31)$$

where

$$x = \frac{\log(P/Pm)}{H}$$

and where PO_3 is the ozone partial pressure. The function is used in this study to describe the ozone profile in a range of altitudes starting near the tropopause and extending upward. The partial pressure in the troposphere is considered to be constant. A plot of this function is shown later in Figure 20.

The goal of the inversion method is to select values for the three parameters P03m, Pm, and H which give a match between $\bar{L}_c(\bar{\nu}_o, 0)$ and $\bar{L}_m(\bar{\nu}_o, 0)$ according to a criterion which is discussed subsequently. The initial step in the solution procedure is to make a linear approximation for the relationship between $\bar{L}_m(\bar{\nu}_o, 0)$, $\bar{L}_c(\bar{\nu}_o, 0)$, and the three parameters as follows

$$\bar{L}_m(\bar{\nu}_o, 0) = \bar{L}_c(\bar{\nu}_o, 0) + \frac{\partial \bar{L}_c(\bar{\nu}, 0)}{\partial PO3m} \Delta PO3m + \frac{\partial \bar{L}_c(\bar{\nu}, 0)}{\partial Pm} \Delta Pm + \frac{\partial \bar{L}_c(\bar{\nu}, 0)}{\partial H} \Delta H \qquad (3.2.32)$$

This is a Taylor's series expansion with the higher order terms truncated. To determine three parameters, at least three equations must be used. The required three equations can be written from (3.2.32) to correspond to measured radiances at three wave numbers. If we drop the parentheses and use a numerical subscript to denote the 1st, 2nd, and 3rd wave number center we have,

$$\begin{aligned}
\bar{L}_{m1} &= \bar{L}_{c1} + \frac{\partial \bar{L}_{c1}}{\partial PO3m} \Delta PO3m + \frac{\partial \bar{L}_{c1}}{\partial Pm} \Delta Pm + \frac{\partial \bar{L}_{c1}}{\partial H} \Delta H \\
\bar{L}_{m2} &= \bar{L}_{c2} + \frac{\partial \bar{L}_{c2}}{\partial PO3m} \Delta PO3m + \frac{\partial \bar{L}_{c2}}{\partial Pm} \Delta Pm + \frac{\partial \bar{L}_{c2}}{\partial H} \Delta H \qquad (3.2.33) \\
\bar{L}_{m3} &= \bar{L}_{c3} + \frac{\partial \bar{L}_{c3}}{\partial PO3m} \Delta PO3m + \frac{\partial \bar{L}_{c3}}{\partial PM} \Delta Pm + \frac{\partial \bar{L}_{c3}}{\partial H} \Delta H
\end{aligned}$$

An iterative procedure is used to determine the final values of the three parameters P03m, Pm, and H. After making initial guesses for the parameters, the quantities $\bar{L}_{ci}$ are computed using (3.2.31), (3.2.8) or

(3.2.24), and (3.2.6). The partial derivitives are computed in a similar manner by letting one parameter at a time change by a small amount in order to obtain the differentials. Upon solving for $\Delta P03m$, ΔPm, and ΔH, these quantities are added to the initial guesses and the process is repeated until some convergence criteria are met.

The system of equations (3.2.33) could be solved directly without further manipulations. But since the measured radiances will contain noise, it is desirable to use a least squares fitting procedure. It is also desirable to use an overdetermined solution method; i.e. use many more equations than are needed to determine the three parameters. By using a large number of measurements (preferably measurements covering the entire ozone band) and by using a least squares solution, the standard deviation of the radiance noise can in effect be reduced.[1] So if N measurements are used, instead of having just three equations, the system (3.2.33) will have N equations. This system of N equations can be expressed in matrix form as follows,

$$\Delta L = B \cdot S \qquad (3.2.34)$$

where ΔL is an Nx1 matrix defined by the differences $(\bar{L}_{mi} - \bar{L}_{ci})$, B is the Nx3 matrix of partial derivitives, and S is the 3x1 matrix defined by the perturbation terms. The least squares solution to (3.2.34) is easily shown to be

$$S = (B^T \cdot B)^{-1} \cdot (B^T \cdot \Delta L) \qquad (3.2.35)$$

---

[1] Currently, it is not possible to use the entire band because of the magnitudes and differences in sign of absorption errors in various parts of the band (refer to Figure 1.). This emphasizes the importance of further work to improve the accuracies of the absorption line parameters.

where the T and -1 superscripts denote the matrix transpose and inverse respectively.

Equation (3.2.35) is unstable in its present form when a small error is added to ΔL; i.e. a small error in ΔL will cause a vastly different solution than when the error is zero. This is because the matrix $(B^T \cdot B)^{-1}$ is almost singular. This condition arises because of the high degree of overlap of the weighting functions. Saying this another way, the solution is unstable because it depends on information which is not available from the measurements. When this solution occurred in the temperature inversion problem, the procedure was to introduce a smoothing matrix and a smoothing parameter γ (Wark and Fleming, 1966). The value of γ, which depends upon the errors that are present, was determined by a trial and error procedure. The approach preferred here is to express the solution in terms of eigenvectors and eigenvalues. This approach has been used by Drayson (1963) and also by Mateer (1964) to deal with the instability of (3.2.35). The advantage of this procedure is that it will show explicitly how many pieces of independent information are available from the measurements.

The matrix $(B^T \cdot B)$ is real, symmetric, and positive definite. Therefore, its eigenvalues will be real and positive. Suppose that the eigenvalues of $(B^T \cdot B)$ designated λ_1, λ_2, and λ_3 are ordered so that $\lambda_1 \geq \lambda_2 \geq \lambda_3$ with corresponding orthonormal eigenvectors v_1, v_2, and v_3. The column matrix $(B^T \cdot \Delta L)$ can be expressed in terms of the eigenvectors of $(B^T \cdot B)$ by

$$(B^T \cdot \Delta L) = \sum_{i=1}^{3} b_i \cdot v_i \qquad (3.2.36)$$

Where b_i is a constant for each eigenvector. Now (3.2.35) becomes

$$S = (B^T \cdot B)^{-1} \sum_{i=1}^{3} b_i v_i = \sum_{i=1}^{3} b_i (B^T \cdot B)^{-1} v_i \qquad (3.2.37)$$

It is known by a property of eigenvalues and eigenvectors that,

$$(B^T \cdot B)^{-1} v_i = \frac{1}{\lambda_i} v_i \qquad (3.2.38)$$

Therefore,

$$S = \sum_{i=1}^{3} \frac{b_i}{\lambda_i} v_i \qquad (3.2.39)$$

Expanding (3.2.39) we have,

$$\begin{pmatrix} \Delta PO3m \\ \Delta Pm \\ \Delta H \end{pmatrix} = \begin{pmatrix} b_1(\frac{a_{11}}{\lambda_1}) + b_2(\frac{a_{12}}{\lambda_2}) + b_3(\frac{a_{13}}{\lambda_3}) \\ b_1(\frac{a_{21}}{\lambda_1}) + b_2(\frac{a_{22}}{\lambda_2}) + b_3(\frac{a_{23}}{\lambda_3}) \\ b_1(\frac{a_{31}}{\lambda_1}) + b_2(\frac{a_{32}}{\lambda_2}) + b_3(\frac{a_{33}}{\lambda_3}) \end{pmatrix} \qquad (3.2.40)$$

where a_{ji} are the components of the eigenvectors v_i, that is,

$$v_i = \begin{pmatrix} a_{1i} \\ a_{2i} \\ a_{3i} \end{pmatrix} \qquad (3.2.41)$$

The errors in the system can be viewed as being contained in the constants, b_i, since in order to determine the b_i's the matrix $(B^T \cdot \Delta L)$ is used. The errors arise in B and in ΔL which, as previously stated, is the difference $(\bar{L}_{mi} - \bar{L}_{ci})$, where i is the wave number subscript. Errors in measurement appear through $\bar{L}_{mi}$ and all other errors occur in computing $\bar{L}_{ci}$. In reality, therefore, (3.2.39) can be written

$$S = \sum_{i=1}^{3} \frac{bo_i}{\lambda_i} v_i + \sum_{i=1}^{3} \frac{\epsilon_i}{\lambda_i} v_i \qquad (3.2.42)$$

where b_{oi} is the value of the constant with no error and ϵ_i represents the error contribution. The reason for the instability of (3.2.35) now becomes clear. If λ_i is very small, then the error term will be very important and could dominate the solution. Recalling that the λ_i's are ordered, when (3.2.42) is expanded, it may be that the second and/or third eigenvalues will be so small and the resulting error terms will be so large that the iteration procedure will either be unstable or will converge to a physically unrealistic solution. It can be shown (Drayson, 1963) that the eigenvectors, v_i, corresponding to these small λ_i's have very little effect upon the calculated radiance at the top of the atmosphere. Thus, these eigenvectors correspond to details of the solution which are easily hidden by a very small amount of noise. Furthermore, it is clear from (3.2.42) that inclusion of the small eigenvalues associated with these eigenvectors can cause instability or unrealistic results. Therefore, the obvious solution is to truncate the terms containing these components. The problem is to determine how many terms can be carried in the summation of (3.2.39) with realistic errors added to the measured radiances and to various quantities in (3.2.6). It is desirable

to carry as many terms as possible since when a term is dropped ozone information is also lost. There is a trade-off involved between an improved solution due to a decrease in noise sensitivity and a degraded result due to loss of information. This is discussed further in section 3. 3. The number of terms which can be carried that still allow a physically realistic solution is by definition, in this report, the number of independent pieces of information available from the measurements.[1] The types and magnitudes of errors used to determine this information and the responses of the solution to these errors are discussed in section 3. 3.

3. 3 ERROR STUDY

The "measured" radiances for the error study were calculated with (3. 2. 6) assuming a clear sky and using vertical ozone and temperature distributions measured by the Air Force Cambridge Research

---

[1] This terminology is based on the following: equations (3. 2. 40) can be viewed as a set of three simultaneous equations in 1) three unknowns (b_1, b_2, and b_3) if three terms are carried, 2) two unknowns (b_1 and b_2) if two terms are included and 3) one unknown (b_1) if one term is used. Assume for illustration purposes that $\Delta P03m$, ΔPm, and ΔH are known. If three terms can be carried then all three equations are needed to solve for b_1, b_2, and b_3; i. e. each equation is independent of the other. Hence, the term-three independent pieces of information. If only two terms can be carried then any two equations are sufficient to define b_1, and b_2 and the third equation is dependent on these values. Thus only two independent pieces of information exist. If only one term can be used then the solution for b_1 from one equation dictates the values in the other two equations and there is only one piece of information available from the measurments.

Laboratories (Hering, 1964, Hering and Borden, 1964, 1965, 1967)[1]. The Planck radiance at the temperature of the ground was used in computing the effective lower boundary emission and the surface emissivity was assumed to be 1.0. Transmittances used in the computations were determined with the Random Exponential band model. The calculations were limited to the spectral range 1044 cm^{-1}-1070 cm^{-1} since this is the region where currently, the absorption line parameters are known with the greatest accuracy (refer to Figure 1). Radiances were calculated at nine wave number centers spaced 3 cm^{-1} apart. After computing the "measured" radiances, these values were used to invert (3.2.6) to obtain ozone information. This procedure gave complete control over all input errors. The "measured" radiances were known perfectly since calculations with (3.2.6) in the inversion procedure were done in exactly the same way as they were done when the synthetic radiances were originally computed. Convergence criteria for these computations were applied to the three perturbation parameters $\Delta P03m$, ΔPm, and ΔH. The iteration was stopped when the following conditions were met simultaneously: $\Delta P03m \leq 1\mu$ mb, $\Delta Pm \leq 1$ mb, and $\Delta H \leq .01$. These limits were selected to give sufficient accuracy in a minimum of computing time. If convergence was not achieved after nine iterations, the initial guess was altered

[1] These observations were made in-situ from a high altitude balloon at twelve stations covering a latitude range extending from the Canal Zone ($\approx 9^{o}N$) to Greenland ($\approx 77^{o}N$). The ozone measurements were made with chemiluminescent type ozonesondes developed by Regener (1960, 1964). The ozone profile above the maximum balloon altitude is determined in this study by extrapolation assuming a constant ozone mixing ratio.

and the procedure was repeated. These same criteria were used in the calculations of section 3.4 which will be discussed later.

The first series of tests were to evaluate the information content of the radiance measurements. Normally distributed random noise was imposed on the "measured" radiances and inversions were performed for various standard deviations σ of the noise. The calculations showed that it was not possible to obtain realistic solutions when three eigenvectors were included in the expansion (3.2.40) even when the radiance noise was as low as σ=1%. But when the third eigenvector was truncated, the inversion was very stable and it gave physically possible solutions for noise as large as σ=5%. It can be concluded, based on these results, that there are at most two pieces of independent information available from the measurements. But it is still necessary to show that it is always best to use two terms in the expansion; it may be better to use only one term if the noise level is very high since, as pointed out in sub-section 3.2.4, successive truncation of terms continually reduces the sensitivity of the inversion method to noise. Also, if there are two pieces of independent information available, the form of this information must be determined. Both of these tasks were accomplished by performing inversions with all input errors equated to zero for various sets of "measured" radiances. These calculations were done using radiances determined for ten different ozone profiles covering the latitude range from 9 to 76.5^{o}N. The inversion results showed that in order to obtain physically realizable solutions no less than two terms should be used in the expansion. Thus, under favorable conditions, there are two pieces of independent information available from the measurements. Furthermore, those two pieces of information are the total ozone (u) and the altitude (hm) of the maximum in the profile.

TABLE I.

Errors in Total Ozone (u) and in the Altitude (hm) of the Maximum Ozone Partial Pressure When All Input Errors Are Set Equal to Zero

Location	Date of sounding used in the study	Error in u (in %)			Error in hm (in km)		
		with $v_1+v_2+v_3$	with v_1+v_2	with v_1	with $v_1+v_2+v_3$	with v_1+v_2	with v_1
Albrook Fld. Canal Zone (9°N)	7/28/65	-1.3	-.68	58.0	-.8	.1	4.8
	11/18/64	-1.9	-.78	44.6	-.3	.7	4.5
Fla. St. U., Florida (30.4°N)	4/21/65	-1.4	-.72	12.0	.5	.6	1.6
	1/11/65	-1.2	.61	37.1	.4	.7	2.8
Green Bay, Winconsin (44.5°N)	3/15/65	.44	1.2	-5.0	.75	.8	.3
	2/18/65	1.2	-.87	-7.7	.6	.2	-.5
Ft. Churchill, Canada (58.8°N)	3/16/65	.89	2.1	-8.0	0	.2	-.2
	9/2/64	-.67	-.55	26.2	.95	.95	4.1
Thule, Greenland (76.5°N)	5/19/65	1.3	-.3	-.1	2.8	2.0	3.1
	10/7/64	-.22	.09	23.7	2.3	.7	3.8
Root-Mean-Square Errors		1.15	.95	28.8	1.27	.86	3.1

The data supporting these conclusions are presented in Table 1. Table I shows errors in the total ozone and in the altitude of the maximum of the ozone profile when one, two, and three eigenvectors are used in the

expansion (3.2.40). There is very little change in the RMS errors for the ten profiles when two eigenvectors are used rather than three but there is a drastic change in going from two eigenvectors to one. In this latter case the error in u goes from .95% to 38.8% and the error in hm goes from .86 km to 3.1 km. It is clear that the second eigenvector contains so much information that it can not be discarded even if the noise level is unusually high. The data of Table I are explicit examples of the trade-off between reduction of noise sensitivity and loss of information when terms of (3.2.40) are truncated. Very little information about u and hm is lost when the third eigenvector is truncated as shown by the small changes in the RMS errors. Yet the random noise study showed that when the third eigenvector is included, the inversion is so sensitive to noise that the solution becomes unstable even for small errors. Therefore this component should clearly be dropped. On the other hand, a great deal of information is contained in the second eigenvector term and it obviously can not be neglected.

The inferred ozone information can not be expressed explicity in terms of the three parameters of Green's ozone function (3.2.31). The inversion gives one of these parameters, Pm (or hm), but the other piece of information is a function of all three parameters through an integral relationship; i.e. the total ozone is expressed as,

$$u \propto \int_0^{P_s} \frac{PO_3}{P} \, dP \qquad (3.3.1)$$

where PO_3 is the ozone partial pressure, P is pressure, and P_s is the pressure at the surface of the earth.

Since the errors of Table I were generated with all input errors equal to zero, these errors are the smallest possible values when Green's

function is used to model the ozone profile. The errors occur because of the mismatch between Green's function and the atmospheric ozone profiles and because of the small amount of information in the measured radiances. The actual distribution and the profile determined by inversion using two eigenvectors with all errors equated to zero are compared for the July-Canal Zone sounding and the March-Canada sounding in Figures 8, and 9. These results are typical of solutions obtained for the ten profiles included in this study. The ozone soundings used for Figures 8 and 9 were selected because they include opposite extremes of latitude, season, and ozone amount.

The remainder of the error study was done with two eigenvectors in the expansion. In the next series of tests, individual errors were imposed one at a time. The types and ranges of errors used in these calculations are given in Table II. The types of errors in Table II are those which probably would be encountered in an actual experiment. The ranges were selected to facilitate unambiguous identification of the most important error effects. The results are presented in Figures 10-18 for the July-Canal Zone profile and the March-Canada profile. The errors in u and hm from Table I have been subtracted from the errors in each figure. The only errors plotted for hm are those due to random radiance noise, lower boundary temperature errors, and temperature profile bias errors. The effects on hm resulting from the remaining types of error were not plotted since the deduced values were very small ($\leq$ 0.4km).

TABLE II

Types and Ranges of Errors Used in the Study of Individual Error Effects in the Nadir Experiment

Type of Error	Range
Random radiance noise, normally distributed with a mean of zero	standard deviation* σ=1%, 3%, 5%
Radiance bias	$\pm$. 3x10^{-5} watts/m-sr
Temperature profile $\pm$	0 – 20 ^{o} K†
Temperature profile bias	$\pm$ 7^{o} K
Ozone absorption line intensity	$\pm$ 15%
Lower boundary temperature	$\pm$ 2^{o} K

* Fifteen inversions were performed for each value of standard deviation.

† This is the maximum difference between the true profile and the error profile at each of six different altitudes in the range from the ground to the stratopause. The errors between any two of these altitudes varied linearly going from a plus value at one level to a minus value at the next.

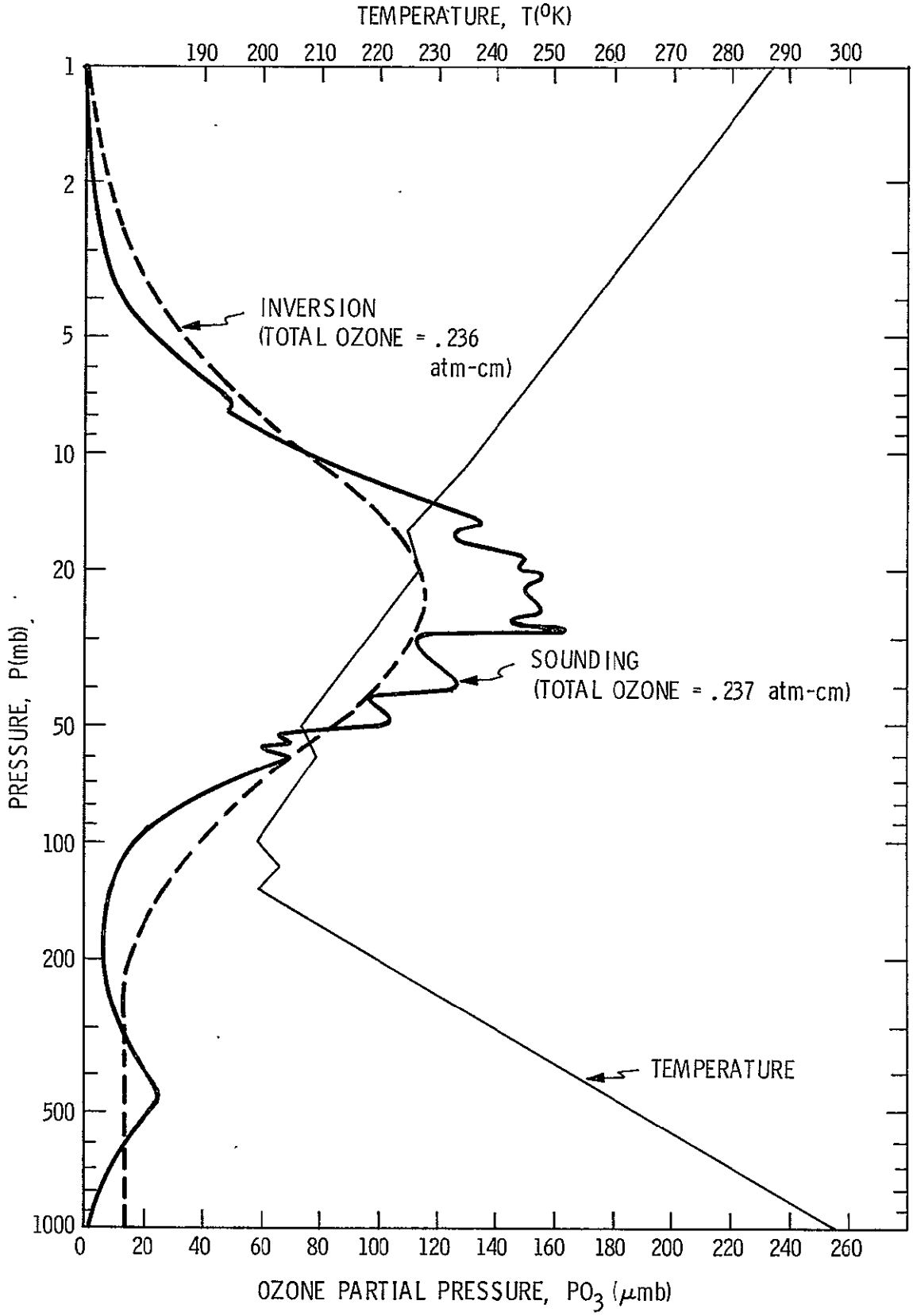

Fig. 8. A comparison of the actual and inferred ozone profiles for a July Canal Zone sounding. All input errors equal zero.

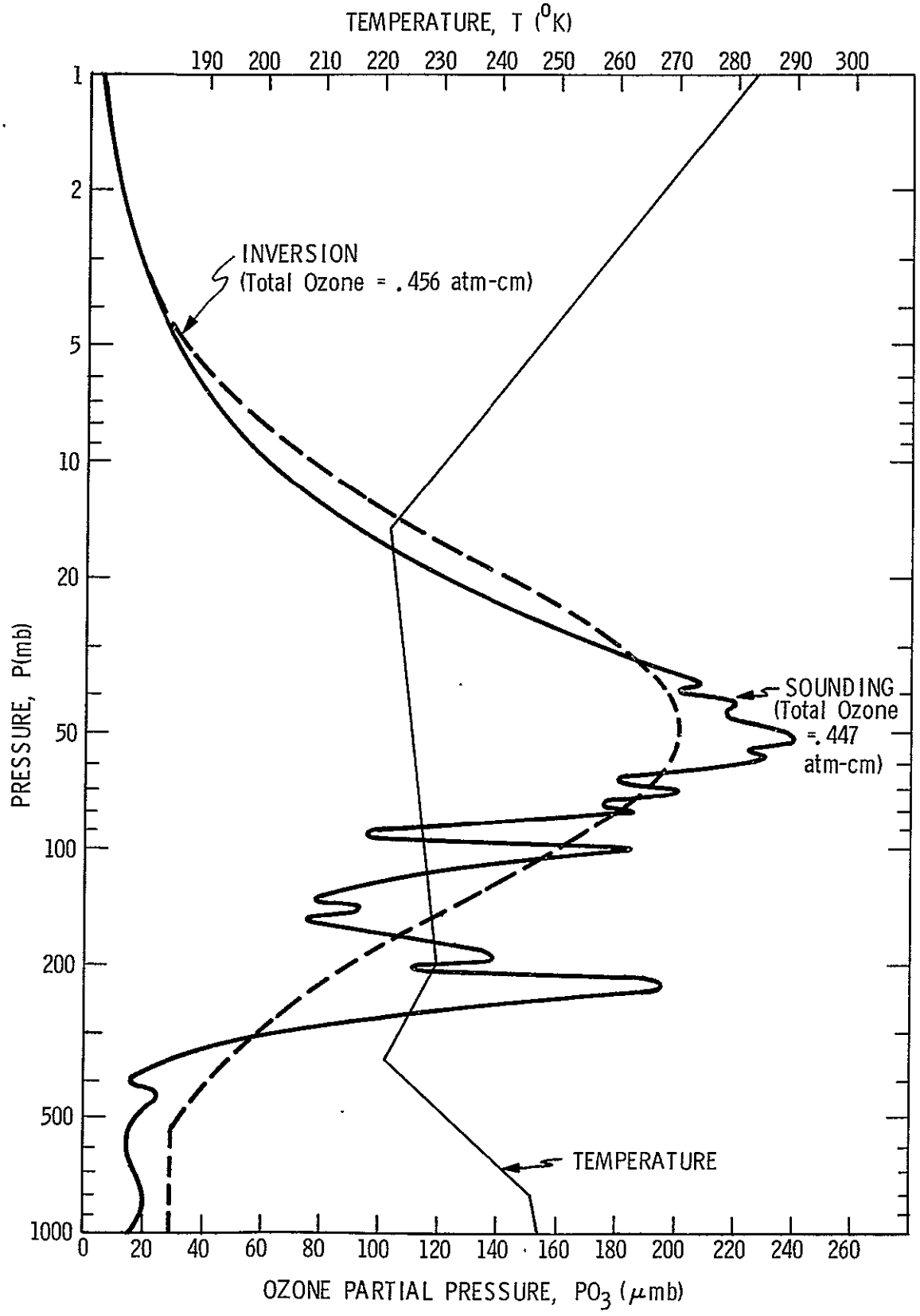

Fig. 9. A comparison of the actual and inferred ozone profiles for a March Canada sounding. All input errors equal zero.

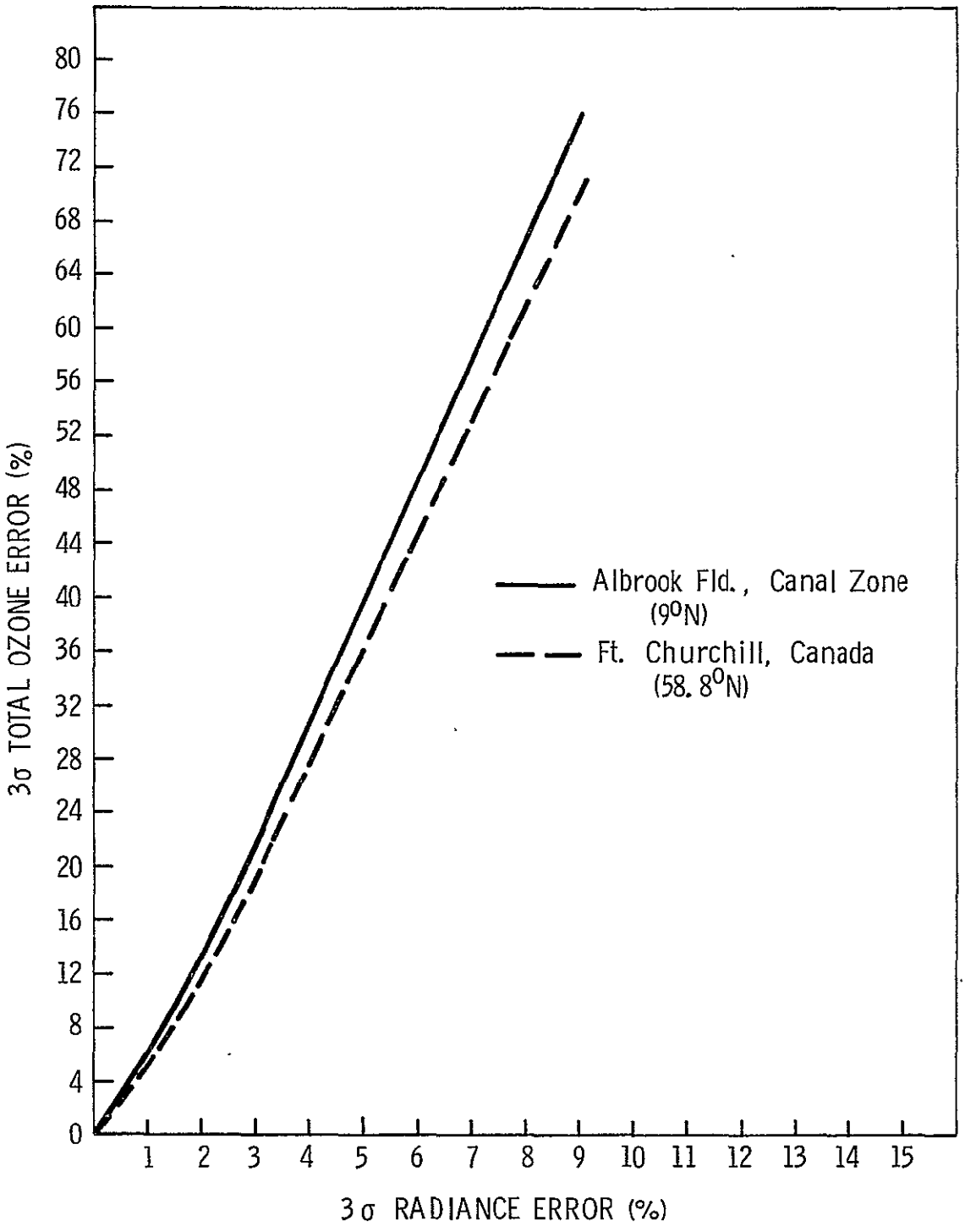

Fig. 10. 3σ total ozone error versus 3σ radiance error for normally distributed random radiance noise with a mean of zero.

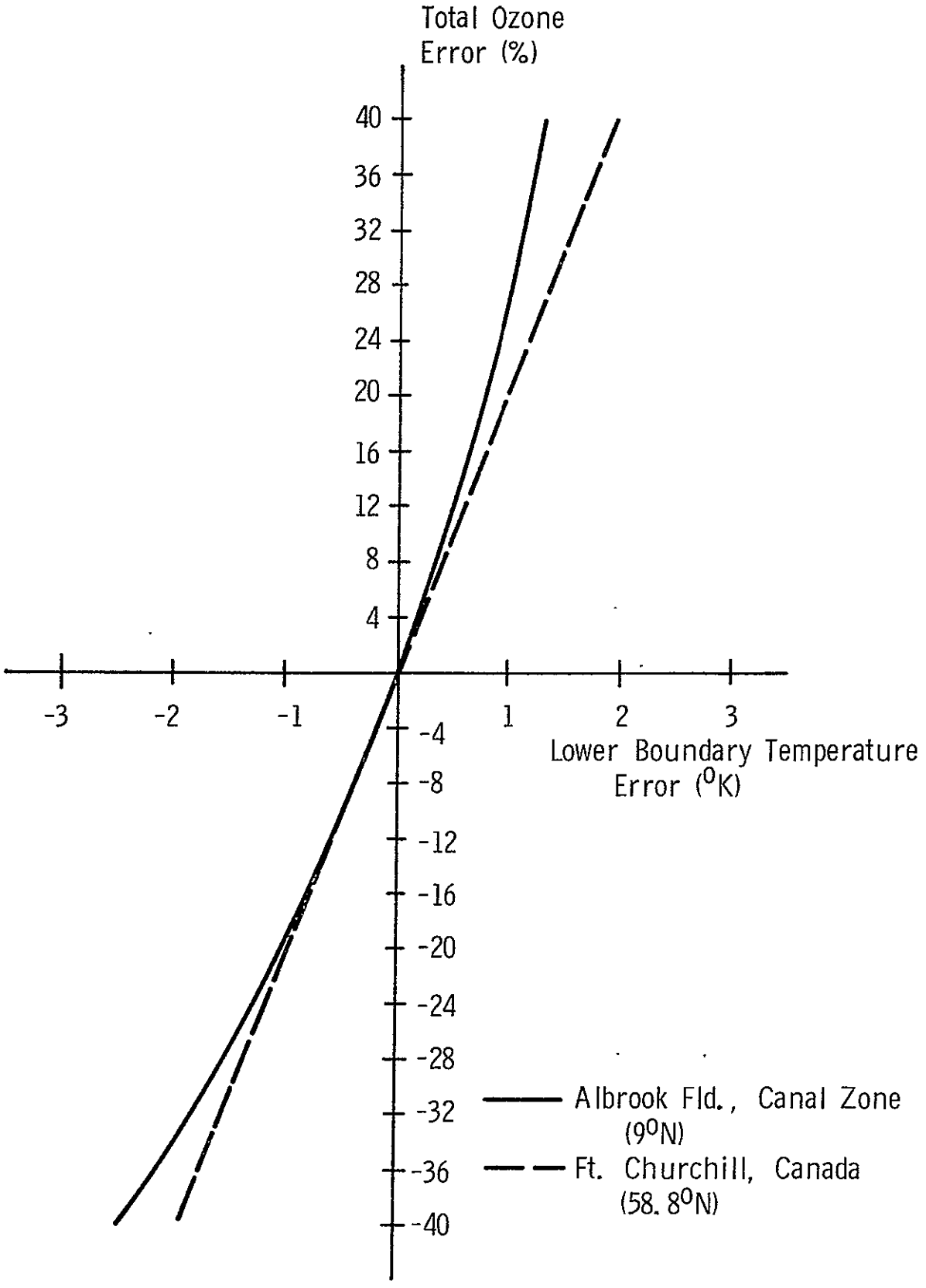

Fig. 11. Total ozone error versus lower boundary temperature error.

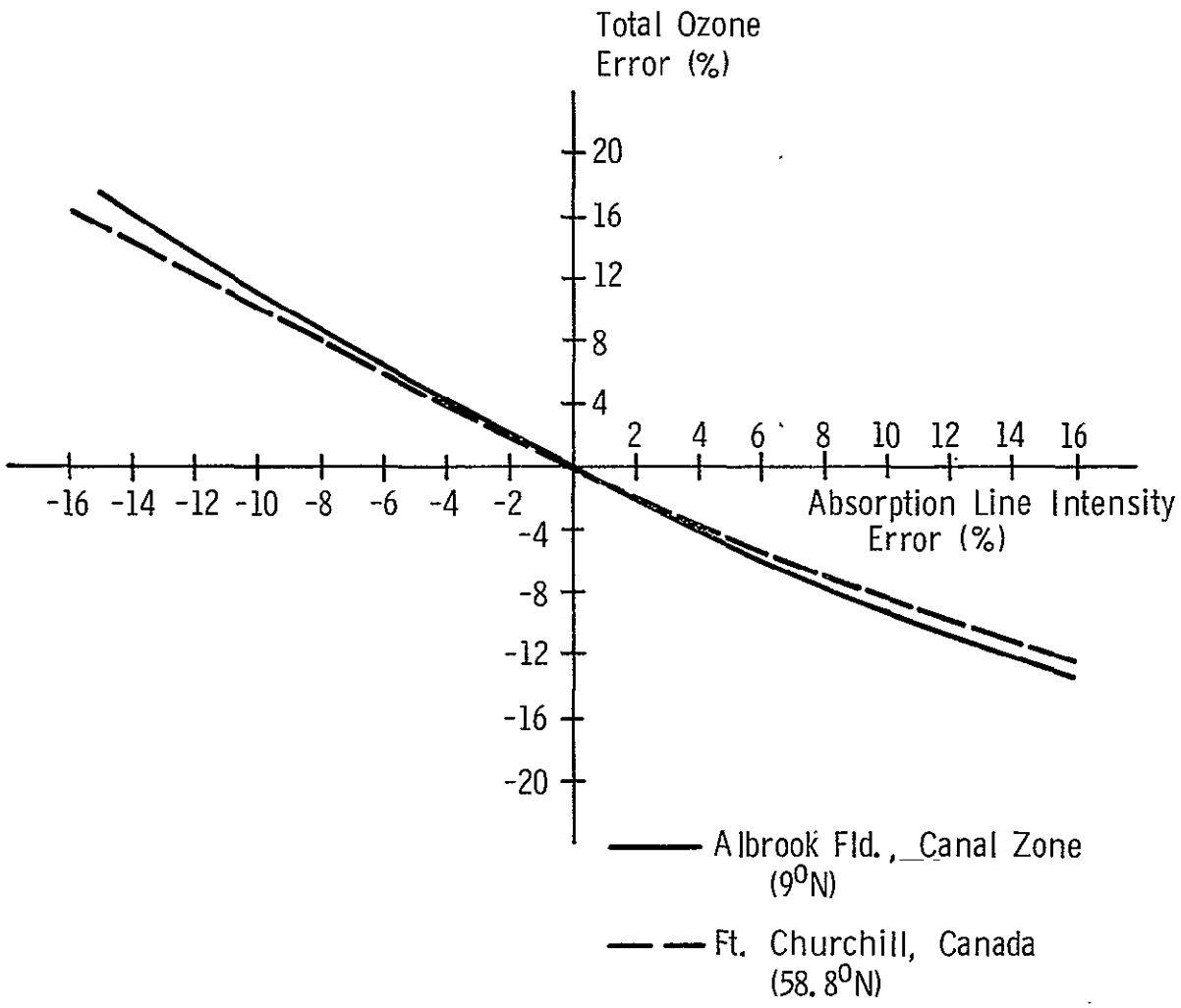

Fig. 12. Total ozone error versus absorption line intensity error.

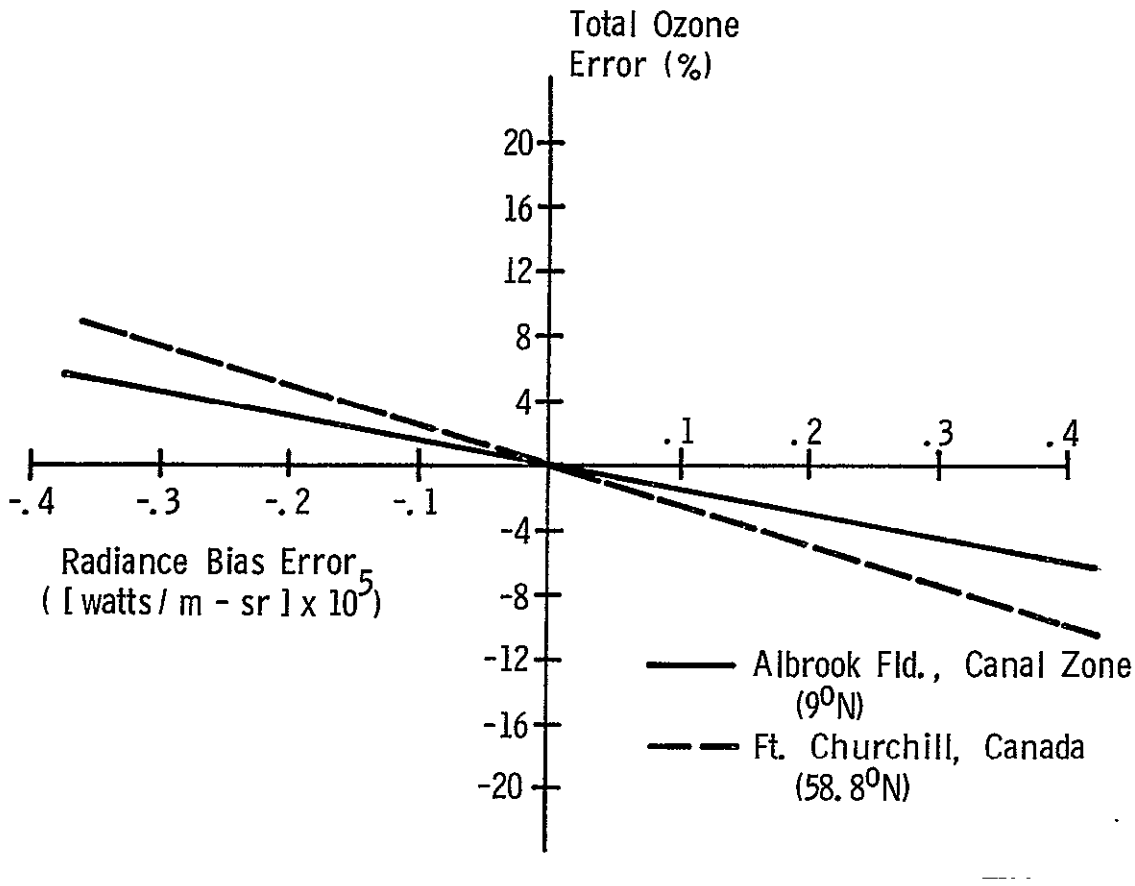

Fig. 13. Total ozone error versus radiance bias error.

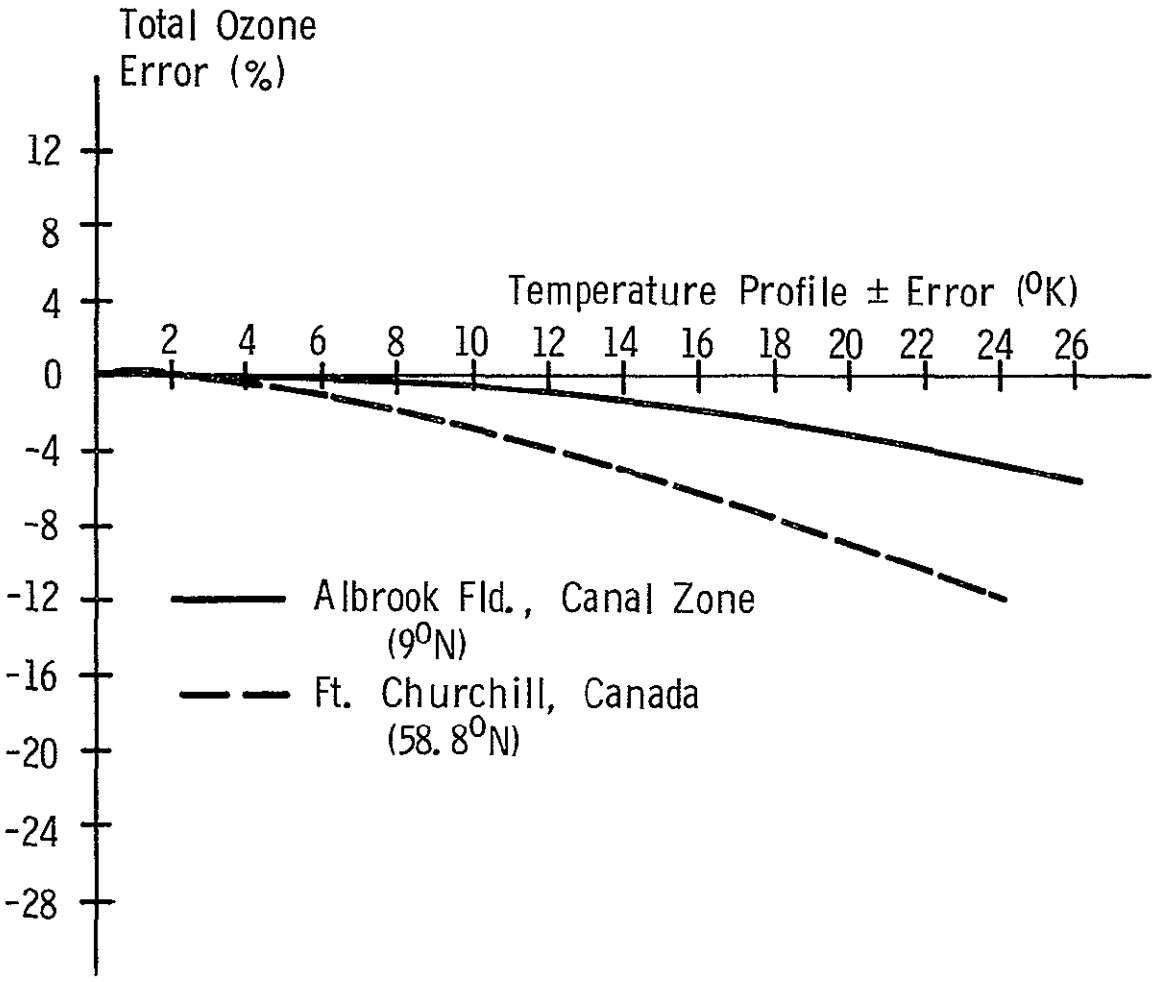

Fig. 14. Total ozone error versus temperature profile ± error.

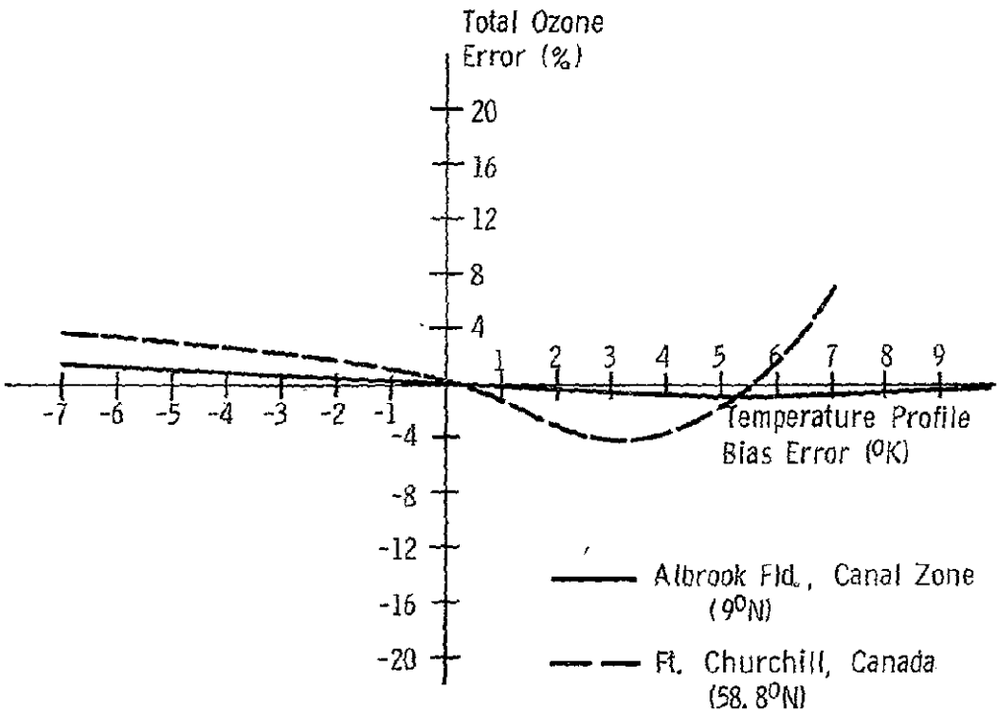

Fig. 15. Total ozone error versus temperature profile bias error.

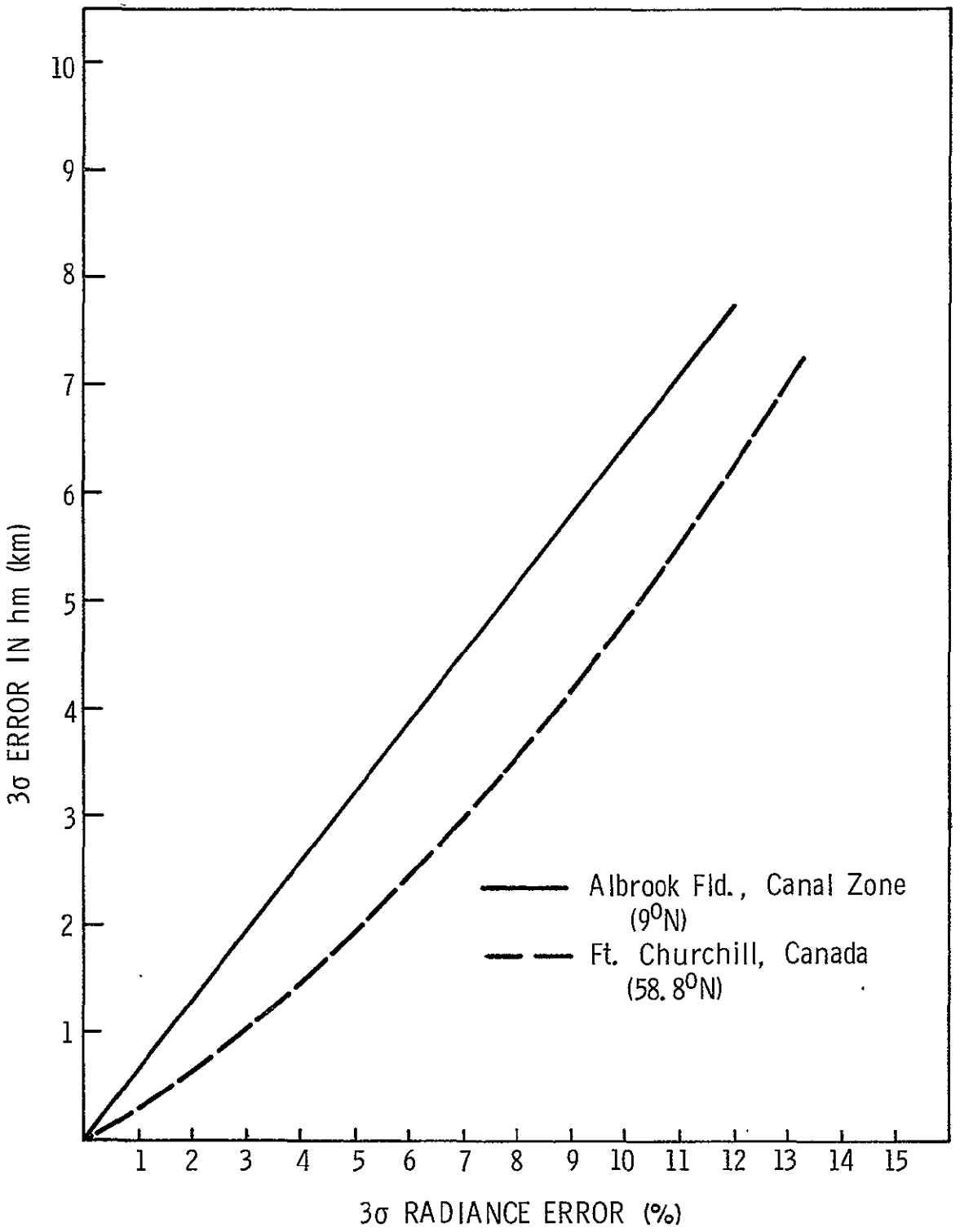

Fig. 16. 3σ error in the altitude, hm, of the maximum ozone partial pressure versus 3σ radiance error for normally distributed random radiance noise with a mean of zero.

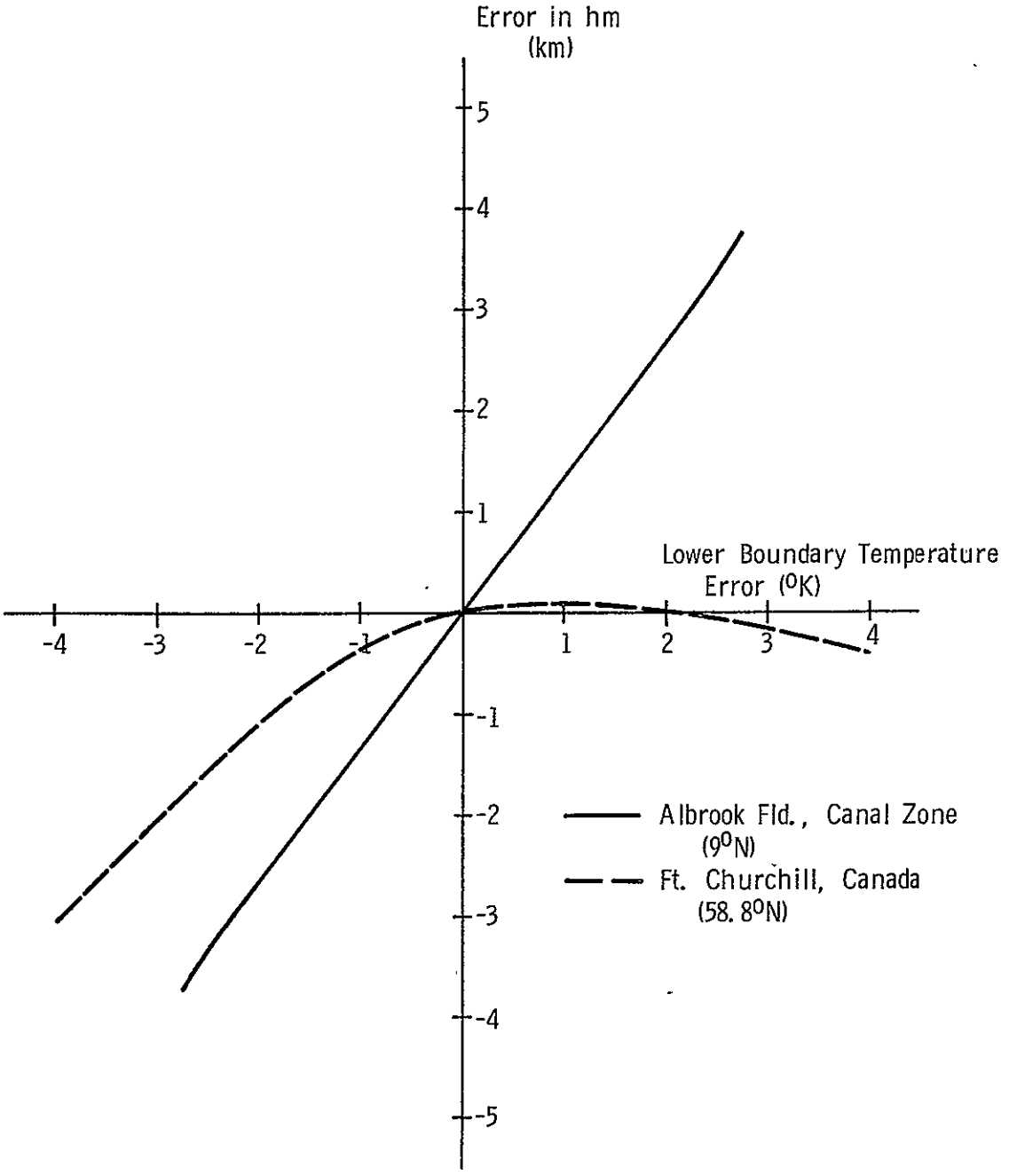

Fig. 17. Error in the altitude, hm, of the maximum ozone partial pressure versus lower boundary temperature error.

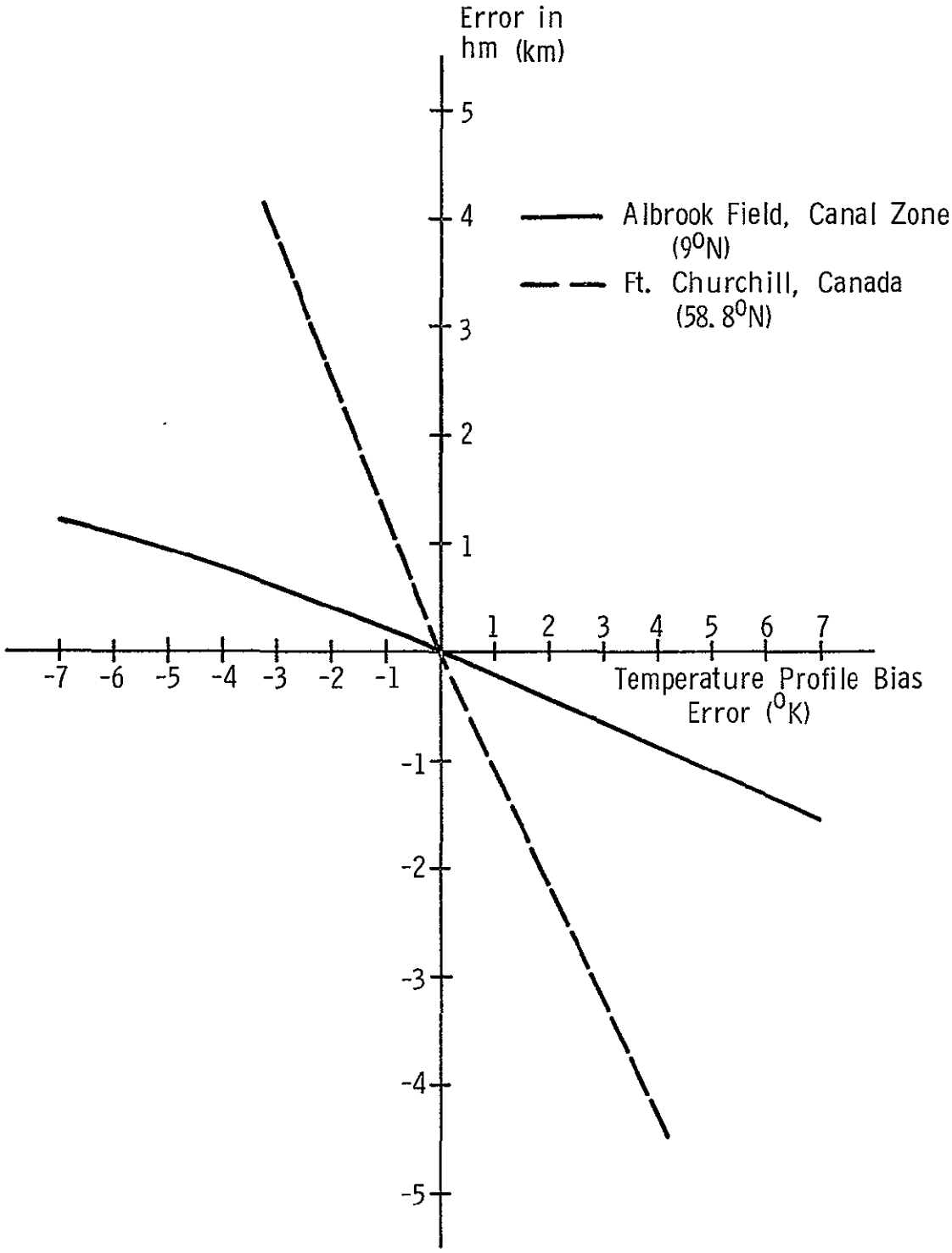

Fig. 18. Error in the altitude, hm, of the maximum ozone partial pressure versus temperature profile bias error.

An examination of the calculations leading to these results showed that radiance changes in the wings of the band cause the greatest changes in u and hm. Accordingly, errors in the lower boundary temperature are magnified considerably since 60 to 85% of the energy emitted by the lower boundary in the wing region of the spectrum reaches the top of the atmosphere. A positive lower boundary temperature error leads to a positive total ozone error. This is because a positive error increases the upwelling radiance at the top of the atmosphere. The only way to reduce the radiance to the level which exists for zero error, assuming other conditions are unchanged, is to add more ozone to the atmosphere; this attenuates the energy emitted from the lower boundary before it reaches the top of the atmosphere. A positive absorption line intensity error leads to a negative total ozone error. This is because a positive absorption error decreases the upwelling radiance. The only way to increase the radiance to the level which exists for zero error (when all other errors equal zero) is to reduce the amount of ozone in the atmosphere and thereby transmit more of the lower boundary energy to the top. A positive radiance bias error also leads to a negative total ozone error for a similar reason. The effect of atmospheric temperature errors on the total ozone error is small since these errors cause the greatest radiance change in the center of the ozone band rather than in the wing regions. The errors in hm are coupled with the total ozone error. The latitudinal hm error responses are reversed for temperature bias and lower boundary temperature errors. The Canada inversion is more sensitive than the Canal Zone calculations to temperature bias errors but the canal zone inversion is more sensitive than the Canada results to lower boundary

temperature errors. This is due to the nature of the errors. The effect of a temperature bias error is greater for the Canada inversion since the ozone profile peaks in a nearly isothermal region of the atmosphere. Because of this, the center of gravity (or hm) of the profile must change significantly to a region where the temperature profile has a strong slope in order to cause a significant radiance change. The Canal Zone solution, on the other hand, is much less sensitive to temperature errors since the profile peaks in a region where the temperature is increasing with altitude. The effect of a lower boundary temperature error is greater for the Canal Zone inversion since the transmittance of the entire atmosphere is larger. The transmittance is larger since the total ozone is smaller than for the Canada profile. With a higher transmittance, a given error in the lower boundary temperature will cause a greater error in the upwelling radiance (and hence in hm).

The error results show a relatively small latitudinal dependence. The errors which have the greatest effect on the error in total ozone are random radiance noise, lower boundary temperature errors, and absorption line intensity errors. Those which have the greatest effect on hm are random radiance noise, lower boundary temperature errors, and temperature profile bias errors. Fortunately, large temperature bias errors are unlikely to occur in practice since the temperature profiles that would be used would come from a temperature inversion method like that of Wark and Fleming (1966) which usually gives $\pm$ errors; i. e. the inverted temperature profile alternates $\pm$ in value around the true profile. Also, the other types of error can be controlled. As was pointed out in sub-section 3.2.3, the effective lower boundary temperature can be determined to within $0.5^{\circ}K$ or less and undoubtedly, errors in the absorption line intensities will eventually

be improved as work advances to eliminate defects in current theories regarding the ozone molecule. Once the accuracies of the absorption line intensities are increased, the entire ozone band can be used in the calculations thereby causing a reduction in the effective value of the random radiance noise. To determine the ultimate accuracy which can be expected for u and hm with the present inversion scheme, the conditions of Table III were imposed simultaneously. The best case values in Table III contain errors which have cancelling effects on each other and the worst case values contain errors which are all additive in effect. The values represent error limits presently attainable (for the lower boundary temperature and temperature profile errors) or limits which probably can be achieved in the future. The standard deviation of the radiance noise was selected in the following way: if the standard deviation of the radiance noise is 1%, which is currently possible, and if thirty wave numbers can eventually be used (once the accuracies of the absorption line intensities are improved), then the effective standard deviation can be reduced to $\sigma_{eff} = \frac{\sigma}{\sqrt{n'}} = \frac{1\%}{\sqrt{30'}} = 0.18\%$. This value can be simulated in the current calculations with $\sigma = .54\%$ since with nine wave numbers $\sigma_{eff} = \frac{.54\%}{\sqrt{9'}} = .18\%$. The remaining quantities of Table III are estimates of final accuracies. The resulting errors are given in Table IV. The mean error in total ozone ranges from 3.4% in the best case to -16% in the worst case with a standard deviation of about 4%. Thus, it is not unreasonable to expect that total ozone can eventually be determined to within 10% or less. Also, the error in hm varies from .15 km in the best case to -1 km in the worst case with a standard deviation of approximately .3 km. It would appear that this parameter can ultimately be determined to within about .5 km. However, some

TABLE III.

Errors Used in the Simultaneous Error Study of the Nadir Experiment

Type of Error	Best Case Values	Worst Case Values
Radiance noise	σ = .54%	σ = .54%
Radiance bias	$-.15 \times 10^{-5}$ watts/m-sr	$.15 \times 10^{-5}$ watts/m-sr
Temperature profile ±	3° K	3° K
Ozone absorption line intensity	4%	4%
Lower boundary temperature	$.4^{\circ}$ K	$-.4^{\circ}$ K

TABLE IV.

Errors in Total Ozone (u) and in the Altitude (hm) of the Maximum of the Ozone Profile When the Errors of Table III are Imposed Simultaneously

Location and date of sounding used in the study	Best Case Errors				Worst Case Errors			
	Error in u(%)		Error in hm(km)		Error in u(%)		Error in hm(k	
	Mean	Std. Dev.	Mean	Std. Dev.	Mean	Std. Dev.	Mean	Std. Dev
Albrook Fld., Canal Zone (9°N) 7/28/65	3.4	4.7	.17	.3	-16.0	3.5	-1.0	.4
Ft. Churchill, Canada (58.8°N) 3/16/65	6.7	3.4	.15	.16	-14.3	3.4	.28	.2

caution should be exercised here since Table I shows several errors in hm which are greater than .5 km even when all input errors are zero. The "all error" study indicates such small discrepancies because the two ozone profiles used in the study were matched reasonably well by Green's ozone function (3.2.31) thereby giving a small "zero error" for hm in both cases. This will not always be true as Table I shows. However, it is reasonable to expect, based on Tables I and IV, that hm can be determined to within about 1.5 km; at least for the large majority of profiles encountered in the atmosphere.

The calculations of Table IV were repeated for varying degrees of cloudiness in the troposphere. To simulate the effect of clouds, the effective lower boundary emission was computed by weighting emissions from the ground and cloud-tops according to the percentage cloud cover.[1] The clouds were considered to be black and the Planck radiance B_{eff} of the effective lower boundary was computed according to the following,

$$B_{eff} = B_{gnd}(1-P_{cL}) + B_{cL} \cdot P_{cL} \qquad (3.3.2)$$

where B_{gnd} is the Planck radiance at the ground temperature, B_{cL} is the Planck radiance at the cloud-top temperature, and P_{cL} is the percentage cloud cover. Altostratus cloud covers of 100% and 8% at 5 km were used for the Canal Zone and values of 100% and 12% at 3 km were

[1] The percentage cloud cover is not required in applying the inversion technique to flight data since cloud effects are treated indirectly by the method discussed in sub-section 3.2.3.

used for the Canada calculations. These conditions, exclusive of the complete cloud covers, are averages for the respective locations according to data published by London(1957). The calculations revealed only a small effect due to the presence of clouds. Negligible changes occurred in the errors of Table IV when partially cloudy conditions were used and the errors increased only slightly when a complete cloud cover was used. The means and standard deviations of the errors in u increased by about 2-3% and the errors in hm increased about .2 km. Therefore, it appears that the presence of clouds will not seriously degrade the inversion results as long as there is some contrast between the ozone spectrum and the effective lower boundary emission spectrum (see Appendix B).

Since the band model used in the error study did not allow for variation in absorption line intensity with temperature, a test was conducted to evaluate this effect. The line-by-line integration technique was used to compute the atmospheric transmittances for a mid-latitude ozone profile and a corresponding temperature profile. This was done for the reference temperature profile and a profile 10° K higher in temperature at every point. These two sets of transmittances were then used along with the reference temperature profile and (3.2.6) to compute the radiances at the top of the atmosphere. The results are plotted in Figure 19. The computations show a slight temperature dependence, mostly in the wings of the ozone band, but the effect is so small that it would not change the results of the error study significantly if it were included in the calculations. The inferred values of u and hm would differ by about 8% and .4 km respectively for the two spectra of Figure 19.

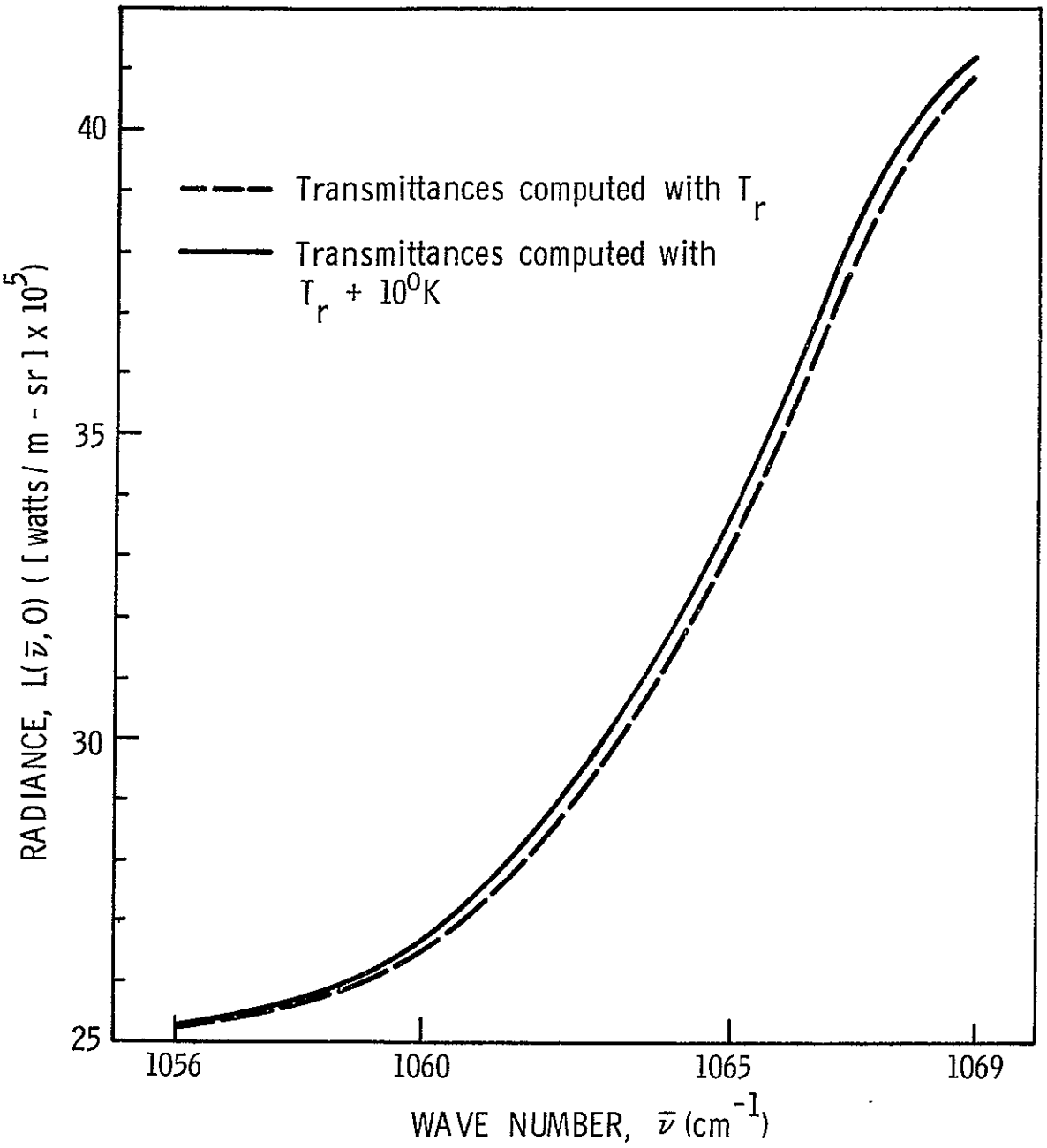

Fig. 19. Effect of temperature on the ozone spectrum.

This effect is large enough that it should not be neglected in precise calculations such as when applying the inversion method to actual radiances measured from a balloon or satellite.

3.4 APPLICATIONS

3.4.1 Palestine Data

The methods of section 3.2 were applied first to radiances measured from a balloon at the 31 km level above Palestine, Texas (31.8°N, 96°W). The measurements were made on May 8, 1966 in a flight conducted by the High Altitude Engineering Laboratory of the University of Michigan. The instrumentation and other details concerning the flight have been discussed in a report by Chaney, et al (1967). A breadboard version of an IRIS having a resolution of 5 cm^{-1} was used to make the radiance measurements and a typical spectrum from the experiment was presented in Figure 2. The data were of very good quality. The standard deviation of the radiance noise was only 0.5×10^{-5} watts/m-sr. which corresponds to a level of about 1.3% in the center of the ozone band and less than 1% in the wing region. This low noise made the data especially well suited to test the inversion method. Unfortunately, neither the total ozone nor the vertical ozone distribution were measured at the time and location of the balloon. Therefore, it was not possible to make a direct comparison between measured quantities and values determined from the inversion. However, the total ozone could be estimated for Palestine based on a Dobson measurement made nearby at Albuquerque, New Mexico (35° N, 106.6°W). The ozone amount at Albuquerque on the day of the balloon flight was .317 atm-cm (Muench,

1969) and since Palestine, Texas is located at a slightly lower latitude, the total ozone there should have been slightly less; a reasonable guess would be a value of .298 atm-cm. This estimate is based on a total ozone latitudinal gradient of .006 atm-cm/degree latitude as determined from data presented by Hering and Borden (1967). There was no vertical sounding at Albuquerque on the day of the balloon flight which could be used to estimate the altitude of the primary maximum in the ozone profile. Past measurements at the same time of year at Albuquerque indicate that the value of hm could lie anywhere in the range from about 23 km to 27 km.

Transmittances used in the inversions were calculated by the direct integration method rather than by the less accurate Random Exponential band model approach. As previously mentioned, direct integration calculations are very lengthy so they could not be performed on the University of Michigan time-sharing computer. The work was accomplished using a large block of free CDC-6600 computer time granted by the NASA Langley Research Center. The transmittances were computed each time they were needed as opposed to determining the values by interpolation in a transmittance library. A library could have been constructed based on the ranges of the three parameters P03m, Pm and H and on the range of temperature normally encountered in the atmosphere, but the time and expense required to construct a library is excessive if it will be used for only a few inversion calculations.

Inversions were attempted using the radiances in Table V and the atmospheric temperature profile measured in-situ from the balloon.

TABLE V

Palestine Data

Wave number (in cm^{-1})	Radiance $\bar{L}(\bar{\nu}, o)$ (in[watts/m-sr] x10^5)
1052.	37.2
1056.	38.6
1060.	45.2
1062.	50.3
1066.	61.5
1068.	66.8
1070.	70.8

A stable solution could be obtained only after water vapor line absorption was neglected in determining the lower boundary emission. This was equivalent to using background radiances which were too high; i. e. it was equivalent to having a positive error in the lower boundary temperature. The most likely reason the higher background emission was needed is that it compensated for a positive absorption line intensity error. Figures 11 and 12 show that positive errors in the lower boundary temperature and the absorption line intensity have cancelling effects on each other. A positive absorption line intensity error should be expected based on Figure 1. which shows that there is too much calculated absorptio over the spectral range of Table V for a homogeneous path. Other calculations with the Nimbus data also show that this is true for an atmospher path. The theory of cancelling error effects is plausible when estimates of the errors involved are considered. For example, the background radiance error was about 10^{-5} watts/m-sr. in the wings of the band.

This corresponds to a lower boundary temperature error of about $1^{o}K$. According to Figure 11, a $1^{o}K$ error, causes a total ozone error of about 25%. The error in absorption line intensity can be estimated from Figure 1. A representative error for the interval of Table V is about 35%. If the curve of Figure 12 is extrapolated, it shows that a 35% error causes a total ozone error of around -30%. When the two sources of error are combined the net result is a total ozone error of only about -5%.

There was almost complete cancellation of error effects for the spectral range 1060 cm^{-1} to 1070 cm^{-1} where the absorption line intensity error is large and positive. But this was not true for the remaining region of Table V (1052 cm^{-1} to 1060 cm^{-1}) where the absorption line intensity errors are different. Figure 1 shows that the absorption errors are smaller in the range 1052 cm^{-1} to 1060 cm^{-1} and the error changes sign; at 1052 cm^{-1} the error is almost zero and it is negative. Thus, when the wave numbers centered at 1052 cm^{-1} and 1056 cm^{-1} were included in the calculations the balance of error effects was upset. The effect of using these wave numbers was to cause the computed spectrum to shift upward in the wing region of the band. The shift was due to a change in slope of the spectrum in the wing region brought about by the least squares fitting procedure. The slope became progressively steeper as first 1056 cm^{-1} and then 1052 cm^{-1} was included. The steeper slope gave higher radiances at every point which corresponded to less ozone absorption and hence smaller ozone amounts. For example, when all wave numbers of Table V were used, the inverted ozone amount was .129 atm-cm; when the 1052 cm^{-1} wave number was dropped, the value of inferred

total ozone increased to .161 atm-cm. Finally, when both wave numbers were dropped to give good cancellation of error effects, the value of inferred total ozone increased to .294 atm.-cm. Since the balloon was not at the top of the atmosphere this value should be increased by about 5% to account for the ozone above the balloon. When this is done the inferred total ozone becomes .309 atm.-cm. This is in excellent agreement with the value estimated for Palestine, Texas. The Green ozone function (3.2.31) corresponding to this inversion is shown in Figure 20. The value of hm is 26.6 km which is within the expected range of values for the latitude and time of year of the measurement. These results, coupled with the results of the error study in section 3.3, prove the validity of the inversion method developed in sub-section 3.2.4. They also suggest a need for further work to increase the accuracy of the absorption line intensities. Because of the low noise level in the Palestine radiances, it was possible to ultimately perform the inversion using only five wave number centers in a narrow spectral interval (1060-1070 cm^{-1}). With this narrow interval, a cancellation of error effects due to absorption line intensity errors was obtained by adding positive background radiance errors. But such a narrow interval will not afford enough suppression of random radiance noise to permit accurate results for noise levels normally encountered (this is vividly illustrated in later calculations with the Nimbus III data); and when a wider interval is used to reduce the effective noise level, error effects no longer cancel for reasons previously discussed. Therefore, future calculations will have to be limited to a narrow spectral interval and to low noise data (less than about 1%) until absorption errors are improved.

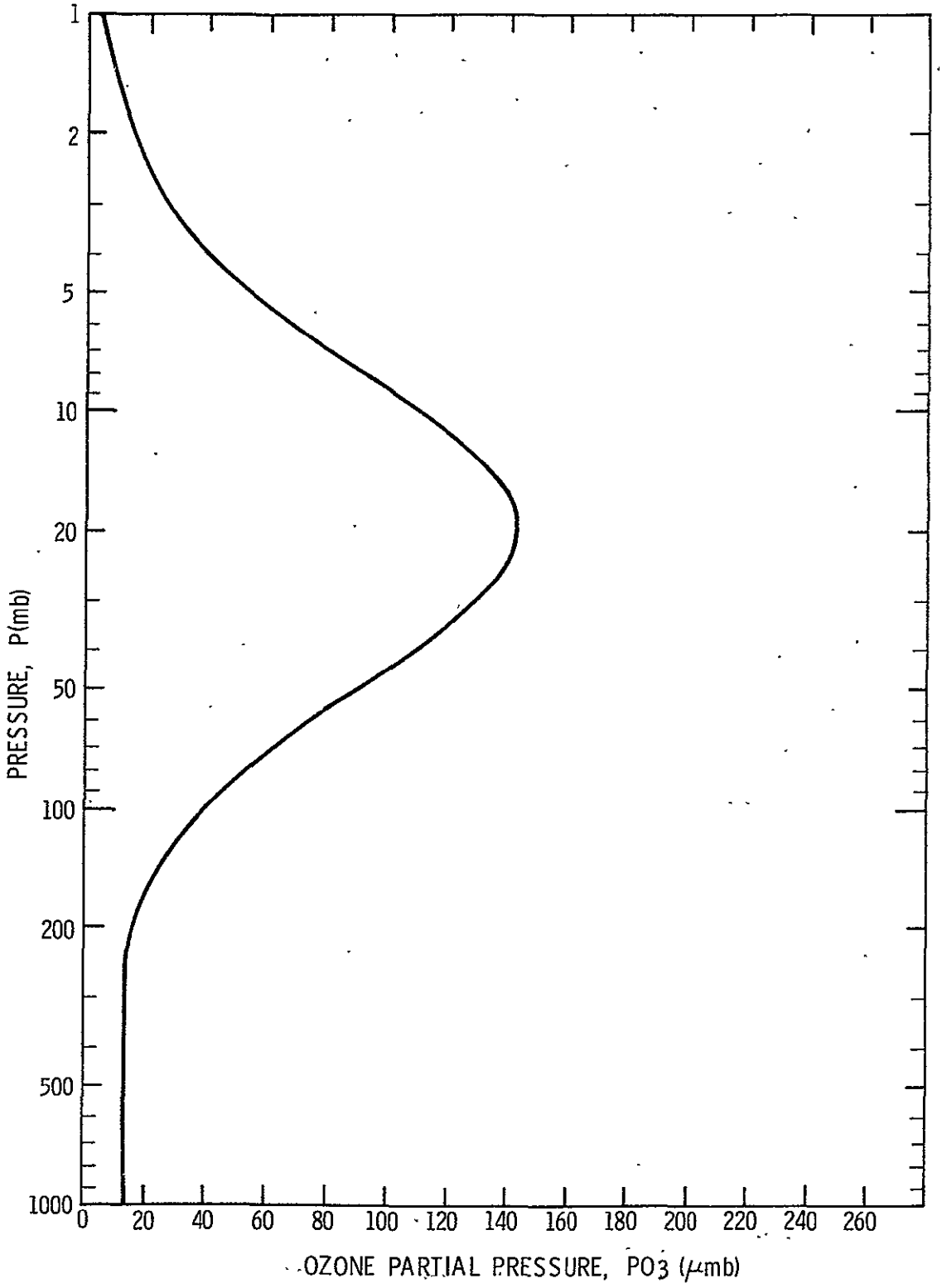

Fig. 20. Ozone profile inferred using radiances measured from a balloon above Palestine, Texas, May 8, 1966.

3.4.2 Nimbus Data

The methods of section 3.2 were also applied to radiances measured by an IRIS mounted on the Nimbus III satellite launched in April 1969. These data were kindly provided to the author before they were released for general distribution by Dr. B. J. Conrath of the NASA, Goddard Spaceflight Center, Greenbelt, Maryland. The location of the subsatellite point at the time of the measurements was 20.8°N, 70.9°W. This is very close to the Grand Turk Air Force Base (21.5°N, 71.1°W) where an ozonesonde observation was made less than twenty four hours before the satellite pass. Since daily ozone variations are quite small in the temperate zone, the ozone profile probably changed only slightly between the time of the ozonesonde launch and the time the radiances were measured. Therefore the ozonesonde data should be a good gauge for evaluating the inversion results.

Unfortunately, the Nimbus III measurements were of poor quality in the vicinity of 1042 cm^{-1}. The noise equivalent radiance was about $2x10^{-5}$ watts/m-sr. (Prabhakara, 1969b). This corresponds to an error of about 5% in the center of the ozone band and approximately 3% in the wing region. Considering the mean error to be 4% gives a 3σ radiance error of 12% and according to figures 10 and 16, this causes a 3σ total ozone error of about 96% and a 3σ hm error of about 7.7 km. Therefore it is anticipated that inversion results using the Nimbus data will be poor

Inversions were performed using the data of Table VI and the tem perature profile measured in-situ at the time of the ozonesonde observat The first inversion was attempted using background radiances that incluc ed water vapor line absorption and as with the Palestine data, the soluti

TABLE VI

Nimbus Data

Wave number (in cm^{-1})	Radiance $\bar{L}(\bar{\nu}, o)$ (in [watts/m-sr] x10^5)
1053.3	40.3
1055.4	42.1
1059.5	45.4
1061.6	49.0
1065.8	56.4
1067.9	59.5
1070.0	60.2

was unstable. Therefore water vapor line absorption was neglected for the same reason as was discussed in sub-section 3.4.1. When wave numbers less than a value of about 1060 cm^{-1} were used, the solution was also unstable. This was probably due to the combined influence of the high radiance noise and the imbalance of error effects brought about by absorption error differences in the spectral region below 1060 cm^{-1} (as discussed in sub-section 3.4.1). Finally, an inversion was performed using the same spectral range as was ultimately used with the Palestine data and the solution was barely stable. It did not converge until the seventh iteration. Usually, convergence is achieved in only three or four iterations. The inversion gave a total ozone of .062 atm-cm and a value for hm of 18.7 km. These correspond to errors of -76% and -6.3 km respectively which, as expected, are large errors. The error magnitudes are consistent with the values predicted from Figures 10 and 16. These results could be improved by using the entire ozone band to reduce the

effective noise level but as previously discussed, existing absorption errors prohibit this.

To evaluate typical absorption errors for an atmospheric path the radiance at the top of the atmosphere was computed using ozonesonde and temperature data taken at Grand Turk. Water vapor line absorption was considered in computing the background radiances and the line-by-line technique was used to compute the transmittances. Computed values were compared to the radiances measured at the satellite and the results are shown in Table VII. The quantity $\Delta L = \bar{L}_{mi} - \bar{L}_{ci}$ is the difference between the measured and calculated radiances. The table shows that there

TABLE VII

Differences Between Radiances Measured on-board Nimbus III and Radiances Computed Using the Corresponding Ozone Profile

Wave number (in cm^{-1})	Radiance Difference ΔL ([watts/m-sr] $x10^5$)
1053.3	-1.6
1055.44	.33
1059.5	1.5
1061.6	4.1
1065.8	4.7
1070.	1.4

is too much calculated absorption in the region 1060 cm^{-1} to 1070 cm^{-1} for the atmospheric path just as it is for the homogeneous path spectrum shown in Figure 1. This supports the argument of sub-section 3.4.1 that justified the need for positive background radiance errors because of the presence of positive absorption line intensity errors.

3.5 SUMMARY

There is only a small amount of information contained in radiances measured vertically from a satellite in the 1042 cm^{-1} spectral region. Because of this low information content, it is not necessary to use an elaborate function to characterize the vertical ozone distribution. A function was used that described the ozone profile in terms of just three parameters - P03m, Pm, and H. These correspond respectively to the maximum ozone partial pressure, the atmospheric pressure at the altitude of the maximum partial pressure, and a width factor. An inversion procedure was designed to select values for these parameters so that the computed ozone spectrum at the top of the atmosphere matched the measured spectrum in a least squares sense. It was shown that the calculations should include the entire ozone band to obtain a maximum reduction of the effective random radiance noise. The atmosphere was divided into two broad layers; an upper layer containing pure ozone and a lower layer devoid of ozone containing the earth's surface and all the atmospheric water vapor and clouds. The problems connected with computing the water vapor continuum and with considering clouds in the analysis were circumvented by following this procedure. The top of the lower layer was taken as the boundary under the satellite and the effective temperature of the layer was used to compute the lower boundary emission in the equation of radiative transfer. The effective temperature could be found to within 0.5^{o}K or less by considering water vapor line absorption in the calculations.

The least squares solution for the three parameters of Green's ozone function (3.2.31) was expanded in terms of the eigenvectors and eigenvalues of a solution matrix. A subsequent analysis using synthetic

clear sky radiances showed that under favorable conditions, measurement in the ozone band contain two pieces of independent information; the total ozone, u, and the altitude, hm (or pressure Pm), at the level of the maximum ozone partial pressure. An error study revealed that errors in u are most affected by random radiance errors, lower boundary temperatur errors, and ozone absorption line intensity errors. Errors in hm are most affected by the former two errors and by temperature profile bias errors. When all error sources were considered simultaneously the results showed that it should ultimately be possible to determine the total ozone to within 10% or less and to determine the altitude of the maximum in the ozone profile to within 1.5 km when the radiance noise level is 1% or less. These latter calculations were repeated for varying degrees of cloudiness in the troposphere. The data showed that the presence of clouc will not seriously effect results as long as there is some contrast between the ozone spectrum and the effective lower boundary emission spectrum (as discussed in Appendix B). Next the inversion technique was applied to balloon data measured over Palestine, Texas and to the Nimbus III satellite data measured over Grand Turk of the Bahamas. The Palestine data contained very low radiance noise and the corresponding inversion gave a value for u which was within about 3% of the value estimated from a nearby Dobson measurement. The value for hm could not be accurately estimated but the result obtained from the inversion was within the possib range of values indicated by past measurements made at the same genera location and time of year. The Nimbus III data were very noisy by comparison to the balloon measurements and this noise was reflected in the inversion. The inferred values for u and hm were off by 76% and 6.3 km respectively when compared to values determined by a simultaneous

ozonesonde observation. These errors are consistent with the predicted values of 96% and 7.7 km respectively as determined from the error study results and the estimated random radiance noise in the Nimbus III data. The application of the inversion technique to the Palestine and Nimbus data proved the validity of the inversion method and demonstrated the usefulness of the error study in predicting errors. The calculations also illustrated a critical need for further work to improve the accuracies of the absorption line intensities. The basic difference between the Palestine and Nimbus data was the radiance noise level; the noise for the Palestine radiances was low while the noise for the Nimbus data was comparatively high. It is believed that this is the underlying reason for the drastic differences in the inversion results for the two sets of data. If the absorption line intensities had been known with greater precision, a much wider spectral interval could have been used in the calculations thereby causing a significant reduction of the effective noise level in the Nimbus III data ans a substantial improvement in the results. These results indicate that to obtain accurate inversions, future calculations will have to be limited to a narrow spectral interval and to low noise data (less than about 1%) until absorption errors are improved.

CHAPTER 4

THE HORIZON EXPERIMENT

4.1 INTRODUCTION

The use of infrared measurements of the horizon (or limb) of the earth is an attractive remote sensing approach. It provides the advantage of no background interference since the radiometer measures atmospheric emissions against the blackness of space. This simplifies the analysis as compared to the analysis of nadir measurements because the lower boundary emission term in the equation of radiative transfer can be neglected. Furthermore, the horizon experiment affords excellent vertical resolution. Figure 21 illustrates the geometry.[1] It can be shown that the path length along the line of sight at a given tangent height Z_k is much greater for the tangent layer than for any other layer. Thus a large percentage of the ozone mass along the line of sight lies in the tangent layer. In addition to this geometrical factor, the ozone density decreases with altitude for level above about 25 km. These factors acting simultaneously assure that most of the ozone mass will be concentrated near the tangent point for a large part of the ozone profile. Consequently, it should be possible to obtain detailed information from horizon measurements regarding the vertical ozone distribution. This is in sharp contrast with the small amount of information which could be inferred from vertically measured radiances.

The energy sensed by a limb viewing radiometer depends on the amount and distribution of the emitting gas as well as the temperature of the atmosphere. Therefore, the temperature distribution must be found

---

[1] Figure 21 is drawn grossly out of scale. In reality the ozone atmosphere (≈60 km and below) crossed by a horizontal ray path is confined within an angle of only ± 6 degrees or less with respect to a vertical line going through the tangent point for tangent heights of 10 km and higher. The tangent height is defined as the altitude above the surface where the line of sight intersects the radius vector of the earth perpendicularly.

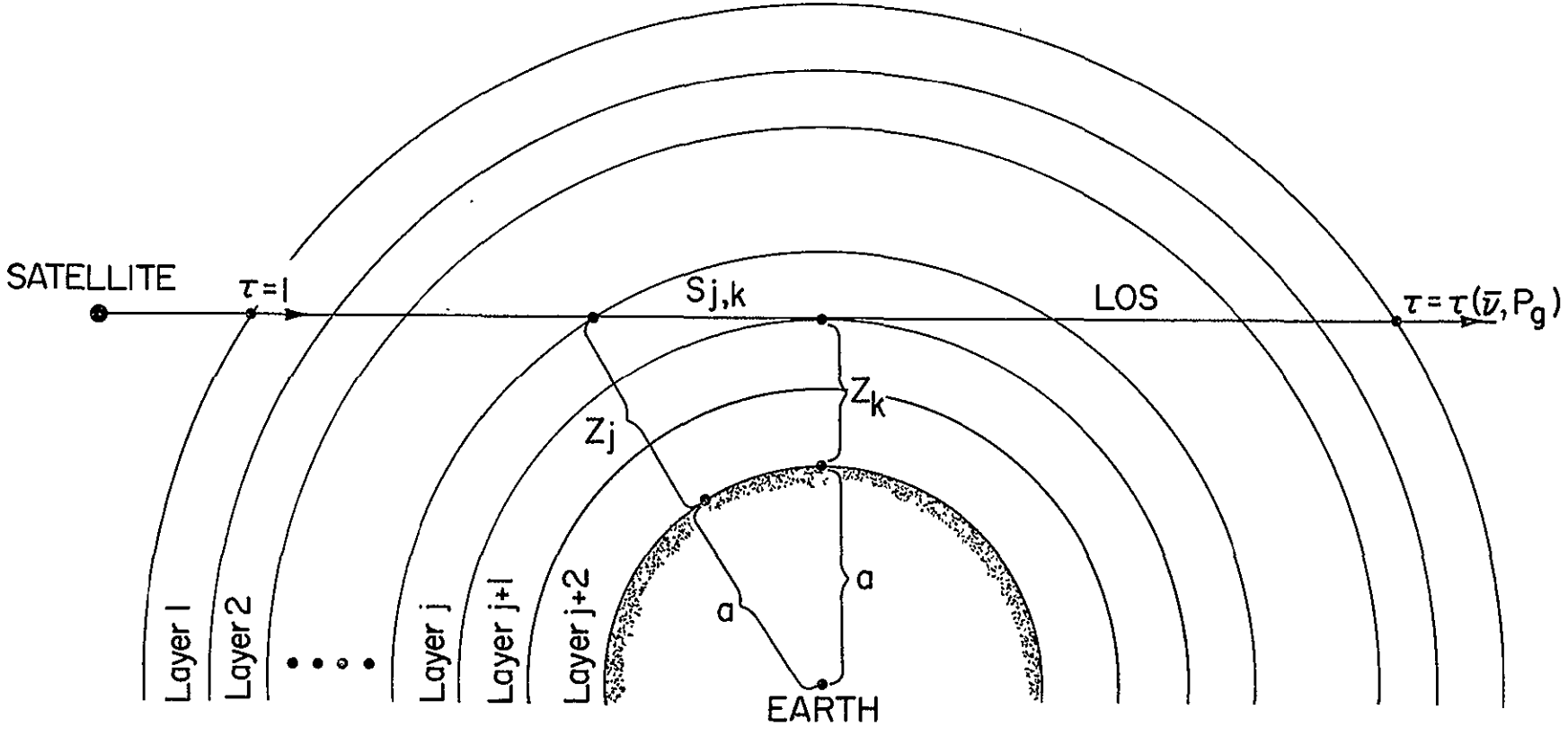

Fig. 21. Horizon geometry.

before a constituent inversion can be performed. This should be done using simultaneous horizon measurements to obtain temperature data at a sufficiently high altitude and to obtain time and space correlation betwee the temperature inferences and other limb measurements.[1] Several authors have analyzed the limb temperature inversion problem and as in t nadir experiment, they used the 667 cm^{-1} band of CO_2 (Gille, 1968b; McKee, et al, 1969a; House and Ohring, 1969; Burn and Uplinger; 1969). Once the temperature profile is known, information regarding the variabl gases, H_2O and O_3, can be inferred from measurements in the appropria absorption bands. House and Ohring (1969) and McKee, et al (1969b) usec the 315 to 475 cm^{-1} spectral region to deduce water vapor profiles and these authors suggested using the 1042 cm^{-1} region to infer ozone information. The purpose of this present work is to evaluate the feasibility of their suggestion.

4.2 ANALYSIS

4.2.1 Basic Relations

Calcuations in this chapter will incorporate the following assumpti

(a) The atmosphere is spherically stratified and spherically symmetric.

(b) Scattering at the wavelengths under consideration can be neglected.

(c) Atmospheric refraction can be neglected.

(d) Ozone is in local thermodynamic equilibrium up to an altitude of 60 or 70 km (Kuhn and London, 1969)

---

[1] While it may be possible in the future to obtain temperature data up to a high altitude from the nadir experiment, current methods allow accurate temperature inferences only up to an altitude of about 30 km.

All of these assumptions are adequate for the current feasibility study, however, in calculations involving flight data, (a) and (c) will have to be reconsidered. The consequences of assuming spherical symmetry and neglecting refraction have been discussed by Davis (1969) and Bates, et al (1967) respectively. The energy detected by a radiometer aimed toward the horizon is related to the gas concentration and atmospheric temperature through the equation of radiative transfer. If measurements are made at altitudes above the clouds, there is no emission from the lower (or far) boundary since the boundary is space. Therefore, the radiative transfer equation for a single wave number $\bar{\nu}$ and a tangent height Z_k can be written,

$$L_{Z_k}(\bar{\nu}) = -\int_1^{\tau(\bar{\nu}, P_g)} B_{Z_k}\left[\bar{\nu}, T(P)\right] \; d\tau_{Z_k}(\nu, P) \qquad (4.2.1)$$

where $\tau(\bar{\nu}, P_g)$ is the transmittance along the line of site (LOS) from the satellite to the far boundary of the atmosphere (refer to Figure 21.) and where the k subscript refers to values for the LOS passing through a tangent point corresponding to Z_k. The radiometer field of view in a horizon experiment is very narrow to allow good vertical resolution and atmospheric emissions are quite weak. Consequently, the detected energy is low. Accordingly, a wide bandwidth instrument is used to collect the maximum possible amount of energy. Thus the measured radiance can be represented analytically by the integral of (4.2.1) over the range of the radiometer bandwidth, that is

$$L_{Z_k} = -\int_{\Delta\bar{\nu}} \int_1^{\tau(\bar{\nu}, P_g)} B_{Z_k}\left[\bar{\nu}, T(P)\right] \, d\tau_{Z_k}(\bar{\nu}, P) \, d\bar{\nu} \qquad (4.2.2)$$

where $\Delta\bar{\nu}$ is the bandwidth. It is assumed in writing (4.2.2), that the radiometer instrument function $\phi(\bar{\nu})$ is square over the interval $\Delta\nu$. However, any function could be used (in the manner described by equation 3.2.7) if its form is known. Equation (4.2.2) is the basic relation needed for all remaining calculations in this chapter. The Planck radiance $B_{Z_k}\left[\bar{\nu}, T(P)\right]$ is computed according to (3.2.2). Since the present work is a feasibility study, the transmittance is calculated by the Random Exponential band model according to (3.2.24) rather than by the more accurate (but very time consuming) direct integration method. Each of these methods was discussed in Chapter 3. Equation (3.2.24) is repeated here for convenience.

$$\overline{\tau_{Z_k}(\bar{\nu}, \bar{P}_{i,k})} = \exp\left[-\frac{(\beta_{\bar{\nu}}/d) \cdot \bar{u}_{i,k}}{\left(1+2\left[\frac{\beta_{\bar{\nu}}}{2\pi\alpha_{Lo}(\bar{\nu})}\right] \cdot \bar{\ell}_{i,k}\right)^{1/2}}\right] \qquad (4.2.3)$$

The k subscript of (3.2.24) has been changed to a double i, k subscript in (4.2.3) which refers to the value in the ith layer along the LOS passing through the kth tangent point. Figure 21 shows that each jth layer is crossed twice during a horizontal pass through the atmosphere. But it is recalled that the quantities $\bar{P}_{i,k}$, $\bar{u}_{i,k}$ and $\bar{\ell}_{i,k}$ must be computed for an equivalent homogeneous layer according to the Curtis-Godson approximation as described in Appendix A. Thus the i subscript refers to the ith Curtis-Godson layer which is crossed only once. The only difference in these calculations as compared to the nadir analysis is that the homogeneous layers are determined in a horizontal direction along the LOS for each tangent point rather than in the vertical direction. Equation (4.2.3) is the transmittance expression for a Lorentz line shape. This

shape was adequate for the nadir analysis since the path length in any layer was very short. But in the horizon experiment, it is possible to have very long paths at low pressures. Therefore, the Voigt and Doppler profile functions should be included in the calculations. This was accomplished through the use of a correction table published by Gille and Ellingson (1968). The table was developed specifically for correcting transmittances computed with the Random Exponential band model and a Lorentz line shape. The corrections were based on the values of the quantities,

$$Y(\bar{\nu}_o) = 2\left(\frac{\alpha_L}{\alpha_D}\right) = \frac{2\,\alpha_{Lo}\cdot c}{P_o}\sqrt{\frac{m_{o_3}\,T_o}{2\,k\,\ell n 2}}\cdot\frac{\bar{P}_{i,k}}{(\bar{\nu}_o\cdot\bar{T}_{i,k})} \qquad (4.2.4)$$

and

$$R(\bar{\nu}_o) = \left[\frac{\beta_{\bar{\nu}_o}}{2\pi\alpha_{Lo}}\right]\cdot\bar{\ell}_{i,k} \qquad (4.2.5)$$

where α_{Lo}, P_o, and T_o are the Lorentz half-width, pressure and temperature respectively at standard conditions. The values of the effective temperatures $\bar{T}_{i,k}$ were computed according to,

$$\bar{T}_{i,k} = \frac{\int_o^{\bar{u}_{j,k}} T_{j,k}\,du}{\bar{u}_{j,k}} \qquad (4.2.6)$$

where the j subscript refers to the temperature values at the boundaries of each layer along the LOS. The remaining relationships used in this chapter involve the pressure P_k, the geometric length $S_{j,k}$ along the LOS, and the mass path $u_{j,k}$ in a layer of length $S_{j,k}$ (refer to figure 21.) Since measurements in a horizon experiment are altitude referenced, it

is necessary to use the hydrostatic relationship to compute the pressure at each tangent point. Thus

$$P_k = P_o \exp\left\{ -\frac{M}{R_o} \left[\int_o^{Z_k} \frac{g(Z)}{T(Z)} \, dZ \right] \right\} \qquad (4.2.7)$$

where M is the mean molecular weight of air and R_o is the universal gas constant. The quantity P_o is the pressure at the surface of the earth taken here to be 1013mb. The quantity $S_{j,k}$ can be computed from the geometry of Figure 21 as follows,

$$S_{j,k} = \left[(a+Z_j)^2 - (a+Z_k)^2 \right]^{1/2} \qquad (4.2.8)$$

where a is the radius of the earth. The value of $S_{j,k}$ in (4.2.8) is the distance from the tangent point out to the boundary of the jth layer. The value of $u_{j,k}$ for a layer starting at the tangent point and extending outward along the LOS can be computed from the relation

$$u_{j,k} = \int_o^{S_{j,k}} \rho O_3 \, dS \qquad (4.2.9)$$

or

$$u_{j,k} = \int_o^{S_{j,k}} q \cdot \rho \, dS \qquad (4.2.10)$$

where q is the ozone mass mixing ratio, ρO_3 is the ozone mass density, and ρ is the atmospheric mass density. Equation (4.2.10) can be further manipulated using the equation of state of an ideal gas to give

$$u_{j,k} = \frac{M}{R_o} \int_o^{S_{j,k}} \frac{q \cdot P}{T} \, dS \qquad (4.2.11)$$

When the mixing ratio is expressed in a form that yields units of atm-cm for $u_{j,k}$ we have,

$$q = \frac{A_v}{M \cdot n_s} \cdot \frac{PO_3}{P} \qquad (4.2.12)$$

where A_v is Avogadro's number, n_s is the number density of air at standard conditions, and PO_3 is the ozone partial pressure. Inserting (4.2.12) into (4.2.11) gives

$$u_{j,k} = \frac{A_v}{R_o \cdot n_s} \int_o^{S_{j,k}} \frac{PO_3}{T} \, dS \qquad (4.2.13)$$

The absorber amounts computed by (4.2.13) are for one-half of the atmosphere on either side of the tangent point along the LOS. The values for the opposite half of the atmosphere are the mirror images of the values for the first half since spherical symmetry is assumed.

4.2.2 The Inversion Method

The purpose of this sub-section is to develop a method for inferring an ozone profile starting with a measured horizon radiance profile and a known temperature distribution. It would appear that it is possible to infer the entire ozone profile since as the radiometer scans the limb from the top of the atmosphere downward, it views a different layer of the horizon at each new tangent point. However, it may be difficult to recover all of the ozone profile in this way. At each

successively lower tangent point, the radiometer must look through the atmosphere above that point and the atmosphere from above could mask any new information provided by energy coming from the lower layer. Fc example if the atmosphere becomes opaque at some low altitude, it would be impossible to infer information about the new layer. Thus it can be expected that there will be a lower limit to the limb technique irrespectiv of the limit which arises because of clouds. This will be discussed in more detail later.

The so-called "onion peeling" approach will be used in this study to develop the inversion procedure. The atmosphere is divided up into layers and the inversion begins with the top-most layer for which there is a measurable radiometer signal. Once the inversion is complete in the first layer, the next lowest slab is added and an inversion is performed for that layer. This procedure continues until the lower altitude limit is reached. This is the approach followed by McKee, et al (1969a and 1969b The initial step in the solution procedure for the current work is to make a linear approximation for the relationship between the measured radianc the calculated radiance, and the ozone partial pressure at the lower boun ary of a layer as follows,

$$L_{mk} = L_{ck} + \frac{\partial L_{ck}}{\partial P0_3} \Delta P0_3 \qquad (4.2.14)$$

where, as before, the k subscript refers to the kth tangent point. Equati (4.2.14) is a Taylor series expension with the higher order terms truncated. The quantities L_{mk} and L_{ck} are the measured and calculated radiances respectively. $P0_3$ is the ozone partial pressure at the bottom of a layer and $\Delta P0_3$ is a pertubation parameter. The final value of the

ozone partial pressure is determined by iteration. The procedure begins with a guess for $P0_3$ at the bottom of the first layer. Next, the partial pressure is computed at the bottom of each successive higher layer assuming a constant ozone mixing ratio.[1] After this, L_{ck} is calculated using (4.2.2), the partial derivitive is determined by letting $P0_3$ change by a small amount, and (4.2.14) is solved for the perturbation term $\Delta P0_3$ according to,

$$\Delta P0_3 = \frac{\Delta L}{\left(\frac{\partial L_{ck}}{\partial P0_3}\right)} \qquad (4.2.15)$$

where ΔL is the difference $(L_{mk}-L_{ck})$. The quantity $\Delta P0_3$ is then added to the original guess for $P0_3$ and the process continues until some convergence criteria are met. These criteria are specified later. Once $P0_3$ is known for the first layer, it is used as an initial guess for the partial pressure at the bottom of the next lowest slab and the iteration is performed for that layer and so on. In reality the quantity ΔL contains errors; measurement errors arise in L_{mk} and all other errors occur in determining L_{ck} Therefore (4.2.15) can be expressed in the form,

$$P0_3 = \frac{\Delta L}{D} + \frac{\epsilon}{D} \qquad (4.2.16)$$

---

[1] It is recalled from Chapter 2 that the assumption of a constant ozone mixing ratio is very good for the upper stratosphere during both the day and night. But this will not be true in the nighttime mesosphere if the secondary maximum at around 70 km exists.

where ϵ represents the equivalent radiance error and D is the derivitive $\partial L_{ck}/\partial P0_3$. The reason for a lower altitude limit is now clear. As the radiometer probes deeper and deeper into the atmosphere the derivitive D continually decreases because the ozone absorption across the horizon approaches opacity. Consequently the error term is magnified. In the extreme, if opacity is reached a solution is not possible since D will equal zero. Equation (4.2.16) is a mathematical statement of the discussion in the first part of this sub-section regarding a lower altitude limit to the horizon technique. This can also be illustrated using the vertical weighting function along a LOS. This function is defined by the change in transmittance along the LOS with respect to the vertical coordinate Z. It shows in an indirect way, the distribution of energy being emitted along the LOS. If the function peaks at the tangent point then the energy emitted along the LOS is localized near the tangent point and the inversion will not be very sensitive to errors. If on the other hand, the function peaks somewhere else and is broad, then the energy emitted by the atmosphere is distributed all along the LOS (the atmosphere is more nearly opaque) and an inversion will be difficult. Since every altitude except the tangent point altitude is crossed twice during a horizontal pass through the atmosphere the weighting functions anterior and posterior to the tangent point must be summed in computing the total vertical weight. Thus

$$W_k = \left[\frac{\partial \tau (\Delta \bar{\nu}, Z)}{\partial Z}\right]_a + \left[\frac{\partial \tau (\Delta \bar{\nu}, Z)}{\partial Z}\right]_p \qquad (4.2.17)$$

where W_k is the weighting function for a LOS passing through Z_k and the subscripts a and p denote anterior and posterior respectively. The $\Delta\bar{\nu}$ argument is to indicate that the transmittance is averaged over the entire ozone band of width $\Delta\bar{\nu}$. Equation (4.2.17) is plotted for various tangent points and a high latitude ozone profile in Figure 22. The figure shows that it will be difficult to infer ozone information at altitudes lower than about 25 km. For example the radiance measured on a LOS passing through Z_k = 17 km would not arise mainly from near the tangent point but would instead come from points all along the LOS covering the vertical range 17 to 50 km. This information can also be displayed quantitatively by plotting the ratio R_L of the radiance coming from the tangent layer to the total radiance. The tangent layer radiance is computed according to

$$L_{Z_k}(\text{tangent}) = -\int_{\Delta\nu}\int_{\tau_b}^{\tau_e} B\left[\bar{\nu}, T(P)\right] d\tau\,(\bar{\nu}, P)\, d\bar{\nu} \qquad (4.2.18)$$

where τ_b and τ_e are the transmittances along the LOS at the beginning and end of the tangent layer respectively. R_L is shown as a function of altitude in Figure 23. The quantity has a value of 43% at 37 km and it steadily decreases at lower altitudes finally becoming less than 9% at 17 km. Plots of W_k and R_L for a low latitude ozone profile are very similar to Figures 22 and 23. Thus, scanning from the top of the atmosphere downward, the inversions should become increasingly sensitive to errors for successively lower tangent points since the proportion of the measured radiance which arises in the tangent layer will continually diminish. The prospects do not appear to be very good for obtaining ozone information in the lower stratosphere. These results suggest that an inversion will

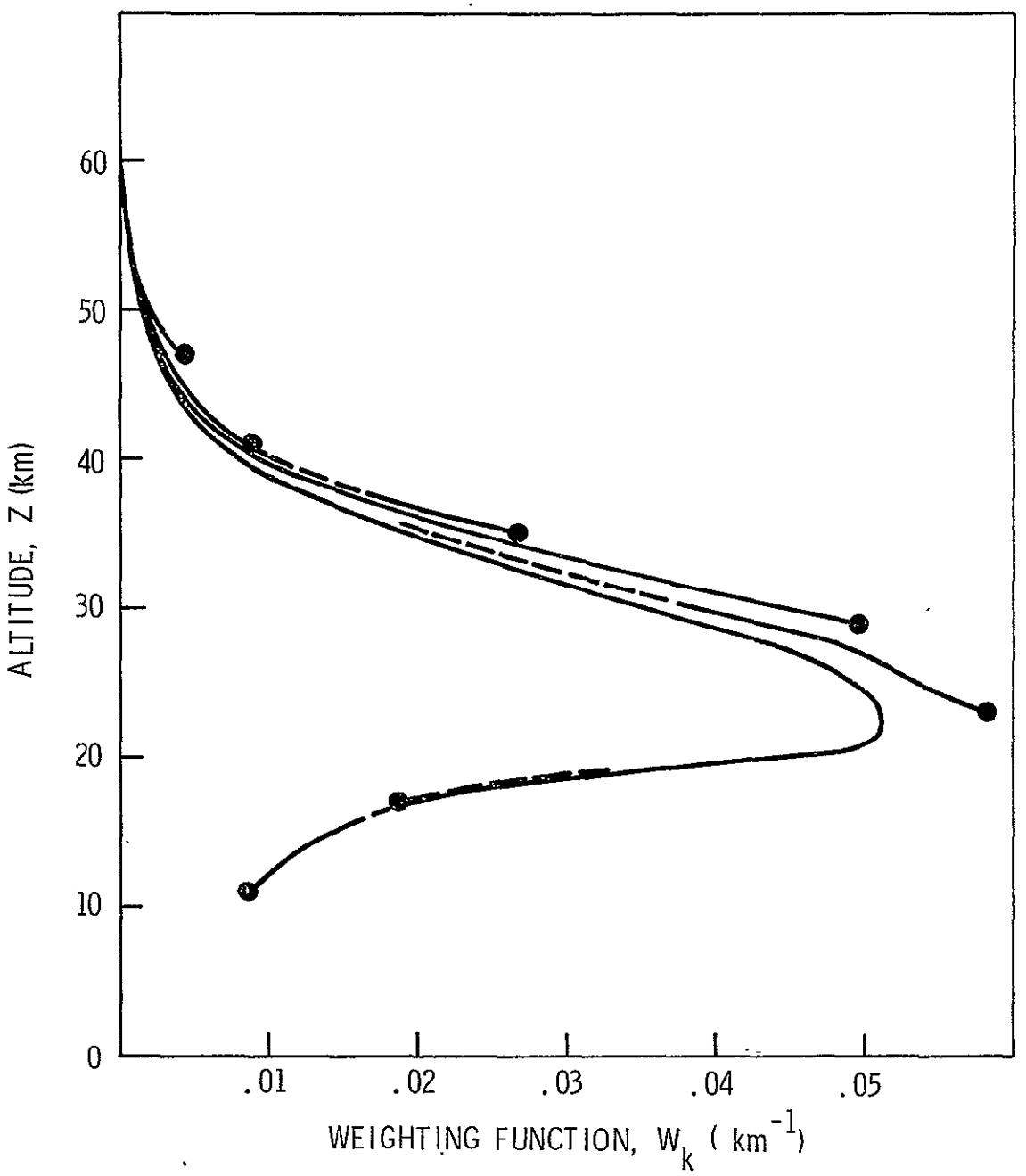

Fig. 22. Vertical weighting function over the interval 995 to 1070 cm^{-1} for a high lattitude ozone profile. Complete weighting function shown at 12-km intervals. Dots indicate tangent heights.

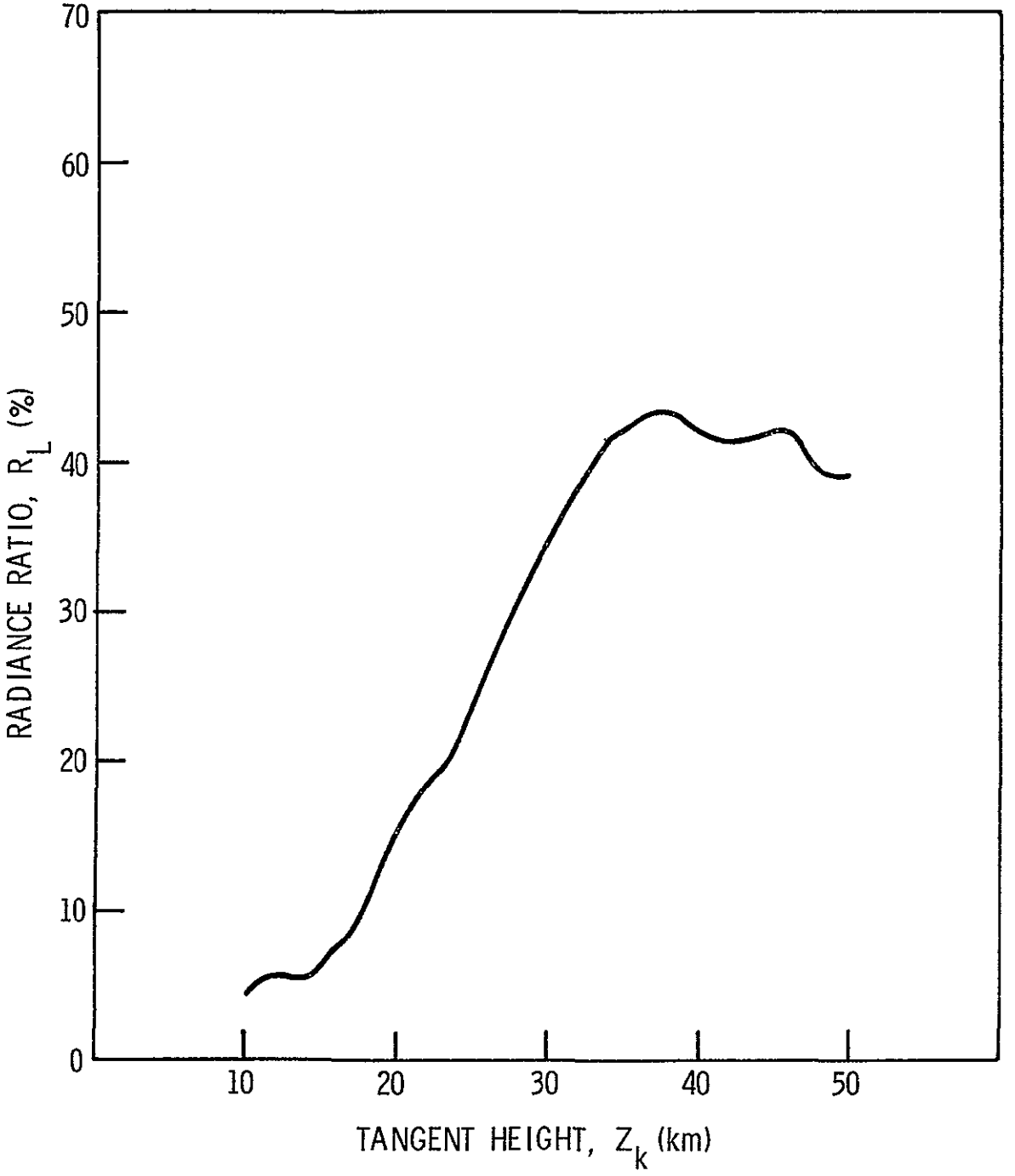

Fig. 23. Ratio of the radiance emitted by the tangent layer to the total radiance versus tangent height for a high latitude ozone profile.

be feasible in the lower region only when the radiance noise is very low and other input errors are small. The sensitivity of the inversion technique to various errors is studied in the next section for the entire range of the ozone profile down to the tropopause.

4.3 ERROR STUDY

The procedures followed in this analysis were similar to those used in the nadir study. Horizon radiance profiles were generated using (4.2.2) and the Air Force Cambridge Research Laboratories measurements referenced in section 3.3 These synthetic radiance profiles were then used as measured values in studying the inversion technique. Transmittances used in the calculations were determined for a temperature of $250^{o}K.$[1] Spectral radiances were computed at 5 cm^{-1} intervals throughout the absorption band and these values were integrated against wave number to give the total radiance. The calculations were performed for 2 km thick layers. This thickness gave radiance differences for two successive tangent points which were sufficiently above the anticipated noise level of a practical radiometer and provided at the same time, sufficient vertical resolution to define the ozone profile. Convergence criteria were imposed on the difference $\Delta L = L_{mk} - L_{ck}$ and on the perturbation parameter $\Delta P0_3$. The iteration was stopped when either $\Delta L \leq .01$ watts/m^2-sr. or $\Delta P0_3 \leq .1$ mb. These limits were selected to give sufficient accuracy in a minimum of computing time.

---

[1] Calculations showed that the variation of transmittance with temperature has a negligible effect on the total band radiance for a given tangent point.

The error study was designed to establish the lower altitude limit of the inversion approach of section 4.2 and to identify those errors which have the greatest effect on the results. Errors in various quantities were added one at a time and inversions were performed to determine the effects. The types and ranges of errors used are given in Table VIII. The types of error in Table VIII are those which normally would be encountered in an actual experiment and the ranges include values which allow clear identification of the most important error effects.

TABLE VIII

Types and Ranges of Errors Used For the

Analysis of Individual Error Effects in the Horizon Experiment

Type of Error	Range
Random Radiance Noise, Normally distributed with a mean of zero	$\sigma = .02$ watts/m^2-sr.
Radiance Bias	$\pm .03$ watts/m^2-sr.
Radiance Scale	$\pm$ 3%
Tangent Height	$\pm$ 1 km
Ozone Absorption Line Intensity	$\pm$ 15%
Surface pressure	$\pm$ 5%
Temperature Bias	$\pm 3^{\circ}K$

The first series of calculations were performed for a Thule, Greenland ($76.5^{\circ}N$) sounding. The ozone, temperature, and horizon radiance profiles used in the computations are shown in Figure 24. These data represent typical high latitude conditions. A series of

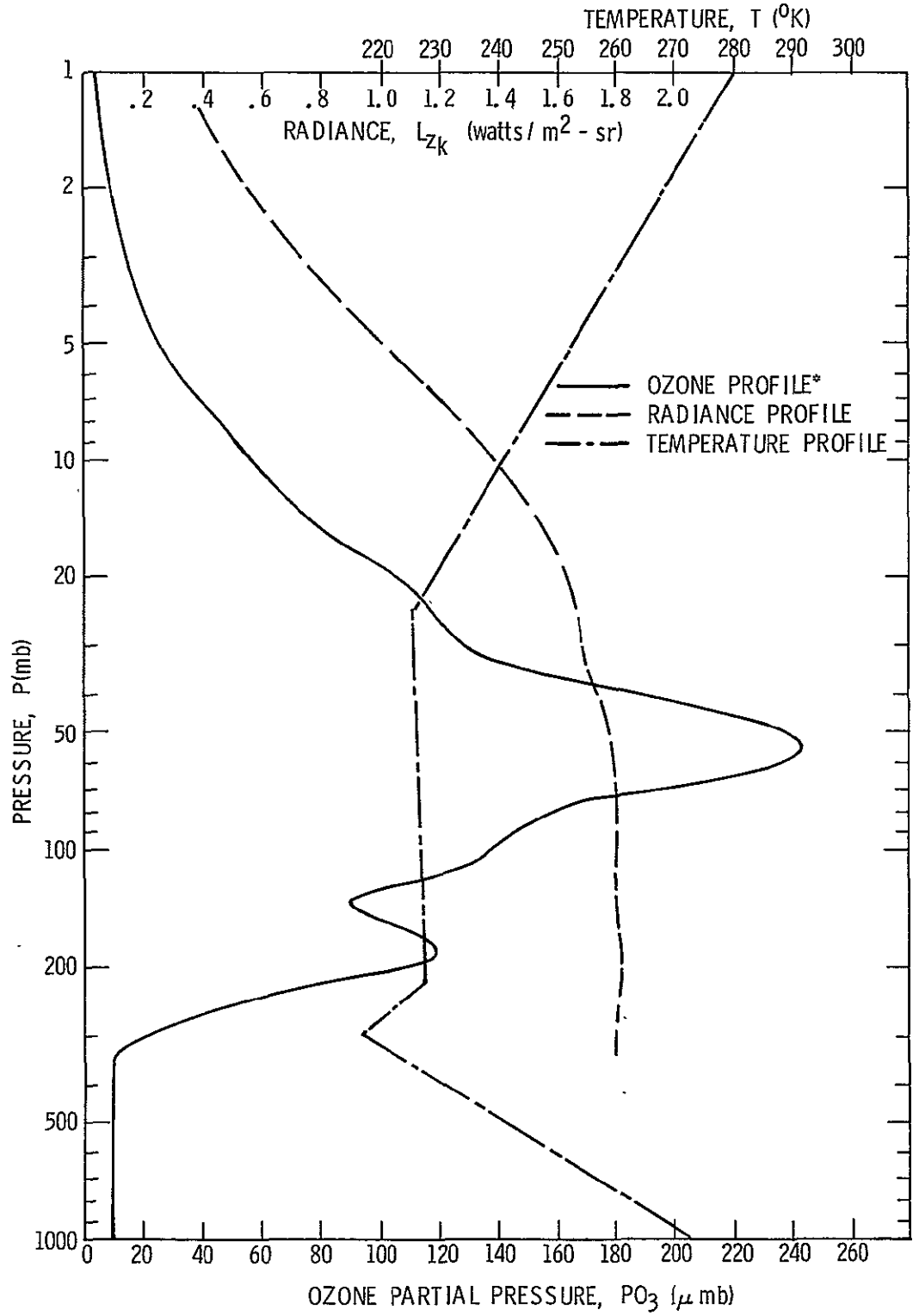

*The ozone profile above 8mb was determined by extrapolation assuming a constant ozone mixing ratio.

Fig. 24. Ozone, radiance, and temperature profiles for a Thule, Greenland (76.5°N) sounding.

calculations were also made for a low latitude sounding and these results are presented later. The effects of specific errors are considered in the following paragraphs.

Random Noise - The inversion of the radiance profile of Figure 24. with random noise added to the radiances is shown in Figure 25. by clear circles. The solid circles will be discussed subsequently. Figure 25. shows that the solution becomes intolerably sensitive to noise near the level of the primary maximum in the profile. A reduction of these errors was accomplished by using segmented quadratic smoothing of the radiance data. The radiance profile was separated into three segments and a quadratic was fitted, in a least squares sense, to each of the segments. The end point of the first quadratic solution was used as the beginning point in finding the next and an average value was taken at the end point of the overlapping quadratics to reduce the magnitude of any discontinuity present. The solid circles are the inversion results using data smoothed in this manner. The results are still strongly effected by the noise but they represent a substantial improvement over the solution obtained using unsmoothed data. Similar results using radiances for a Green Bay, Wisconsin and an Albrook, Field Canal, Zone sounding are shown in Figures 26 and 27 respectively. The inversions in an actual experiment may not be as poor as these results indicate since practical noise levels will probably be only one-half the value used in the calculations (McKee, et al, 1969b). Even though the inversion is irregular in the lower stratosphere, it still contains information regarding the ozone profile. Some of this information can be recovered by fitting, in a least squares sense, the three parameter Green function (3. 2. 31) to the solution.

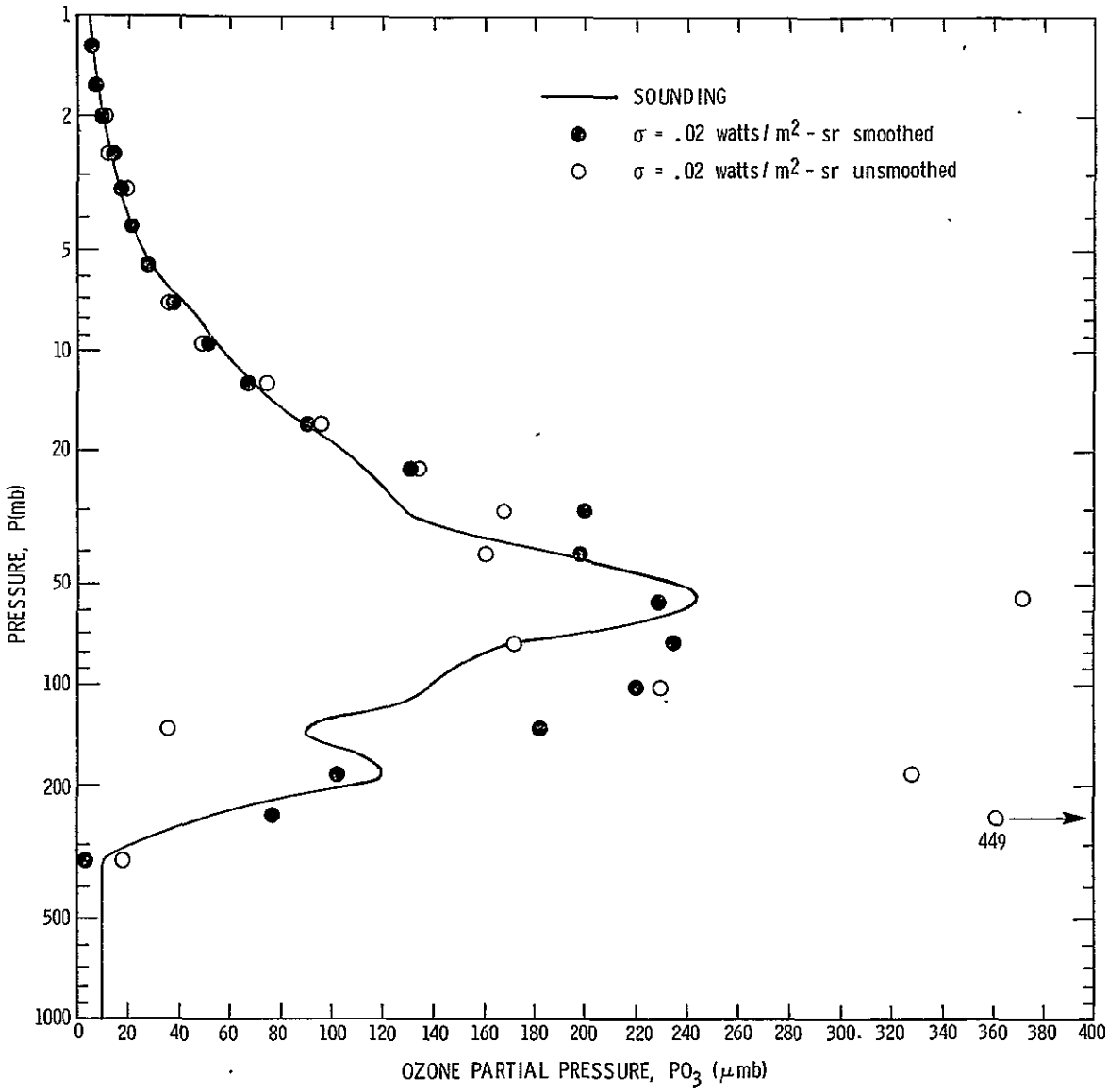

Fig. 25. Radiance random noise results—Thule, Greenland (76.5°N).

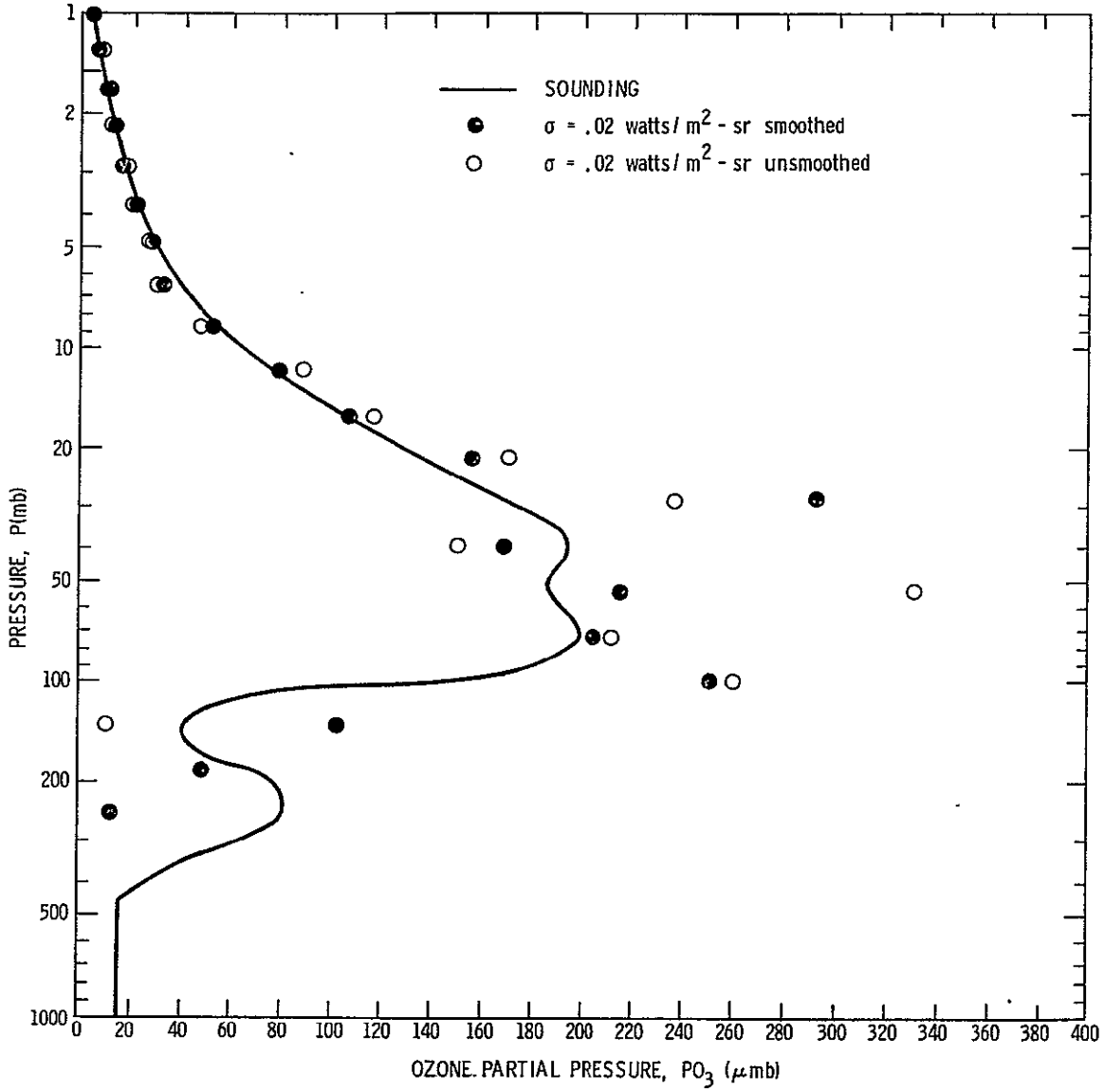

Fig. 26. Radiance random noise results—Green Bay, Wisconsin (44.5°N).

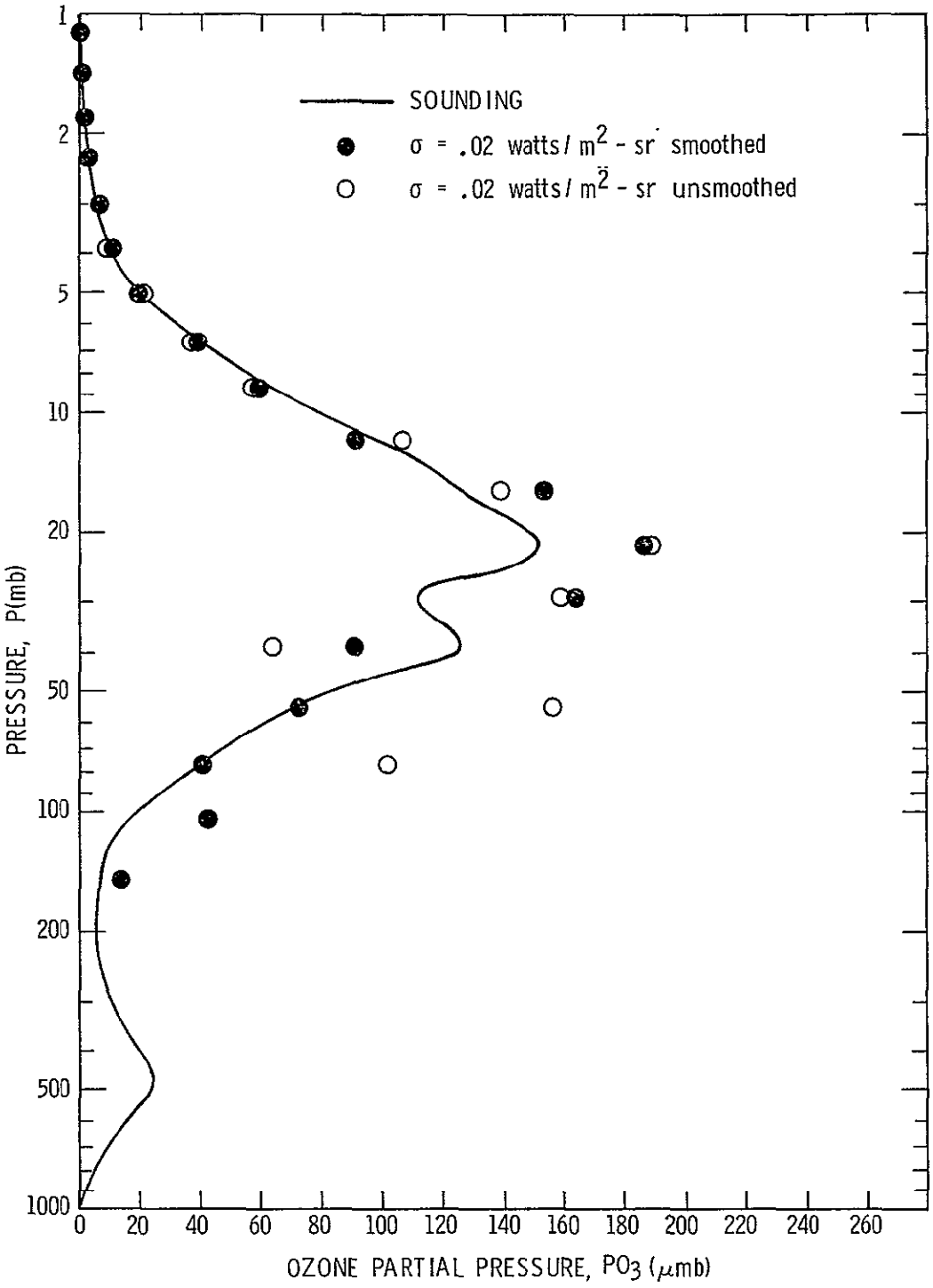

Fig. 27. Radiance random noise results—Albrook Field, Canal Zone (9°N).

This was done for six different inversions, corresponding to six different ozone profiles. The inversion points near the peak of the ozone profile were excluded in this procedure since they correspond to the region of the atmosphere which is nearest to opacity and hence the region where the inversion is most sensitive to errors. The results are presented in Table IX which shows the error in the altitude, hm, of the primary maximum in the ozone profile. The results show that it should be possible to determine hm to within 2 km by this method. Certainly the determination of hm will not always be as good as the values of Table IX would suggest since other error sources will influence the result. Also, an estimate of the ultimate accuracy should be based on a larger number of cases. The main significance of these calculations is they show the feasibility of a method for determining hm which can be used even when fairly large random noise is present. The effects of the remaining types of error on inversions with the Thule, Greenland data will now be considered.

TABLE IX

Error in the Altitude (hm) of the Primary Maximum in the Ozone Profile for the Horizon Experiment with Random Radiance Noise of σ=. 02 watts/m^2-sr.

Location of Sounding Used in the Study	Error in hm (in km)
Canal Zone (9°N)	.25
Florida (30.4°N)	-.05
Wisconsin (44.5°N)	-.7
Canada (58.8°N)	-.3
Greenland (Spring) (76.5°N)	.1
Greenland (Fall) (76.5°N)	1.35

Radiance Bias Error- The errors in ozone partial pressure for radiance bias errors are shown in Figure 28. A positive radiance bias, i. e. a higher measured radiance, would appear as a higher atmospheric emission. More emission is obtained by adding ozone to the atmosphere. Hence the ozone error is positive. A negative radiance bias yields converse results. The ozone error steadily increases as pressure increases at 30 mb the error is $\pm$ 8% and it increases greatly for higher pressures. McKee, et al (1969b) states that bias errors of .01 watts/m^2-sr (which is one-third the value used for Figure 28.) are currently possible.

Radiance Scale Error - The effects of radiance scale errors are shown in Figure 29. Each radiance is multiplied by a fixed percentage and the result is added to the original value. The same response as for the bias error is expected and was obtained. The errors in the lower section of the profile are much greater than corresponding values for a bias error since the magnitude of the scale error is greater in those regions. At 30 mb the ozone error is $\pm$ 23% and it increases for higher pressures. According to McKee, et al (1969b) scale errors of $\pm$ 1% are possible at the present time. Again, these are only one-third the values of errors used in calculations for Figure 29.

Tangent Height Error- The error in ozone partial pressure for a tangent height error is shown in Figure 30. In this calculation, a +1 km tangent height error means that each radiance is measured at a tangent p 1 km higher than the altitude used in the inversion calculations; for a -1 k tangent height error the converse is true. Thus with a +1 km error the entire curve is shifted downward and with a -1 km error it is shifted upward. Again the resulting error in ozone partial pressure is magnified significantly at higher pressures. At 30 mb, the error in PO_3 is +23%

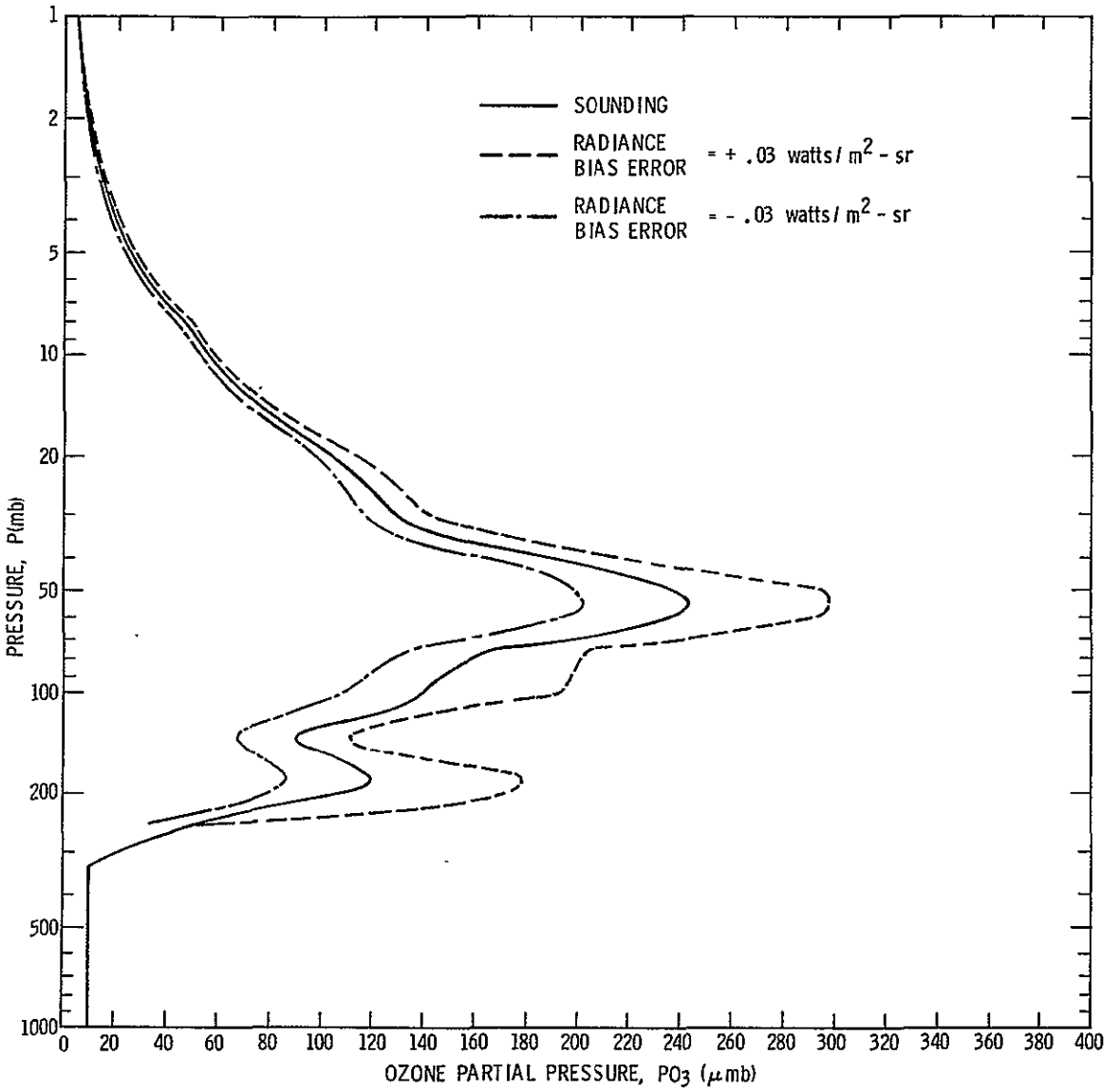

Fig. 28. Radiance bias error results—Thule, Greenland (76.5°N).

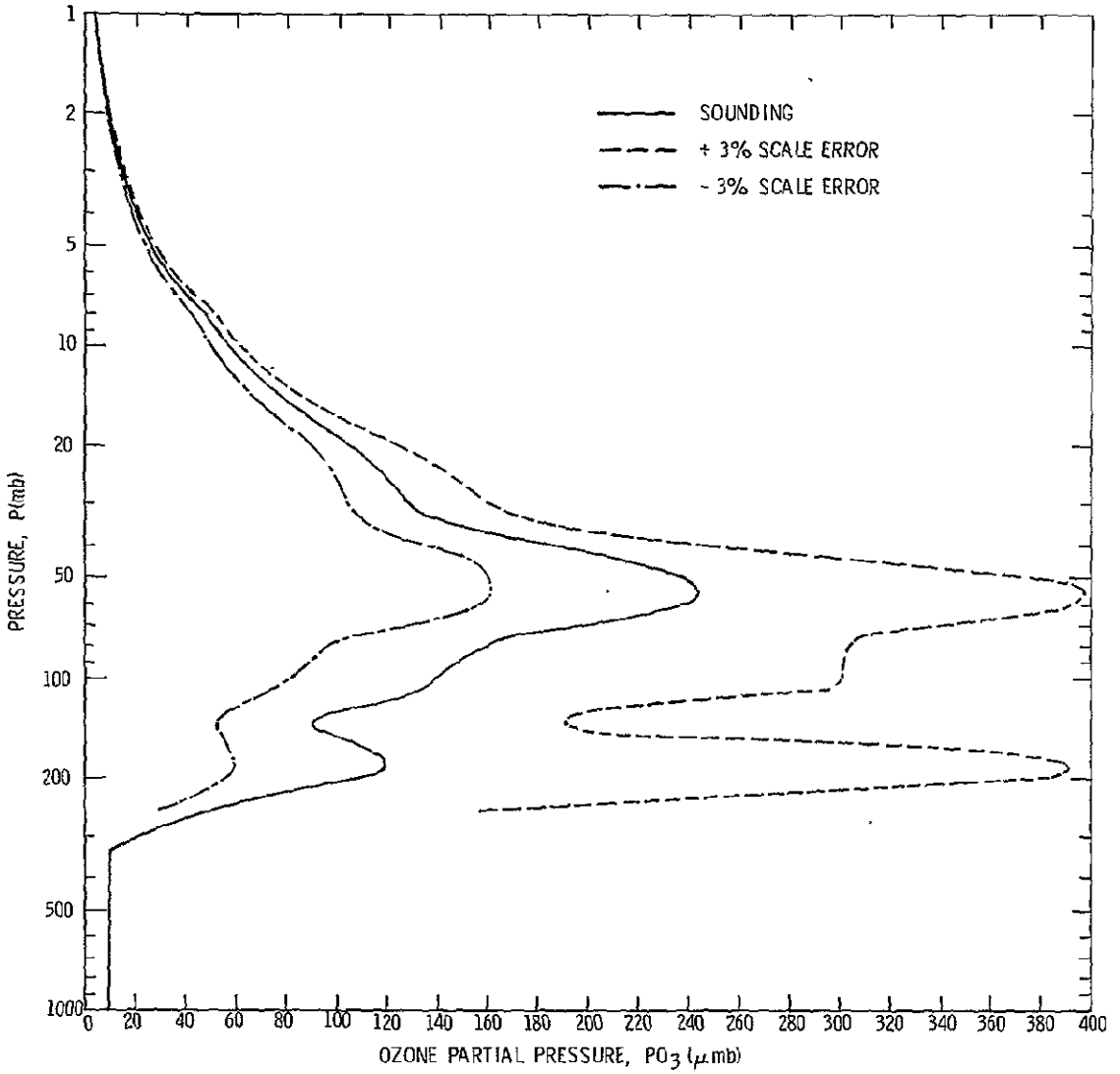

Fig. 29. Radiance scale error results--Thule, Greenland (76.5°N).

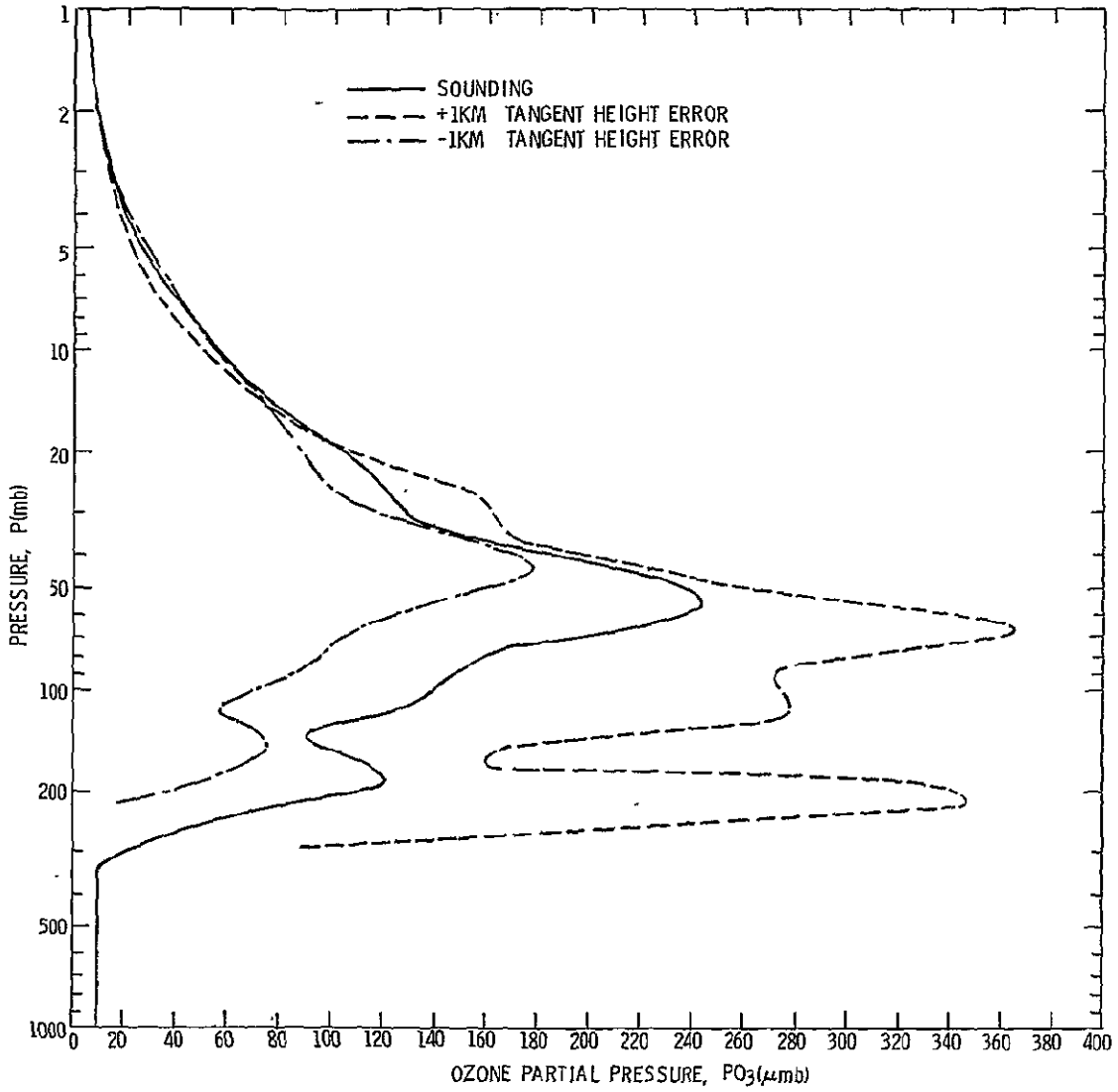

Fig. 30. Tangent height error results—Thule, Greenland (76.5°N).

and -8%; at 40 mb it is +8% and -15%; at 60 mb it is ± 50% and it increases at all higher pressures. A ± 1 km tangent height discrepancy is realistic for current experiments.

Temperature Bias Error - The resulting inversions for temperature bias errors are shown in Figure 31. This error source causes a larger ozone error than any other single factor for the error magnitudes considered in this report. This is because the radiance emitted by the atmosphere is such a strong function of the temperature. Figure 32 shows the equivalent radiance error as a function of pressure for a $3^{o}K$ temperature bias error. These errors are much larger, particularly at the higher pressures than any other errors used in this study. The ozone error at 30 mb is -50% and + 100%. As the pressure is increased further the error rapidly increases and for a negative temperature bias it becomes infinite. The instability arises because a negative temperature bias requires an increased ozone partial pressure to give the same atmospheric emission as when the temperature error is zero and in this case, the required increase is so great that the atmosphere becomes opaque. When the temperature error is positive, smaller ozone partial pressures occur and the shape of the curve is retained. Data presented by McKee, et al (1969a) indicates that it would be difficult to achieve a temperature error much smaller than ± $3^{o}K$ in an actual experiment. Thus the sensitivity of the inversion to this error source is critical.

Ozone Absorption Line Intensity Error - The effects of absorption errors are shown in figure 33. For a given ozone amount, the transmittance of the atmosphere along the LOS is less when the absorption error is positive. Therefore to increase the transmittance (and to decrease the atmospheric emission) to the value which exists when the

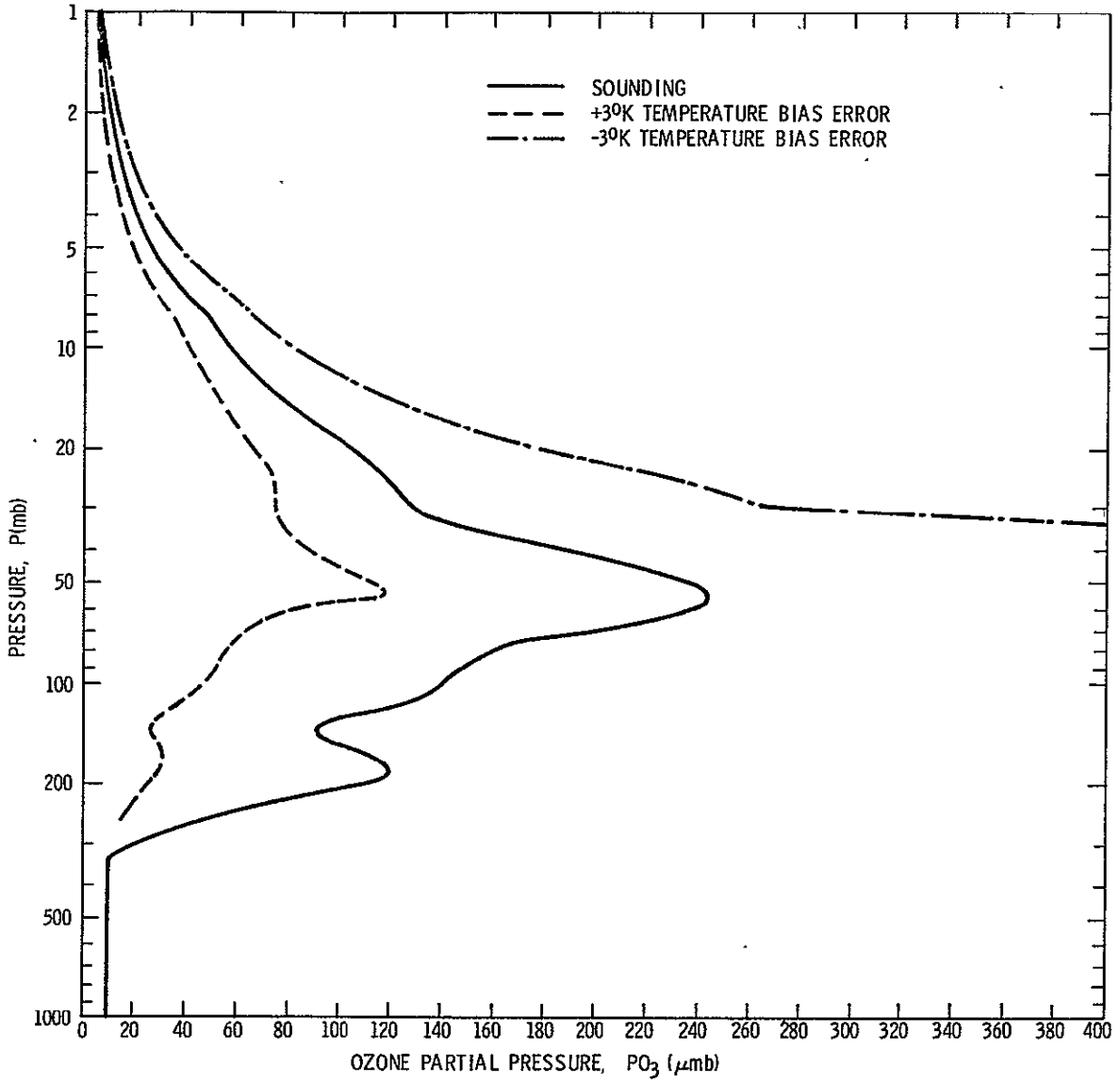

Fig. 31. Temperature bias error results—Thule, Greenland (76.5°N).

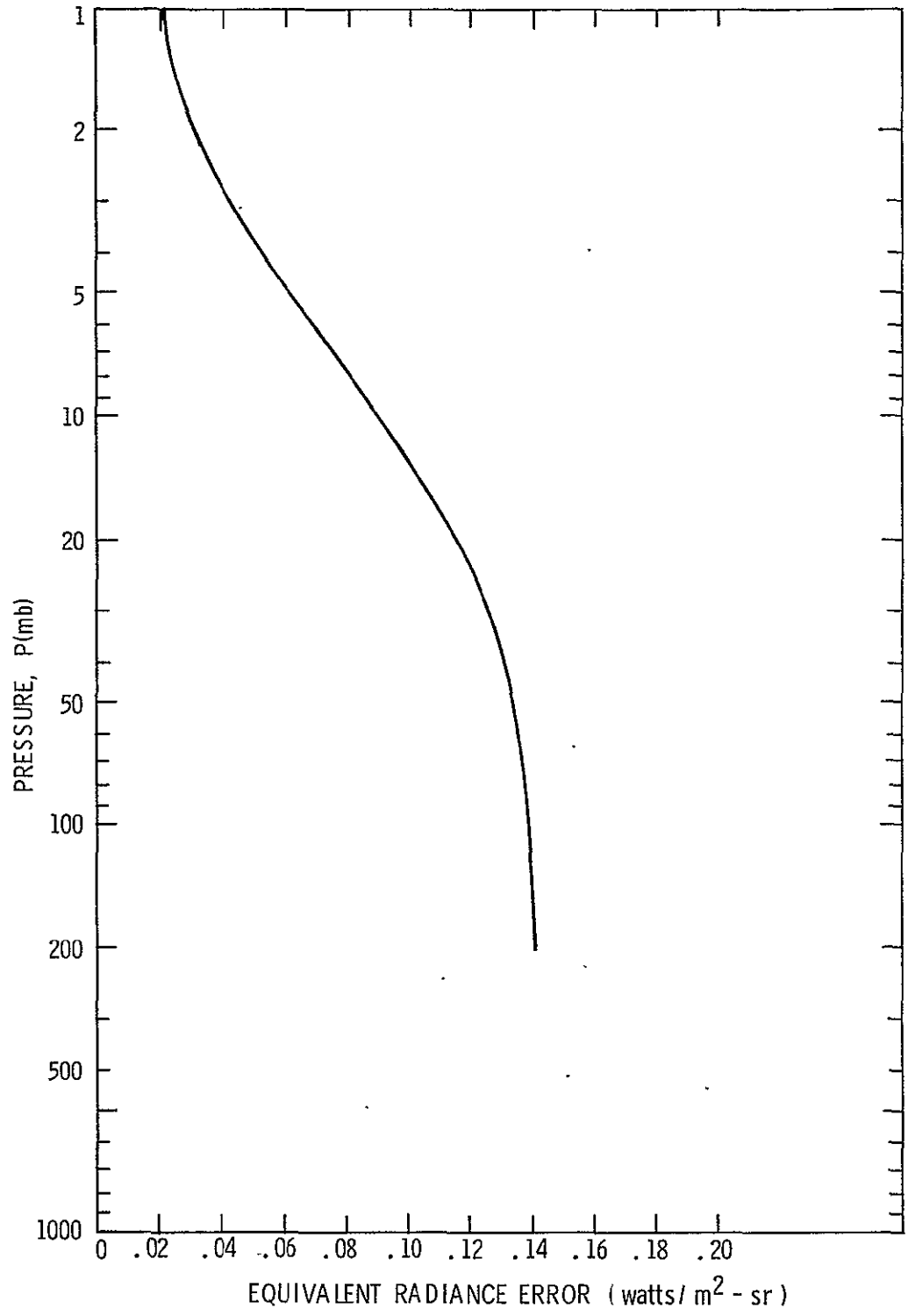

Fig. 32. Equivalent radiance error for a 3^{0}K temperature bias error.

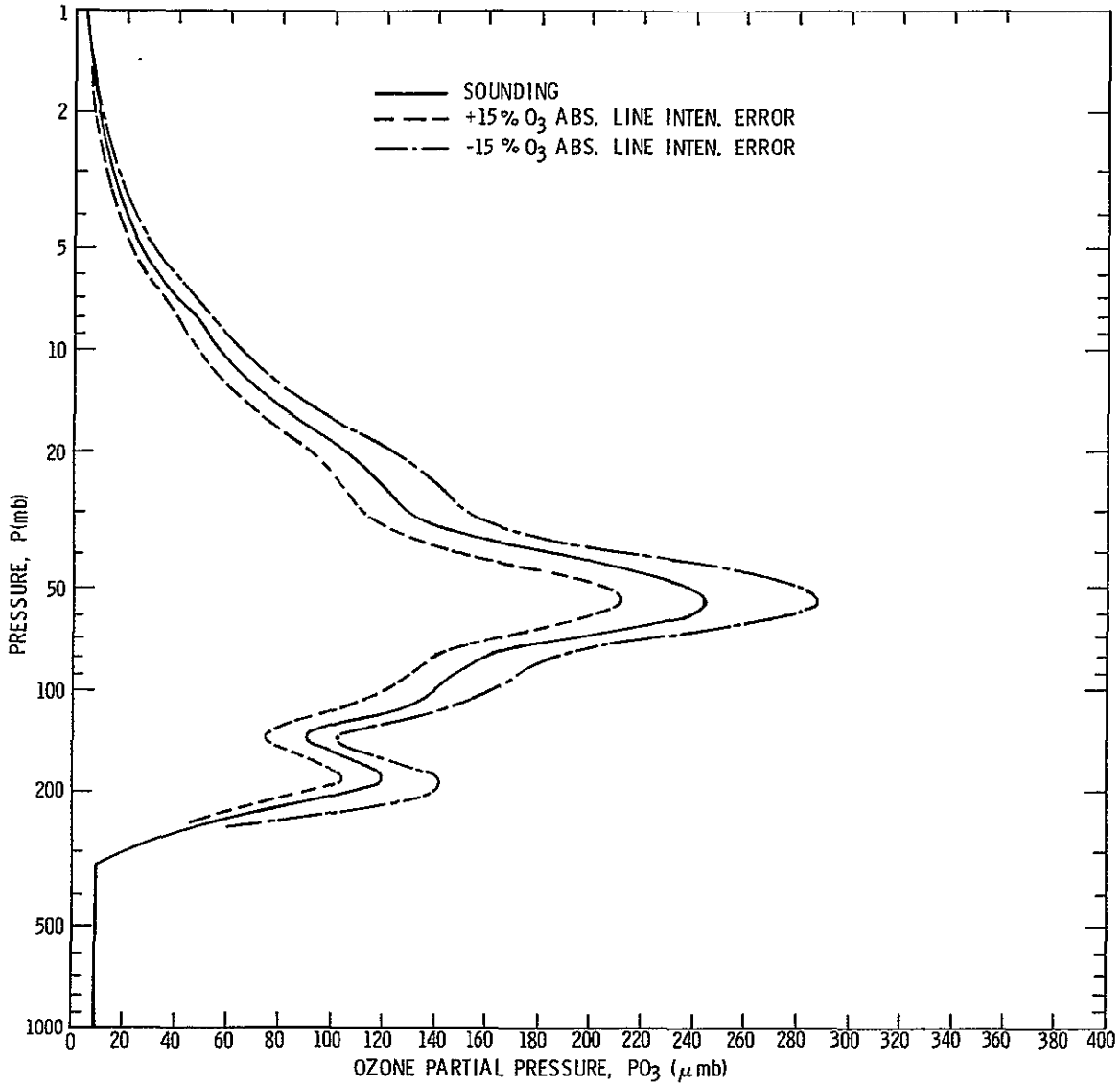

Fig. 33. Ozone absorption line intensity error results—Thule, Greenland (76.5° N).

absorption error is zero, it is necessary to reduce the ozone amount. The converse is true for a negative absorption line intensity error. The error in PO_3 at 30 mb is $\pm$ 15% and it changes only slightly for higher pressures. Currently, absorption line intensity errors may be as high as 35% or more in parts of the band, but eventually the error should be improved to 4% or less.

Surface Pressure Error - This error source arises because measurements in a horizon experiment are referenced to altitude rather than pressure. Since pressure values are needed to determine transmittances, the pressure variation with altitude must be computed and to do this a reference pressure at a reference altitude must be assumed (if it is not known from other measurements). The reference altitude in this report was taken as the surface of the earth. The effect of surface pressure errors are shown in Figure 34. The result of assuming a pressure either too low or too high is to shift the solution profile either upward or downward respectively. The greatest ozone error occurs at about 6 mb and it is about 20%. Actually, the surface pressure in the Northern Hemisphere is known from climatology most of the time to within about one-fourth of the error magnitude used for computing Figure 34. (Smith, et al, 1963). So the ozone error due to this source should be small.

Figure 34. concludes the analysis of individual error effects using the high latitude data. Next, all of the error calculations were repeated for radiances computed from a Canal Zone sounding. This was done to determine if any latitudinal effects exist regarding the error sensitivity of the inversion. In every calculation, the ozone error was smaller than for the corresponding high latitude inversion. The most significant difference was in the ozone partial pressure error for a negative bias

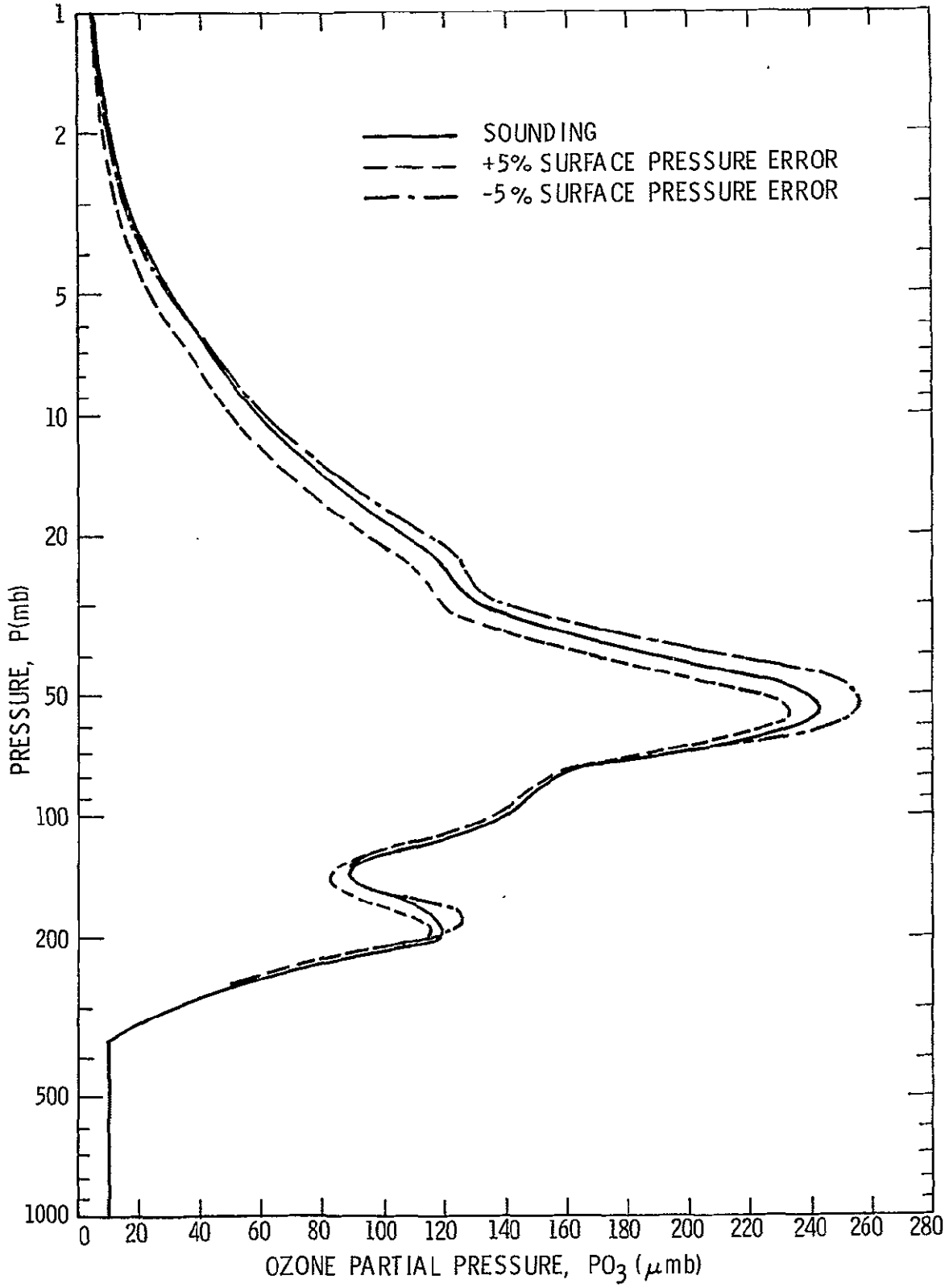

Fig. 34. Surface pressure error results—Thule, Greenland (76.5°N).

error in the temperature profile. The ozone error never reached 100% which contrasts sharply with the infinite error obtained for the Thule, Greenland inversion. The reduced error magnification is due to a combination of effects which arise because of the shape of the temperature profile and the greater transparency of the atmosphere at low latitudes. The greater transparency occurs since characteristically, the ozone partial pressures are smaller and the profiles peak at a lower pressure thereby causing less absorption.

When all of the error results are considered collectively, it appears doubtful that an inversion will be possible below an altitude of about 25 km. The success, if achieved, will depend on the probability of different error effects cancelling each other or on the ability to control errors to finer limits than those used in this study. Even for altitudes above 25 km, the inversions may be quite inaccurate. The factor having the most significant effect upon the accuracy is an error in the atmospheric temperature profile. The ozone error at 25 km for a temperature bias error of only $\pm$ 3^{o}K is -40%, +90% for a high latitude inversion and -37%, +70% for low latitude calculations. The errors converge in both cases (high and low latitude) in the upper stratosphere to a value of about $\pm$ 30%. These values do not represent limits because the ultimate ozone error may be better or worse depending upon how all the different error sources combine in a statistical sense. But these discrepancies do emphasize the critical importance of controlling temperature errors in an experiment. The next most significant effect after temperature errors is an error in the tangent height. The ozone error due to +1 km tangent height errors is about $\pm$ 20% at 25 km and it diminishes to a very small value in the upper stratosphere. After this there

is no preferred ordering if current estimates of the appropriate magnitudes are correct. Using these estimates and assuming the ozone error varies approximately linearly as a function of any single error magnitude, it is predicted that the maximum ozone error caused by any one of the remaining types of error will not exceed 7% at 25 km and it will be smaller at higher altitudes. To determine the ultimate ozone partial pressure accuracy which might be expected from the horizon experiment, the conditions of Table X were imposed simultaneously using the Thule, Greenland radiances. The error limits of Table X are either presently attainable or the values will most likely be possible in the future.

TABLE X

Types and Ranges of Errors Used in

The Horizon Experiment Simultaneous Error Study

Type of Error	Range	
	Best Case	Worst Case
Random Radiance Noise Normally distributed with a mean of zero	$\sigma = .02$ watts/m^2-sr	$\sigma = .02$ watts/m^2-sr
Radiance Bias	.02 watts/m^2-sr.	.02 watts/m^2-sr.
Radiance Scale	2%	2%
Tangent Height	-1 km	1 km
Ozone Absorption Line Intensity	-4%	-4%
Surface Pressure	-2%	-2%
Temperature Bias	$0^{\circ}K$	$0^{\circ}K$
Random Temperature normally distributed with a mean of zero	$\sigma = 3^{\circ}K$	$\sigma = 3^{\circ}K$

Excluding random errors, the worst case values are all additive in effect. The best case errors are identical to the worst case values with the exception of tangent height error which is opposite in sign. Thus in the best case, the effect of tangent height error tends to cancel effects caused by other errors. The radiance errors are conservative values since each is greater than the value estimated to be currently possible by McKee, et al (1969b). The tangent height and surface pressure errors are realistic values at the present time and the ozone absorption line intensity error should be achievable in the future. The temperature bias error was set equal to zero for these calculations and a random temperature error was used in its place. Although temperature bias errors probably will never be exactly zero, they should be minimized in a properly designed experiment. The results of inversions using best and worst case values are shown in Figures 35. and 36. respectively. The circles are the ozone partial pressures determined in the inversion for each tangent point. The radiance values were smoothed in these calculations using the segmented quadratic least squares technique previously described. The worst case inversion is unstable for pressures higher than about 150 mb. In the range 1 to 25 mb (50 to 25 km) most worst case inversion points are within 20% or less of the actual sounding. A few points are in error by 30% and a couple are in error by about 40%. For the same pressure range in the best case, most points are within 15% or less of the true profile, some are in error by 20%, and a couple of points are in error by 30%. When Green's ozone profile function, equation (3. 2. 31), was least squares fitted to each solution (best case and worst case) in the range 1 to 25 mb, all points on the curve were within 10% or less of the

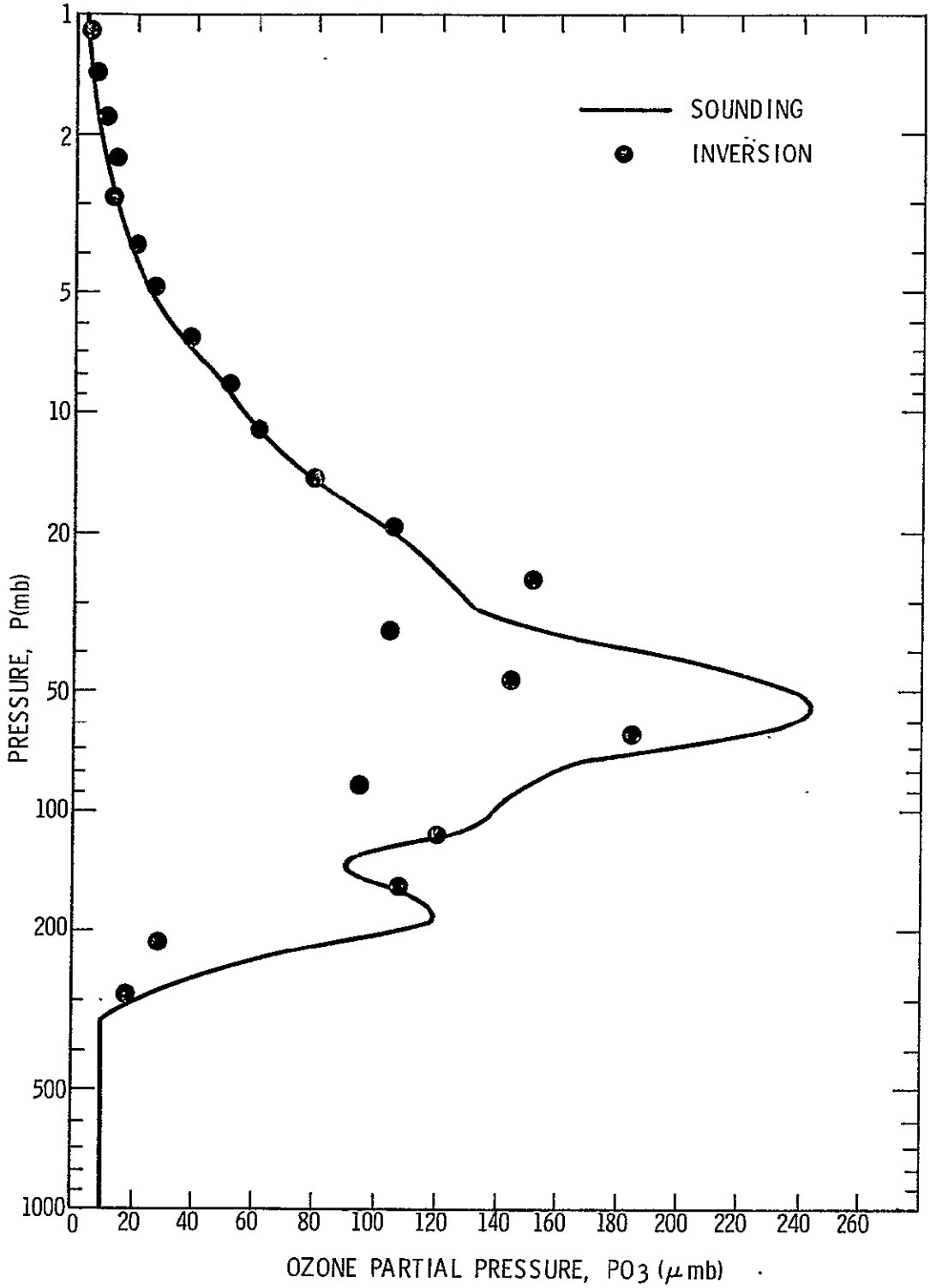

Fig. 35. Best case simultaneous error study results—Thule, Greenland (76.5°N).

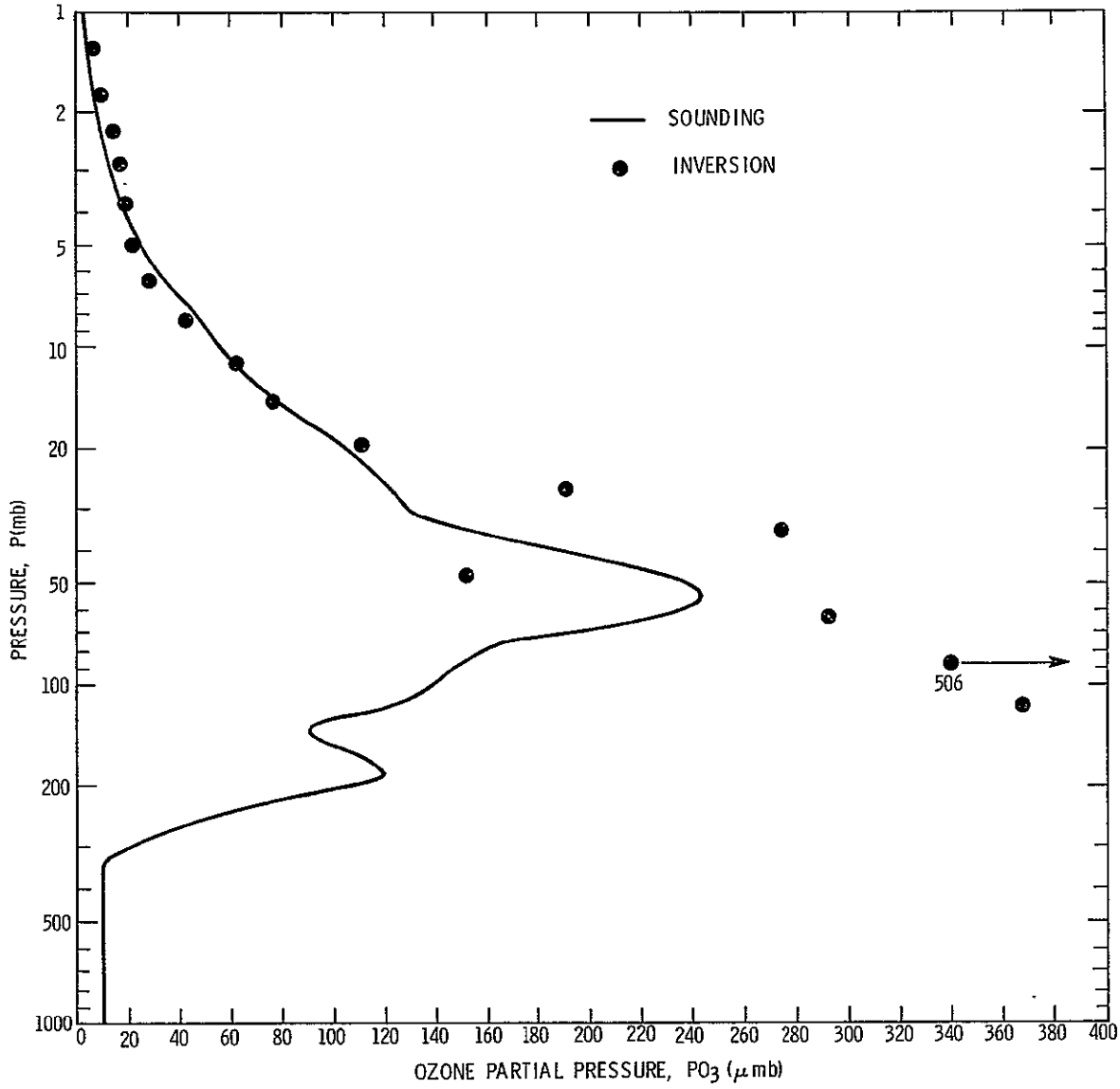

Fig. 36. Worst case simultaneous error study results—Thule, Greenland (76.5°N).

true profile in both cases. So based on these calculations, it should be possible to determine the ozone partial pressure to within 15 or 20% over most of the pressure range 1 to 25 mb and possibly this error can be reduced to 10% or less. These numbers should be conservative since fairly large radiance errors were used.

When the inversion technique is applied to real data, it may not be as sensitive to errors as it was in this study. The true ozone absorption spectrum extends to a lower wave number and has a smaller slope in the low wave number region than the theoretical spectrum determined with current ozone absorption line parameters (refer to Figure 1.). Consequently a larger percentage of the energy will come from the more weakly absorbing part of the spectrum in an actual measurement and the percentage energy coming from the tangent layer will be greater at every altitude. Therefore, the solution should be less sensitive to errors. This effect is not large but it should provide some improvement in the results.

The horizon experiment is compared with three other techniques in Table XI. As shown by the table, the horizon approach is the only method which is applicable on both the day and night side of the planet and it is the only technique which provides middle and upper stratospheric ozone data during the night. Furthermore, it extends the lower altitude limit for determining ozone partial pressure from a satellite and thereby compliments the other methods.

TABLE XI . A Comparison of Different Satellite Methods for Measuring High Altitude Atmospheric Ozone.

Method	Range (km)	Comments	References
Measurement of infrared radiation coming from the horizon	25 to 50	No geographic limitation. Applicable on both the day and night side of the planet.	This report
Measurement of backscattered uv solar radiation *	35 to 55	No geographic limitation. Applicable only on the day side of the planet.	Singer and Wentworth (1957), Sekera and Dave (1961), Twomey (1961), Dave and Mateer (1967), Herman and Yarger (1969), Anderson, et. al. (1969)
Measurement of visible and near uv solar radiation	45 to 65	Geographically limited. Applicable only on the day side of the planet.	Frith (1961), Rawcliffe (1963), Duardo (1967), Miller (1969)
Measurement of a stellar uv spectrum during occultation from a satellite	55 to 100	Geographically limited. Applicable only on the night side of the planet.	Hays and Roble (1967)

* This method may be extended to a lower altitude in the future if current difficulties caused by multiple scattering can be reduced or eliminated.

CHAPTER 5

CONCLUSIONS AND SUGGESTIONS FOR FUTURE WORK

Two basic approaches to the measurement of ozone from a satellite using the 1042 cm^{-1} band have been analyzed: the nadir experiment and the horizon experiment. The conclusions relevant to each approach will be discussed in succession.

A workable technique has been developed for inverting nadir measurements to obtain ozone information. The success of the method depends critically on the accuracy of the quantity which represents the energy emitted from the lower boundary under a satellite. A method was formulated for computing this quantity which circumvents the troublesome problems caused by the water vapor continuum absorption and by atmospheric clouds. By incorporating water vapor line absorption in the calculations, the effective temperature of the lower boundary could be found to within $.5^{\circ}K$ or less. The inversion equations were expanded in terms of the eigenvectors and eigenvalues of a least squares solution matrix and an analysis was performed using synthetic clear sky radiances computed for ten different ozone profiles. The results showed that under favorable conditions, infrared radiance measurements in the ozone band contain two pieces of independent information: the total ozone (u)and the altitude (hm) of the primary maximum in the ozone profile. It is not possible to obtain the value of the maximum ozone partial pressure or the width of the ozone profile from these data. A comprehensive study using a variety of error sources revealed that errors in u are most sensitive to random radiance errors, lower boundary temperature errors, and ozone absorption line intensity errors. Errors in hm are most effected by the former two errors and by temperature profile bias errors. In the next series of tests, all error sources were considered simultaneously.

The results showed that it should ultimately be possible to determine u to within 10% or less and to determine hm to within 1.5 km when the RMS radiance noise level is 1% or less. These calculations were also done for varying degrees of cloudiness in the troposphere. The data showed that the presence of clouds will not seriously effect results as long as there is some contrast between the ozone spectrum and the effective lower boundary emission spectrum. Sometimes, in high latitude areas of the globe, there may be little or no contrast between these spectra due to the effects of temperature profile and cloud condition Under these circumstances, it may be difficult or impossible to infer ozone information from the measurements. Finally, the inversion technique was applied to balloon data measured over Palestine, Texas and to the Nimbus III satellite data measured over Grand Turk of the Bahamas The two sets of measurements were in sharp contrast with each other; the balloon data contained very little noise while the satellite data were very noisy by comparison. The inversion results reflected this contrast. The Palestine inversion was satisfactory considering the uncertainties which existed. The errors in u and hm were estimated to be well within the limits of 10% and 1.5 km respectively. But the Nimbus results were poor. The total ozone was off by 76% and hm was in error by 6.3 km. If absorption errors throughout the band had been smaller, the Nimbus results could have been substantially improved by using the entire ozone band to reduce the effective radiance noise level. Future calculations will have to be limited to a narrow spectral interval and consequently to low noise data (less than 1%) until the accuracies of the absorption line intensities are improved.

A method was also developed for inferring ozone information from horizon radiance measurements. An analysis of the horizon experiment revealed that the ozone partial pressure can be determined in the altitude range from 50 km down to 25 or 30 km. The top limit arises because of the small optical depth of the atmosphere in the upper layers and the bottom extreme occurs because the atmosphere is almost opaque in the lower layers. A study of individual error effects using a high latitude synthetic radiance profile showed that inversions will probably be quite inaccurate unless the atmospheric temperature profile can be determined with great precision. The ozone partial pressure error for a temperature bias error of only $\pm$ 3^{o}K was $\pm$ 30% in the upper stratosphere and it deteriorated to about 80% at 25 km. The next most significant error effect was caused by tangent height errors. The effect was negligible in the upper stratosphere, but at 25 km, a tangent height error of only $\pm$ 1 km caused an ozone partial pressure error of $\pm$ 20%. The ozone error caused by any other individual error was small. The maximum effect due to any other error source probably will not exceed 7% at 25 km in actual experiment. All ozone errors were slightly less for a similar study performed with a low latitude snythetic radiance profile. The last set of calculations was a simultaneous error study. The temperature bias error was set equal to zero for these calculations and a normally distributed random temperature error was used instead with σ=3^{o}K. The results showed that it should ultimately be possible to determine the ozone partial pressure to within 15 or 20% for most of the range 25 to 50 km. It may be possible to reduce this error to 10% or less by smoothing the solution profile. Since a temperature bias error of only 3^{o}K would critically degrade these results, great stress should be placed on methods of minimizing this source of error in an actual experiment.

A comparison of the horizon experiment with three other satellite techniques which provide high altitude ozone data showed that it is the only method which is applicable on both the day and night side of the planet and it is the only technique which provides middle and upper stratospheric data during the night. Furthermore, it extends the current lower altitude limit for determining ozone partial pressure from a satellite.

One may well inquire into the usefulness of the information provided by these two experiments. With an accuracy of 10% or less, total ozone measurements provided by the nadir experiment would compete favorably with similar ground-based measurements made with a Dobson instrument. Therefore, instead of measuring ozone amount at just a few ground locations, it could be measured almost as accurately from a satellite over vast areas of the globe daily. The experiment would yield measurements on a routine basis over previously unsounded areas such as the oceans and remote locations in the Southern Hemisphere. The measurements would provide an extensive map of the latitudinal and longitudinal distribution of ozone amount in both hemispheres which could not be realistically obtained in any other way. In addition, the data would be sufficiently accurate to resolve daily variations of total ozone particularly in high latitude areas of the globe where the changes are most pronounced. Such measurements would facilitate good documentation of the relation between ozone amount and weather conditions and the data should lead to a better understanding of global air mass circulation. Total ozone data would also be valuable in studying the sudden stratospheric warming phenomena which occur in the Northern Hemisphere winter and the Southern Hemisphere spring. The combination of total

ozone data and information on the altitude of the primary maximum in the ozone profile would be useful in constructing more realistic models of the vertical ozone distribution for use in studies of the general circulation.

Measurements provided by the horizon experiment would be especially significant since the regime of the measurements would include the upper stratosphere. This atmospheric region has been probed only a few times in rocket experiments and it is beyond the reach of high altitude balloons. The horizon experiment would yield upper stratospheric ozone data routinely at a multitude of locations around the globe. Such information would reveal for the first time, the latitudinal, longitudinal, seasonal, and short term variability of ozone partial pressure in the high stratosphere of both hemispheres. These data would be helpful in studying the causes of the large ozone amount which accompanies a sudden stratospheric warming. According to Willet(1968), reliable measurements of ozone partial pressure in the range 30 to 50 km would significantly aid in such studies. Furthermore, these measurements would be useful in studying interhemispheric differences in the nature and timing of sudden warmings. Finally, the data would be helpful in clarifying unanswered questions regarding the photochemistry of the stratosphere.

The most pressing area for future work in both the nadir and horizon experiments is the problem of accurately determining the ozone absorption line parameters. This problem was beyond the scope of the current work but it is mentioned here because of its significant importance in these experiments. After more accurate parameters are obtained

the calculations of Chapter 3 using the balloon and satellite data should be repeated. Regarding other work, the microwave region of the spectrum should be investigated for application in the nadir experiment. It may be possible, because of the high resolution provided by a microwave instrument, to obtain more information from nadir measurements regarding the vertical ozone distribution. The infrared 701 cm^{-1} $\bar{\nu}_2$ ozone band should also be studied for use in the horizon experiment. This band is much weaker than the $\bar{\nu}_1$ and $\bar{\nu}_3$ bands used in this study. Consequently, the atmospheric transmittance due to ozone should be greater and the inversion should be less sensitive to errors. Carbon dioxide has a strong absorption band at 667 cm^{-1} which may nulify any gains that would be realized but the magnitude of the CO_2 effect can not be determined until a study is completed. Some future work should also be devoted to methods of combining data from the nadir and horizon experiments. It should be possible to obtain a good indication of the maximum ozone partial pressure from these data.

Appendix A

Relationships for the Random Exponential Band Model and the Curtis-Godson Approximation

The transmittance through a homogeneous layer is given by Goody, 1964a, Chapter 4 as

$$\overline{\tau(\bar{\nu}, \bar{P}_k)} = \exp\left[- \frac{(\beta_{\bar{\nu}}/\bar{d}) \cdot \bar{u}_k}{\left(1 + 2\left[\frac{\beta_{\bar{\nu}}}{2\pi\,\alpha_{Lo}(\bar{\nu})}\right] \cdot \bar{\ell}_k\right)^{1/2}} \right] \qquad (A.1)$$

and he shows that, in order to force a fit in the weak line ($\bar{u}_k << 1$) and strong line ($\bar{u}_k >> 1$) regions, the following expressions should be used,

$$\frac{\beta_{\bar{\nu}}}{\bar{d}} = \frac{\sum_{i=1}^{N'} S_i}{\Delta\bar{\nu}} \qquad (A.2)$$

$$\frac{\beta_{\bar{\nu}}}{2\pi\alpha_{Lo}(\bar{\nu})} = \frac{1}{8}\left\{ \frac{\sum_{i=1}^{N'} S_i}{\sum_{i=1}^{N'} (S_i \cdot \alpha_{io})^{1/2}} \right\}^{1/2} \qquad (A.3)$$

where N' is the total number of lines in the interval $\Delta\bar{\nu}$ and α_{io} is the Lorentz half-width of the ith line at standard temperature and pressure.

According to the Curtis-Godson approximation the effective pressure of the atmosphere between the satellite and an arbitrary pressure P_o is

$$\overline{P_k} = \frac{\int_o^{P_o} P \cdot S[T(P)] \cdot \frac{q}{g}\, dP}{\int_o^{P_o} S[T(P)] \frac{q}{g}\, dP} \qquad (A.4)$$

where q is the absorber mass mixing ratio and g is the acceleration of gravity. The effective absorber amount is

$$\bar{u}_k = \frac{\int_o^{P_o} S[T(P)]\frac{q}{g}\, dP}{S(\bar{T})} \qquad (A.5)$$

where $\bar{T}$ is a mean temperature. But if $S[T(P)] = S(\bar{T})$, i.e. if the line intensity does not vary with altitude, then (A.4) and (A.5) become

$$\bar{P}_k = \frac{\int_o^{P_o} P\,\frac{q}{g}\, dP}{\int_o^{P_o} \frac{q}{g}\, dP} \qquad (A.6)$$

$$\bar{u}_k = \int_o^{P_o} \frac{q}{g}\, dP \qquad (A.7)$$

The effective length of the homogeneous path is computed by,

$$\bar{\ell}_k = \frac{\bar{u}_k}{\bar{P}_k} \qquad (A.8)$$

These last three equations, along with (A.1), (A.2), and (A.3), are used throughout this report to compute the transmittance when the Random-Exponential band model is used. The line intensities required to compute (A.2) and (A.3) were taken from Clough and Kneizys (1965). The half-width was considered to be the same for all lines and equal to .08 cm^{-1} at STP. This value was suggested by Clough and Kneizys (1965) and used by Goldman and Kyle (1968).

APPENDIX B

Effect of the Lower Boundary Emission on the Ozone Spectrum

The energy emitted by the underlying boundary can have a significant effect on the ozone spectrum measured at the top of the atmosphere. Assume, for the present, that the emissivity of the lower boundary is one and that the ozone layer is isothermal at a temperature $T(P_r)$ which is different from the temperature $T(P_g)$ of the lower boundary. These conditions are represented in Figure B-1. In this case (3.2.6) can be written,

$$\overline{L(\bar{\nu}_o, 0)} = B\left[\bar{\nu}_o, T(P_g)\right] \overline{\tau(\bar{\nu}_o, P_g)} - B\left[\bar{\nu}_o, T(P_r)\right] \int_1^{\overline{\tau(\bar{\nu}_o, P_T)}} d\,\overline{\tau(\bar{\nu}_o, P)} - \int_{\overline{\tau(\nu_o, P_T)}}^{\overline{\tau(\bar{\nu}_o, P_g)}} B\left[\bar{\nu}_o, T(P)\right] d\,\overline{\tau(\bar{\nu}_o, P)} \qquad (B.1)$$

where P_T is the pressure at the top of the effective lower boundary. If it is assumed that $\overline{\tau(\bar{\nu}_o, P_T)} \approx \overline{\tau(\bar{\nu}_o, P_g)}$ then (B.1) reduces to the following after integration:

$$\overline{L(\bar{\nu}_o, 0)} = \left\{B\left[\bar{\nu}_o, T(P_g)\right] - B\left[\bar{\nu}_o, T(P_r)\right]\right\} \overline{\tau(\bar{\nu}_o, P_g)} + B\left[\bar{\nu}_o, T(P_r)\right] \qquad (B.2)$$

The spectrum defined by (B.2) and different values of $\bar{\nu}_o$, will show the structure of the ozone band because of the factor $\overline{\tau(\bar{\nu}_o, P_g)}$. However, if the lower boundary is at the same temperature as the ozone layer i.e. $T(P_g) = T(P_r)$ then (B.2) reduces to

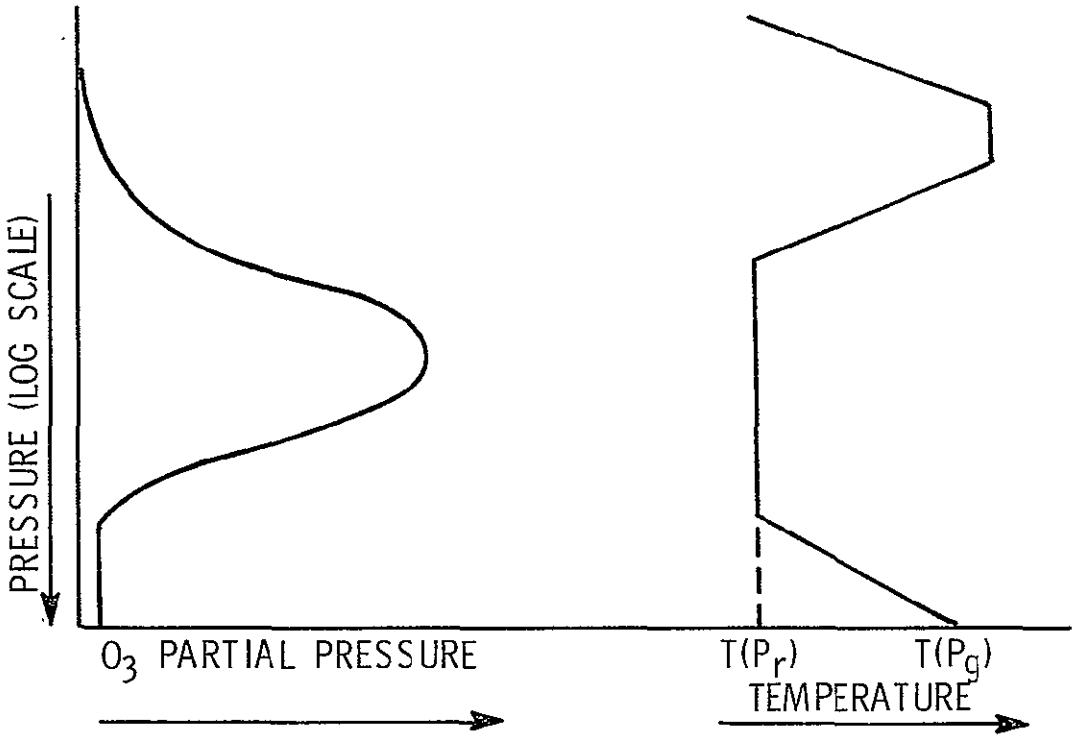

Fig. B-1. Isothermal ozone layer with $T(P_r) \neq T(P_g)$.

$$\overline{L(\bar{\nu}_o, 0)} = B\left[\bar{\nu}_o, T(P_r)\right] \qquad \text{(B. 3)}$$

which shows no structure. Such a spectrum contains no ozone information. Ways in which (B. 3) can occur are illustrated in Figures B-2 and B. 3. In Figure B-2, the underlying boundary is the earth's surface and in Figure B-3 it is the top of a cloud layer for a completely overcast condition. If the troposphere is partly cloudy the effective lower boundary temperature, for a temperature profile like that of Figure B-3, will be at some intermediate value between the ground and tropopause temperatures. There would be structure in the ozone band for this partly cloudy condition but the structure would not be as pronounced as for the clear sky case. In fact, (B. 2) shows that as the value of $T(P_g)$ approaches the value of $T(P_r)$ the structure in the ozone band decreases and finally dissappears when the two temperatures are equal.

A broad, nearly isothermal region in the middle and lower stratosphere is typical of the temperature profile in the high latitude areas of the globe. Therefore, the entire range from full to no structure in the ozone band may be encountered at high latitudes depending upon the temperature profile and cloud conditions. Consequently, it sometimes may be difficult or impossible to determine ozone information from satellite measurements in the high latitude regions.

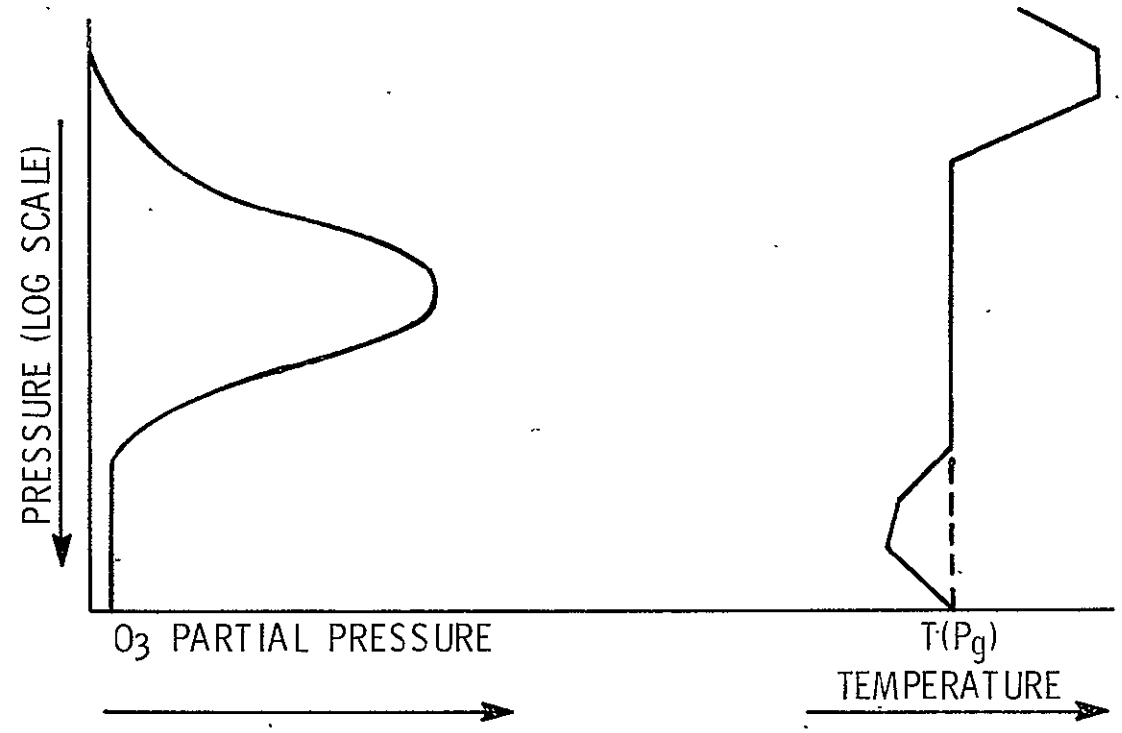

Fig. B-2. Isothermal ozone layer with $T(P_r)=T(P_g)$.

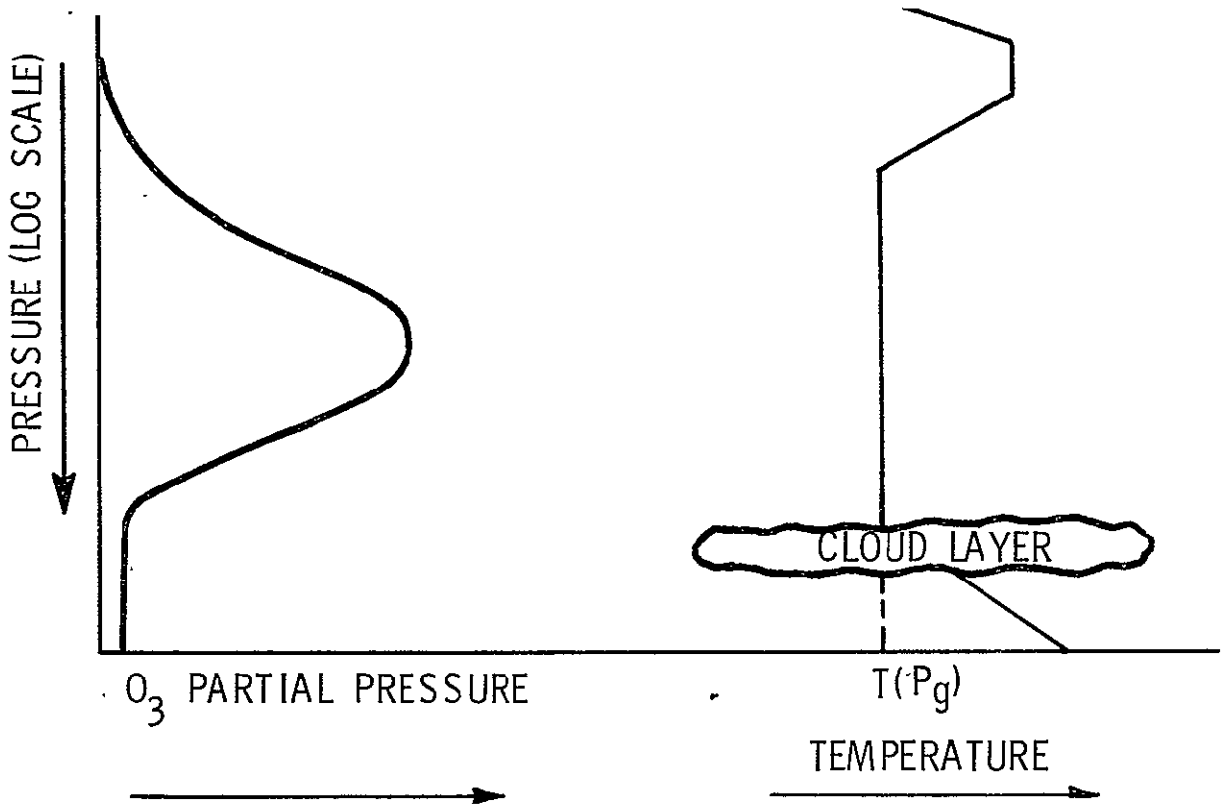

Fig. B-3. Isothermal ozone layer with a total cloud cover in the troposphere [$T(P_r)=T(P_g)$].

BIBLIOGRAPHY

Alishouse, J. C , Crone, L. J., Fleming, H. E., Van Cleef, F. L., and Wark, D. Q., 1967: A Discussion of Empirical Orthogonal Functions and Their Application to Vertical Temperature Profiles. Tellus, 19, 477-482.

Anderson, G. P., Barth, C. A., Cazla, F., and London, J., 1969: Satellite Observations of the Vertical Ozone Distribution in the Upper Stratosphere. Ann. Geophys., 25, No. 1, 341-345.

Armstrong, B. H., 1968: Analysis of the Curtis Godson Approximation and Radiation Transmission Through Inhomogeneous Atmospheres. J. Atmos. Sci., 25, 312-322.

Bandeen, W. R., 1968: Experimental Approaches to Remote Atmospheric Probing in the Infrared from Satellites. Doc. X-622-68-146, NASA, Goddard Space Flight Center.

Bates, J. C., Hanson, D. S., House, F. B., Carpenter, R., and Gille, J., 1967: The Synthesis of 15μ Infrared Horizon Radiance Profiles from Meteorological Data Inputs. NASA CR-724.

Bekoryukov, V. I., 1965: Computation of the Effect of Closed Air Circulation on the Equilibrium Distribution of Ozone in the Earth's Atmosphere. Geomagn. and Aeronomy (U. S. A.), Vol. 5, No. 3, 357-361.

Benedict, W. S. and Calfe, R. F., 1967: Line Parameters for the 1.9 and 6.3 Micron Water Vapor Bands. ESSA, Professional Paper 2, U. S. Department of Commerce.

Benson, S. W. and Axworthy, A. E., 1965: Reconsideration of the Rate Constant from the Thermal Decomposition of Ozone. J. of Chem. Phys., 42, 2614-2615.

Bojkov, R. D., 1968: The Mean Pole to Pole Vertical Distribution of Ozone. In the Proceedings of the Stanstead Seminar on the Middle Atmosphere (7th), edited by B. W. Boville, McGill Univ. Pub. in Meteorology, No. 90, 221.

Brieland, J. G., 1964: Vertical Distribution of Atmospheric Ozone and its Relation to Synoptic Meteorological Conditions. J. Geophys. Res., 69, 3801.

Burn, J. W. and Uplinger, W. G., 1969: The Determination of Atmospheric Temperature Profiles from Planetary Limb Radiance Profiles. Lockheed Missiles and Space Company, Report LMSC-681950, prepared under NASA contract NAS1-8048.

Chandrasekhar, S., 1960: Radiative Transfer. Dover, New York, 393.

Chaney, L. W., Loh, L. T., and Surh, M. T., 1967: A Fourier Transform Spectrometer for the Measurement of Atmospheric Thermal Radiation. Univ. of Mich., Engr. College, Report No. 05863-12-T.

Chapman, S., 1930: A Theory of Upper Atmospheric Ozone. Mem. Roy. Meteorol. Soc., 3, 103.

Clough, S. A., and Kneizys, F. X., 1965: Ozone Absorption in the 9.0 Micron Region. Physical Sciences Research Papers No. 170, Air Force Cambridge Research Laboratories.

Clough, S. A., and Kneizys, F. X., 1966: Coriolis Interaction in the $\bar{\nu}_1$ and $\bar{\nu}_3$ Fundamentals of Ozone. J. of Chem. Phys., 44, No. 5, 1855-1861.

Conrath, B. J., 1966: On a Mathematical Formulation of the Constituent Inversion Problem for Planetary Atmospheres. Doc. X-622-66-542, NASA, Goddard Space Flight Center.

Conrath, B. J., 1967: Remote Sensing of Atmospheric Water Vapor and Ozone Using Interferometry. NASA TMX -53711, 277-296.

Conrath, B. J., 1968: Inverse Problems in Radiative Transfer: A Review. Proc. of the XVIII International Astronautical Congress, Belgrade, 1967, 339-360. (Also available as Doc. X-622-67-57, NASA, Goddard Space Flight Center.)

Conrath, B. J., 1969: On the Estimation of Relative Humidity Profiles from Medium - Resolution Infrared Spectra Obtained from a Satellite. J. Geophys. Res., 74, No. 13, 3347-3361.

Craig, R. A., 1950: The Observations and Photochemistry of Atmospheric Ozone and their Meteorological Significance, A. M. S. Met. Monographs, 1, No. 2, 50.

Craig, R. A., 1965: The Upper Atmosphere, Meteorology and Physics, Chapter 5, Academic Press.

Dave, J. V., and Mateer, C. L., 1967: A Preliminary Study on the Possibility of Estimating Total Atmospheric Ozone from Satellite Measurements. J. Atmos. Sci., 24, No. 4, 414-427.

Davis, R. E., 1969: A Limb Radiance Calculation Approach for Model Atmospheres Containing Horizontal Gradients of Temperature and Pressure. NASA TND-5495.

Dobson, G. M. B., 1930: Observations of the Amount of Ozone in the Earth's Atmosphere and its Relation to Other Geophysical Conditions. Part IV. Proc. Roy. Soc., London, A129, 411-433.

Drayson, S. R., 1963: Errors in Atmospheric Temperature Structure Solutions from Remote Radiametric Measurements. Univ of Mich., Engr. College, Report 05863-4-T.

Drayson, S. R., 1965: Atmospheric Slant Path Transmission in the 15μ CO_2 Band. NASA - TN-D-2744.

Drayson, S. R., 1967: The Calculation of Long-Wave Radiative Transfer in Planetary Atmospheres. Univ. of Mich., Engr. College, Report No. 07584-1-T.

Drayson, S. R., and Young, C., 1966: Theoretical Investigations of Carbon Dioxide Radiative Transfer. Univ. of Mich., Engr. College, Report No. 07349-1-F.

Drayson, S. R., and Young, C., 1967: Private communication, Univ. of Mich., Ann Arbor, Michigan.

Duardo, J. A., 1967: Study to Develop a Technique for Measurement of High Altitude Ozone Parameters. Contract NAS 12-137, prepared for ERC, Cambridge, Mass.

Dütsch, H. U., 1962: Ozone Distribution and Stratospheric Temperature Field over Europe During the Sudden Warming in January/February 1958. Beitr. Phys. Atmos., 35, 87-107.

Fabry, C., and Buisson, M., 1913: L'Absorption de l' Ultraviolet par l'Ozone et la Limit du Spectra Solaire. J. Phys. Rad., 3, 196.

Frith, R., 1961: Measuring the Ozone Above the Earth. Discovery, 390-391.

Gille, J. C., 1968a: Inversion of Radiometric Measurements. Bull. Amer. Meteor. Soc., 49, No. 9, 903-912.

Gille, J. C., 1968b: On the Possibility of Estimating Diurnal Temperature Variation at the Stratopause from Horizon Radiance Measurements. J. Geophys. Res., 73, No. 6, 1863-1868.

Gille, J. C., and Ellingson, R. G., 1968: Correction of Random Exponential Band Transmissions for Doppler Effects. J. Appl. Optics, 7, 471-474.

Godson, W. L., 1960: Total Ozone and the Middle Stratosphere Over Arctic and Sub-Arctic Areas in Winter and Spring. Quart. J. Roy. Meteorol. Soc., 86, 301-317.

Goldman, A., and Kyle, T. G., 1968: A Comparison Between Statistical Model and Line by Line Calculation with Application to the 9.6μ Ozone and the 2.7μ Water Vapor Bands. J. Appl. Optics, 7, No. 6, 1167-1177.

Goody, R. M., 1952: A Statistical Model for Water-Vapor Absorption. Q. J. R. M. S., 78, 165-169.

Goody, R. M., 1964a: Atmospheric Radiation I: Theoretical Basis. Oxford University Press, 4-36.

Goody, R. M., 1964b: The Transmission of Radiation Through an Inhomogeneous Path. J. Atmos. Sci., 21, No. 6, 575-581.

Gotz, F. W. P., Meetham, A. R., and Dobson, G. M. B., 1934: The Vertical Distribution of Ozone in the Atmosphere. Proc. Roy. Soc., A145, 416-446.

Green, A. E. S., 1964: Attenuation by Ozone and the Earth's Albedo in the Middle Ultraviolet. J. Appl. Optics, 3, No. 2, 203-208.

Griggs, M., 1966: Atmospheric Ozone. The Middle Ultraviolet: Its Science and Technology, edited by A. E. S. Green, Chapter 4, John Wiley and Sons.

Hanel, R. A., and Chaney, L. W., 1966: The Merits and Shortcomings of a Michelson Type Interferometer to Obtain the Vertical Temperature and Humidity Profile. Proc. of the XVII International Astronautical Congress, Madrid, 1966. Vol. II. (Also available as Doc. X-620-66-476, NASA, Goddard Space Flight Center.)

Hanel, R. A., and Conrath, B. J., 1969: Interferometer Experiment on Nimbus 3: Preliminary Results. Science, 165, 1258-1260, Sept. 19.

Hays, P. B., and Roble, R. G., 1967: Stellar Spectra and Atmospheric Composition. Univ. of Mich., Engr. College, Report No. 08953-1-T.

Hering, W. S., 1964: Ozonesonde Observations over North America, 1, AFCRL Research Report, AFCRL-64-30 (I).

Hering, W. S., and Borden, T. R., 1964: Ozonesonde Observations over North America, 2, Environmental Research Paper No. 38, AFCRL-64-30 (II).

Hering, W. S., and Borden, T. R., 1965: Ozonesonde Observations over North America, 3, Environmental Research Paper No. 133, AFCRL-64-30(III).

Hering, W. S., and Borden, T. R., 1967: Ozonesonde Observations over North American, 4, Environmental Research Paper No. 279, AFCRL-64-30(IV).

Herman, B. M. and Yarger, D. N., 1969: Estimating the Vertical Atmospheric Ozone Distribution by Inverting the Radiative Transfer Equation for Pure Molecular Scattering. J. Atmos. Sci., 26, 153-162.

Herzberg, G. H., 1945: Molecular Spectra and Molecular Structure Volume II, Infrared and Raman Spectra of Polyatomic Molecules. D. Van Nostrand Co., Princton, N. J. , 285-287.

House, F. B., and Ohring, G., 1969: Inference of Stratospheric Temperature and Moisture Profiles from Observations of the Infrared Horizon. NASA CR-1419.

Hunt, B. G., 1966a: The Need for a Modified Theory of the Ozonosphere. J. Atoms. Sci., 23, No. 1, 88-95.

Hunt, B. G., 1966b: Photochemistry of Ozone in a Moist Atmosphere. J. Geophys. Res., 71, 1385.

Kaplan, L. D., 1959: Inference of Atmospheric Structure from Remote Radiometric Measurements. J. Opt. Soc. Amer., 49, No. 10, 1004-1007.

Karandikar, R. V., and Ramanathan, K. R., 1949: Vertical Distri - bution of Atmospheric Ozone in Low Latitudes. Proc. India Acad. Sci., 29, 330-348.

Kellogg, W. W., and Schilling, G. F., 1951: A Proposed Model of the Circulation in the Upper Atmosphere. J. Meteor., 8, 222-230.

King, J. I. F., 1956: The Radiative Heat Transfer of Planet Earth. In: Scientific Uses of Earth Satellites. Edited by J. A. Van Allen. The University of Michigan Press, Ann Arbor, Michigan, 133-136.

Kuhn, W. R., and London, J., 1969: Infrared Radiative Cooling in the Middle Atmosphere (30-110 km). J. Atmos. Sci., 26, No. 2, 189-204.

Lindzen, R., and Goody, R. M., 1965: Radiative and Photochemical Processes in Mesopheric Dynamics. Part I., Models for Radiative and Photochemical Processes. J. Atmos. Sci., 22, 341.

London, J., 1957: A Study of the Atmospheric Heat Balance. Research Div., Engr. College, N. Y. Univ., Final Report AF 19(122)-165, July.

London, J., 1962: The Distribution of Total Ozone over the Northern Hemisphere. Sun at Work, 7, No. 2, 11-12.

Mateer, C. L., 1964: A Study of the Information Content of Umkehr Observations. Univ. of Mich., Engr. College, Report 04682-2-T.

Mayer, H., 1947: Los Alamos Scientific Lab. Report LA-647(1947).

McCaa, D. J., and Shaw, J. H., 1967: The Infrared Absorption Bands of Ozone. Ohio State University Research Foundation Contractor Report, AFCRL-67-0237, Scientific Report No. 2.

McKee, T. B., Whitman, R. I., and Lambiotte, J. J., 1969a: A Technique to Infer Atmospheric Temperature from Horizon Radiance Profiles. NASA TN D-5068.

McKee, T. B., Whitman, R. I., and Lambiotte, J. J., 1969b: A Technique to Infer Atmospheric Water-Vapor Mixing Ratio from Measured Horizon Radiance Profiles. NASA TN D-5252.

Miller, D. E., 1969: The Measurement of Ozone from a Satellite. Star, 8, No. 1, 94. N70-11271. (Paper presented at the NATO/ Brit. Interplanet. Soc. Inter. Summer School on Earth Observation Satellites, Cambridge, England, July 14-25, 1969).

Muench, H. S., 1969: (Private communication). Air Force Cambridge Research Laboratories, Bedford, Massachusetts.

National Academy of Sciences, 1965: Atmospheric Ozone Studies - An Outline for an International Observation Program. NAS Publ. No. 1348.

Normand, C., 1951: Some Recent Work on Ozone. Quart. J. Roy. Meteorol. Soc., 77, 474-478.

Paetzold, H. K., 1953: The Mean Vertical Ozone Distribution Resulting from the Photochemical Equilibrium, Turbulence, and Currents of Air. J. Atmos. Terr. Phys., 3, 125-131.

Perl, G., and Dutsch, H., 1959: Die 30-jahrige Aroser Ozonmessreihe. Ann. Schweiz. Meteor. Zentralamstalt, 8.

Prabhakara, C., 1969a: Feasibility of Determining Atmospheric Ozone from Outgoing Infrared Energy. Mon. Wea. Rev., 97, No. 4, 307-314.

Prabhakara, C., 1969b: Remote Sensing of Atmospheric Ozone Using the 9.6 Micron Region. NASA TM-X-63733.

Rawcliffe, R. D., Meloz, G. E., Friedman, R. M., and Rogers, E.H., 1963: Measurement of the Vertical Distribution of Ozone from a Polar Orbiting Satellite. J. Geophys. Res., 68, 6425-6429.

Reed, E. I. and Scolnick, R., 1964: International Ozone Symposium, Albuquerque, New Mexico.

Reed., R. J., 1965: The Present Status of the 26-Month Oscillation. Bull. Amer. Meteoro. Soc., 46, No. 7, 374-387.

Regener, V. H., 1960: On a Sensitive Method for the Recording of Atmospheric Ozone. J. Geophys. Res., 65, No. 12, 3975-3977.

Regener, V. H., 1964: Measurement of Atmospheric Ozone with the Chemiluminescent Method. J. Geophys. Res., 69, No. 18, 3795-3800.

Roney, P. L., 1965: On the Influence of Water Vapor on the Distribution of Stratospheric Ozone. J. Atmos. Terr. Phys. 27, 1177-1190.

Sekera, Z., and Dave, J. V., 1961: Determination of the Vertical Distribution of Ozone from the Measurement of Diffusely Reflected Ultraviolet Solar Radiation. Planet. Space Sci., 5, 122-136.

Sekihara, K., and Walshaw, C. D., 1969: The Possibility of Ozone Measurements from Satellites Using the 1043 cm^{-1} Band. Ann. Geophys., 25, No.1, 233-241.

Singer, S. F., and Wentworth, R. C., 1957: A Method for the Determination of the Vertical Ozone Distribution from a Satellite. J. Geophys. Res., 62, No. 2, 299.

Smith, O. E., McMurray, W. M., and Crutcher, H. L., 1963: Cross-Sections of Temperature, Pressure and Density near the 80th Meridian West. NASA TN-D-1641.

Sticksel, P. R., 1966: The Vertical Distribution of Ozone over Tallahassee, Florida. Scientific Report No. 1, Contract AF 19(628)-4953.

Trambarulo, R., Ghosh, S. N., Burrus, C. A., and Gordy, W., 1953: The Molecular Structure, Dipole Moment, and g Factor of Ozone from Its Microwave Spectrum. J. Chem. Phys., 21, No. 5, 851-854.

Twomey, S., 1961: On the Deduction of the Vertical Distribution of Ozone by Ultraviolet Spectral Measurements from a Satellite. J. Geophys. Res., 66, 2153-2162.

Vassy, A., 1965: Atmospheric Ozone. Advances in Geophys., 11, 115.

Walshaw, C. D., and Rogers, C. D., 1963: The Effect of the Curtis-Godson Approximation on the Accuracy of Radiative Heating-Rate Calculations. Quant. J. Roy. Meteoro. Soc., 89, 122-130.

Wark, D. Q., and Fleming, H. E., 1966: Indirect Measurements of Atmospheric Temperature Profiles from Satellites: 1. Introduction. Mon. Wea. Rev., 94, No. 6, 351-362.

Willet, H. C., 1968: Remarks on the Seasonal Changes of Temperature and of Ozone in the Arctic and the Antarctic Stratospheres. J. Atmos. Sci., 25, No. 3., 341-360.

Wulf, O. R., 1945: The Distribution of Atmospheric Ozone. Proc. Eighth Amer. Sci. Cong., Washington, 439-446.